

Ballistic strength of multi-layer fabrics against fragment simulating projectiles

by

Ying Ma

B.S., Sichuan University, China, 2008

AN ABSTRACT OF A DISSERTATION

submitted in partial fulfillment of the requirements for the degree

DOCTOR OF PHILOSOPHY

Department of Mechanical and Nuclear Engineering
College of Engineering

KANSAS STATE UNIVERSITY
Manhattan, Kansas

2017

Abstract

Ballistic performance of textile fabric is affected by numerous elements, such as fabric architecture, material property, and projectile characteristics. Near fiber-level microstructures of soft body armor composed of multi-layer Kevlar KM-2 fabrics are generated for numerical simulation. The modified digital element approach (DEA) is applied to determine the ballistic limit of textile fabrics against fragment simulating projectiles (FSP). Different from other numerical models, the DEA takes a considerable amount of fiber-level detail into consideration and models the fabric at filament-level. In this approach, fabric is an assembly of yarns weaved and relaxed into pre-arranged pattern; yarn is simulated as a bundle of digital fibers. When the number of digital fibers per yarn reaches the number of actual fibers per yarn, fiber-level simulation is achieved.

The DEA model successfully simulates real scale multi-layer fabric impacted by spherical projectile and accurately predicted fabric displacement and failure mechanism. It was assumed that the digital fiber is fully flexible and its bending rigidity is negligible. Shear force was thus neglected. However, for projectiles with sharp edge(s), such as FSP, due to resultant shear force, fabric failure starts where it interacts with projectile edge. As a result, the numerical results derived from the previous DEA overestimated the impact strength of fabrics against projectiles with sharp edges. Therefore, shear force and fiber bending rigidity must be considered.

In the modified DEA approach, numerical tests are employed to determine the effective bending rigidity of digital fiber. A combined tension-shear failure model is then incorporated into the DEA in order to calculate the shear force applied to fibers. 3-D microscope is applied to measure the radius of FSP along the edge. The surface of the FSP is meshed into triangle

elements. A unique algorithm is developed and employed to search contacts between textile fabric and projectile of arbitrary shape.

In this research, first, an overview of ballistic impact analysis is discussed; the previous DEA model used in simulating ballistic impact and penetration process is presented. Second, the modified DEA approach used in simulating arbitrary shape projectile perforation process is established and verified. The method of searching and calculating contacts between textile fabric and solid body projectile is explained. The convergence and accuracy of digital element mesh are investigated statistically using tension-shear failure model. Third, fabric shear force and fiber bending rigidity is investigated using tension-shear failure model. The effective digital fiber area moment of inertia is numerically determined. Fourth, standard ballistic tests of real scale multi-layer Kevlar KM2 fabrics are simulated using FSP. Numerical results are compared to high-resolution experimental test data. The modified DEA is validated.

Ballistic strength of multi-layer fabrics against fragment simulating projectiles

by

Ying Ma

B.S., Sichuan University, China, 2008

A DISSERTATION

submitted in partial fulfillment of the requirements for the degree

DOCTOR OF PHILOSOPHY

Department of Mechanical and Nuclear Engineering
College of Engineering

KANSAS STATE UNIVERSITY
Manhattan, Kansas

2017

Approved by:

Major Professor
Youqi Wang

Copyright

© Ying Ma 2017.

Abstract

Ballistic performance of textile fabric is affected by numerous elements, such as fabric architecture, material property, and projectile characteristics. Near fiber-level micro-structures of soft body armor composed of multi-layer Kevlar KM-2 fabrics are generated for numerical simulation. The modified digital element approach (DEA) is applied to determine the ballistic limit of textile fabrics against fragment simulating projectiles (FSP). Different from other numerical models, the DEA takes a considerable amount of fiber-level detail into consideration and models the fabric at filament-level. In this approach, fabric is an assembly of yarns weaved and relaxed into pre-arranged pattern; yarn is simulated as a bundle of digital fibers. When the number of digital fibers per yarn reaches the number of actual fibers per yarn, fiber-level simulation is achieved.

The DEA model successfully simulates real scale multi-layer fabric impacted by spherical projectile and accurately predicted fabric displacement and failure mechanism. It was assumed that the digital fiber is fully flexible and its bending rigidity is negligible. Shear force was thus neglected. However, for projectiles with sharp edge(s), such as FSP, due to resultant shear force, fabric failure starts where it interacts with projectile edge. As a result, the numerical results derived from the previous DEA overestimated the impact strength of fabrics against projectiles with sharp edges. Therefore, shear force and fiber bending rigidity must be considered.

In the modified DEA approach, numerical tests are employed to determine the effective bending rigidity of digital fiber. A combined tension-shear failure model is then incorporated into the DEA in order to calculate the shear force applied to fibers. 3-D microscope is applied to measure the radius of FSP along the edge. The surface of the FSP is meshed into triangle

elements. A unique algorithm is developed and employed to search contacts between textile fabric and projectile of arbitrary shape.

In this research, first, an overview of ballistic impact analysis is discussed, the previous DEA model used in simulating ballistic impact and penetration process is presented. Second, the modified DEA approach used in simulating arbitrary shape projectile perforation process is established and verified. The method of searching and calculating contacts between textile fabric and solid body projectile is explained. The convergence and accuracy of digital element mesh are investigated statistically using tension-shear failure model. Third, fabric shear force and fiber bending rigidity is investigated using tension-shear failure model. The effective digital fiber area moment of inertia is numerically determined. Fourth, standard ballistic tests of real scale multi-layer Kevlar KM2 fabrics are simulated using FSP. Numerical results are compared to high-resolution experimental test data. The modified DEA is validated.

Table of Contents

List of Figures	xii
List of Tables	xv
Acknowledgements	xvi
Dedication	xvii
Chapter 1 - Introduction	1
Chapter 2 - Overview of ballistic impact analysis	7
2.1 Projectile geometry	7
2.2 Ballistic fibers	9
2.2.1 Background	9
2.2.2 Types of fibers	11
2.2.3 Properties of Kevlar KM2	13
2.2.3.1 Fiber strength	13
2.2.3.2 Constitutional relationship of a single fiber	16
2.2.3.3 Tribological properties of 2D-woven Kevlar KM2	20
2.3 Ballistic impact strength of fabrics	21
2.3.1 Homogenous model	22
2.3.1.1 Membrane model	24
2.3.2 Yarn level model	26
2.3.2.1 Roylance's model	26
2.3.2.2 Finite element model	28
2.3.3 Filament level model	31
2.3.3.1 Digital element model	32
2.3.3.2 Textile fabric impact of rigid body projectile	33
2.3.3.3 Convergence	34
2.3.3.4 Elasto-plastic analysis	35
2.3.3.5 Deterministic and statistical analysis	36
2.3.3.6 Conclusions	37
2.3.4 Other models	38
2.3.4.1 Hybrid	39

2.4	Remarks	41
Chapter 3 - Validation of explicit DEA in determining micro-geometry of 3-D woven fabrics		
	44	
3.1	Introduction.....	44
3.2	Modified fiber-to-fiber contact	46
3.3	Comparison between numerical and experimental results.....	48
3.3.1	Experimental observation	48
3.3.2	Fibers.....	50
3.3.3	Fabric weaving patterns and micro-geometries	51
3.3.4	Comparison of micro-geometries	53
3.3.4.1	Surface appearances.....	53
3.3.4.2	Interior yarn structure	54
3.3.5	Comparison between fabric thickness	55
3.3.6	Fabric thickness discrepancy analysis	57
3.4	Conclusion	57
Chapter 4 - Combined DEA-FEM model		
	59	
4.1	Previous version of DEA	59
4.2	Ballistic impact to fabric using rigid body projectile of arbitrary shape	60
4.2.1	Generate projectile with arbitrary shape	60
4.2.1.1	Element type	60
4.2.1.2	Meshed method.....	61
4.2.1.3	Generate projectile surface	63
4.2.2	Contact search.....	63
4.2.2.1	Node to surface contact.....	66
4.2.2.2	Node-to-line contact.....	67
4.2.2.3	Node to node contact	69
4.2.3	Contact calculation.....	70
4.2.3.1	Tension induced nodal force.....	70
4.2.3.2	Contact induced nodal force	71
	Elastic.....	71
	Elasto-Plastic.....	72

4.2.3.3	Friction force.....	73
4.2.4	Failure algorithm.....	75
4.2.5	The explicit algorithm.....	76
4.3	Ballistic impact to fabric using deformable projectile of arbitrary shape.....	77
4.3.1	Mass lumping.....	77
4.4	Validations	79
4.4.1	Material properties and projectile geometry	80
4.4.2	Ballistic impact simulation using rigid body projectile	81
4.4.2.1	Mesh convergence check	81
4.4.3	Ballistic impact simulation using deformable projectile	86
4.4.3.1	High modulus projectile simulation results	87
4.4.3.2	Low modulus projectile simulation results	89
4.5	Conclusion	91
Chapter 5 -	Modified DEA	93
5.1	Previous version of the DEA	93
5.2	Modified DEA Formulation.....	93
5.2.1	Shear force and bending rigidity relations	93
5.2.2	Fiber strength and failure criterion	94
5.2.3	Effective bending rigidity of the digital fiber	95
5.3	Estimate effective moment of inertia.....	98
5.4	Conclusion	101
Chapter 6 -	Numerical simulation.....	103
6.1	Convergence analysis.....	103
6.1.1	Single fiber.....	103
6.1.2	Conclusion	109
6.2	Ballistic strength of multi-layer fabrics against FSP	109
6.2.1	Edge radius measurement	109
6.2.2	Numerical results	111
6.2.2.1	Comparison between experimental and numerical set-up	111
6.2.2.2	Simulation results.....	112
6.3	Conclusion	114

References	117
------------------	-----

List of Figures

Figure 1-1 Basic Concepts of DEA and Fabric Simulated under Ballistic Impact.....	3
Figure 2-1 Four Common Types of Bullets.....	8
Figure 2-2 Shot Patterns [6].....	15
Figure 2-3 Yarn Pull out Pattern and Shooting Results [6]	15
Figure 2-4 Cartesian Coordinates of Single Fiber Model [8]	17
Figure 2-5 Stress Strain Relationship of Longitudinal Tensile Tests [8].....	18
Figure 2-6 Stress Strain Relationship of Transverse Compressive Test without Tensile Loading [9].....	19
Figure 2-7 Stress Strain Relationship of Transverse Compressive Tests with Tensile Loading [9]	20
Figure 2-8 Fabric Structure	22
Figure 2-9 Mathematical Model of Impacted Textile Fabric [18].....	23
Figure 2-10 Multi-layer Model of Impacted Textile Fabric [19].....	23
Figure 2-11 Multi-layer Model: [19]	24
Figure 2-12 Membrane Model [20]	25
Figure 2-13 Roylance's Model [26].....	27
Figure 2-14 Improved Roylance's Model [31]	28
Figure 2-15 Yarn Level FE mesh Model [34]	29
Figure 2-16 Talebi's Model [37].....	30
Figure 2-17 Luan Kun's Model [39].....	31
Figure 2-18 Digital Element Approach.....	32
Figure 2-19 Projectile Displacement versus Time after Striking [1].....	34
Figure 2-20 Projectile Energy Loss versus Time after Striking [1].....	34
Figure 2-21 Comparison of Fabric Deflection in Impact Area (Elastic) [1].....	35
Figure 2-22 Comparison of Fabric Deflection in Impact Area (Plastic) [43].....	35
Figure 2-23 Zohdi and Powell's Model [45]	38
Figure 2-24 Various Cross-Sectional Shape of Discretization Patterns [46].....	39
Figure 2-25 Hybrid Model [47] (The yarns in red are made of 19 fibers per yarn. The yarns in green have 4 fibers per yarn.).....	41

Figure 3-1 Modification of Contact Elements	47
Figure 3-2 Modification of Diameter.....	48
Figure 3-3 Comparison of Surface Appearances	54
Figure 3-4 Comparison of Interior Microgeometry: Specimen 2	55
Figure 3-5 Comparison of Interior Microgeometry: Specimen 5	55
Figure 4-1 8-Node Element	61
Figure 4-2 ANSYS Meshed Solid Body	62
Figure 4-3 Solid Mesh FSP.....	63
Figure 4-4 Contact Search	65
Figure 4-5 Node to Surface Contact	67
Figure 4-6 Node to Line Contact	68
Figure 4-7 Contact between Node and the Intersection Line	68
Figure 4-8 Tension Induced Force	70
Figure 4-9 Elastic Contact Induced Force	71
Figure 4-10 Transverse Nominal Stress and Strain Curve of Kevlar KM2 Fibers [43]	73
Figure 4-11 Friction Force	75
Figure 4-12 Projectile Force Comparison for Spherical Projectile.....	83
Figure 4-13 Projectile Force Comparison for RCC Projectile.....	85
Figure 4-14 Spherical Projectile Comparison.....	88
Figure 4-15 RCC Projectile Comparison.....	88
Figure 4-16 Spherical Projectile with Different Modulus Comparison.....	89
Figure 4-17 RCC Projectile with Different Modulus Comparison.....	90
Figure 4-18 FSP Projectile with Different Modulus Comparison	90
Figure 5-1 Shear Force Calculation	94
Figure 5-2 Comparison between 19-d Fibers and Actual Fibers per Yarn	96
Figure 5-3 Digital Fiber Area Moment of Inertia	97
Figure 5-4 Effective Moment of Inertia and Friction Coefficient Relation.....	98
Figure 5-5 Single Yarn Model	98
Figure 5-6 V_{50} of 4- to 196-digital Fibers per Yarn.....	101
Figure 6-1 Fiber Stress of Element Length/ Fiber Diameter=0.5	105
Figure 6-2 Fiber Stress of Element Length/ Fiber Diameter=0.125	106

Figure 6-3 Element Stress Comparison between Ratio 0.5 and Ratio 0.125 Fiber	108
Figure 6-4 Projectile Force Comparison between Ratio 0.5 and Ratio 0.125 Fiber	108
Figure 6-5 FSP Projectile Edges	110
Figure 6-6 3D View and Radius Profile of FSP Edges.....	110
Figure 6-7 Comparison between Experimental and Numerical Set-up	112
Figure 6-8 Fabric V_{50} Impacted by FSP	113

List of Tables

Table 3-1 Given Fiber Properties.....	50
Table 3-2 Measured Fiber Properties.....	50
Table 3-3 Fiber Properties	51
Table 3-4 Measured Fiber Properties.....	51
Table 3-5 Weaving Pattern and Microgeometry of Nicalon CG Specimens.....	52
Table 3-6 Weaving Patterns and Microgeometries of S-Glass Fiber Specimens	53
Table 3-7 Comparison of Thicknesses.....	56
Table 4-1 Material Properties of Kevlar KM2.....	81
Table 4-2 Projectile Geometry	81
Table 4-3 Simulation Results for FE Spherical Projectiles	82
Table 4-4 Simulation Results for FE Cylindrical Projectiles.....	84
Table 4-5 Projectile Modulus.....	87
Table 5-1 Single Yarn Cross-section Shape	99
Table 5-2 V_{50} of a Single Yarn Impacted by Cylindrical Projectile using I^∞ and I_0	99
Table 5-3 V_{50} of 64 Digital Fiber per Yarn Model using I_0	100
Table 6-1 Fabric V_{50} of Impacted by FSP	113

Acknowledgements

I would like to express my sincere gratitude to my major professor and academic advisor Dr. Youqi Wang for her intellectual guidance throughout the pursuing of my Ph.D. research. I am also thankful for her inspiring discussions and constructive criticism.

I would also like to thank my committee members Dr. X.J. Xin, Dr. Kevin B Lease, Dr. Daniel Andresen, and last but not the least Dr. Chian-Fong Yen for the insightful discussions we had on my research topic.

This research work is financially supported by the U.S. Army Research Laboratory (ARL), PEO-Soldier, and Materials Research & Design (MR&D), Inc. I would like to express my deepest appreciation and special thanks to Dr. Chian-Fong Yen from ARL, James Q Zheng from PEO-Soldier, and Mr. Brian J. Sullivan from MR&D for their most appreciated help, cooperation and guidance in completing projects.

It was a great pleasure for me to work in the composite group with these amazing colleagues: Dr. Yuyang Miao, Dr. Lejian Huang, Dr. Xiaoyan Yang, Mario M. Dippolito, Habib Ahmadi, and Lun Li for the stimulating discussions and the time we have worked together.

Finally, I would like to show immense appreciation to my families and friends for their support and encouragement in completion of this degree.

Dedication

To my beloved mother and father.

Chapter 1 - Introduction

The strength of textile fabrics under projectile impact is of high importance to soldier protection applications. Researches on ballistic impact started around 1850. Before 1900, silk was used as the major material for bulletproof vest. To absorb impact energy, the silk strength was enhanced by putting 18 to 30 layers of silk together. During the World War I, British Army Design Committee made the first official attempt to research body armor for military use. Possible materials for body armor were steel, silicon, and ceramic. Due to the excessive weight and stiffness, early types of ballistic material were heavy and mobility restricting, therefore failed to have practical use.

In 1973, an innovative aramid fiber Kevlar was introduced by DuPont, followed by the development of ballistic fibers, such as Dyneema, Spectra, Twaron, and Zylon. Aramid fibers are noted for highly oriented, long-chain molecules along fiber axis for strong chemical bonds. Those long chemical chains serve to effectively transfer load, force, and stress generated by impact, resulting in a high strength material. Because of the extremely low weight-to-strength ratio, materials like Kevlar are ideal for military use.

Bullet resistant body armor is designed to protect soldiers against projectile penetration and blunt trauma. Textile armor is evaluated for both penetration resistances by bullets and for impact energy transmitted to the wearer. There are two major types of armor panel: woven and non-woven. Spectra fibers are an assembly of filaments, by laying Spectra fibers parallel to each other and coating them together with resin, a sheet of Spectra cloth is made. Unlike Spectra, Kevlar panel cloth is made of yarns woven in plain or tabby weave, the structure of which makes it a popular target for numerical simulation.

Early approaches model fabrics as isotropic and homogeneous plate. Based on ballistic experiments and experiences, numerical model assumes when bullet hits the textile fabric, the fabric deforms into the shape of a conical shell. The mechanical behavior of textile fabrics is modeled as an anisotropic continuum. Parameters related to fabric and projectile upon impact was mainly determined by projectile shape, impact velocity and force, speed of the energy dissipation inside the fabric, fabric material properties, and fabric dimension calculated via mathematical formulas. In this approach, Textile fabrics are considered unidirectional composite layers. The microstructural behavior of fabrics is neglected for simplification. A continuum damage mechanics (CDM) model was served as impact failure algorithm.

As the development of computer power, yarn level approach became popular in 1990s. Explicit finite element commercial simulation tools, such as LS-DYNA, ABAQUS, and AUTODYN are used intensively in failure modeling for searching impact mechanism. A damage initiation criterion for material model was implemented in the software as subroutine, which embraces fiber failure, matrix damage, and delamination under tensile, compressive, shear, and crush loadings. Although, the introduction of fabric level and yarn level constitutive models have provided insight to the mechanics response of textile fabrics under ballistic impact, fiber level details of fabric microstructure are overlooked.

A near fiber-level digital element approach (DEA) for simulating impact and penetration of textiles is established by Wang and Miao [1] in 2010. This approach is based on explicit digital element method (DEM) which has been developed for simulating fabric micro-geometry. Numerical tool Dynamic Fabric Mechanics Analyzer (DFMA) was introduced by Huang and Wang [2] in 2013. DFMA is designed to model the dynamic relaxation process of textile fabric and simulate ballistic impact and penetration process on personal computer (PC) with computer

friendly resource. During the simulation, each yarn is discretized into several equal length digital fibers. Digital fibers are modeled as digital chain. Digital chain, imitating the physical behavior of an actual fiber, embodied the sub-yarn scale properties of fabrics. Therefore, fiber strength, fiber-to-fiber contact and friction can be modeled. Figure 1-1 shows three key elements of DEA and the relaxation process of a unit cell, and a fabric simulated under ballistic impact.

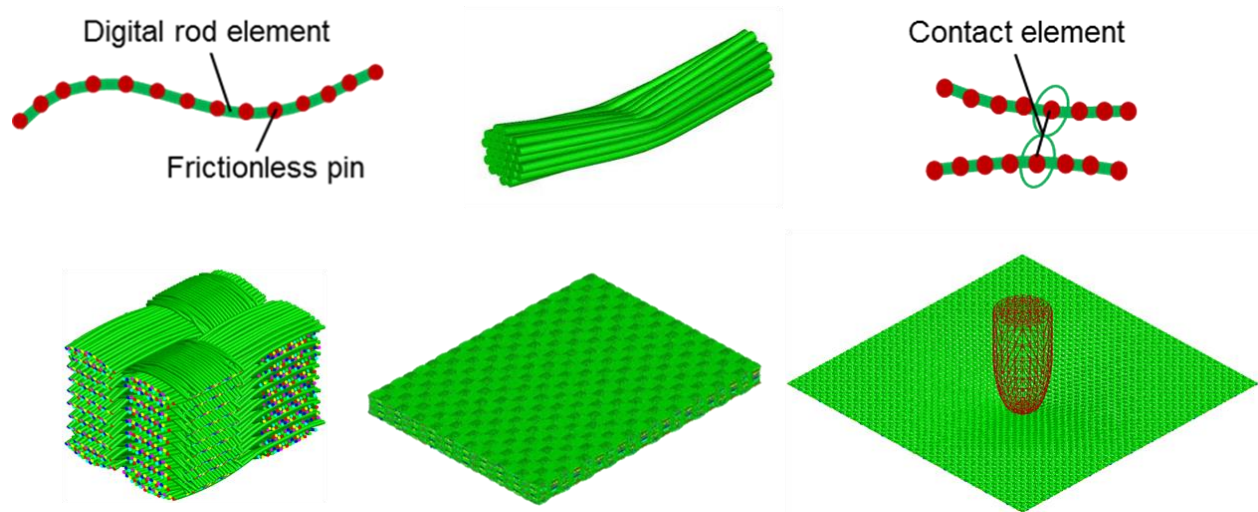


Figure 1-1 Basic Concepts of DEA and Fabric Simulated under Ballistic Impact

The DEA model successfully simulates real scale multi-layer fabric impacted by spherical projectile and accurately predicted fabric displacement and failure mechanism. Well-known experimentally and numerically, fabric failure under spherical projectile impact is largely due to tension applied to principle yarns. The previous version of DEA assumed that the digital fiber is fully flexible and its bending rigidity is negligible. Shear force was thus neglected. However, for projectiles with sharp edge(s), due to high shear force, fabric failure first starts where it interacts with projectile edge, which is not captured by the previous DEA model. As a result, the numerical results derived from the previous version overestimated the impact strength

of fabric against projectiles with sharp edges. Shear force is determined by the fiber bending rigidity. In this research, a modified version of the DEA is developed. The shear force and fiber bending rigidity is incorporated into the numerical model. Because the size of the digital fiber is much larger than the actual fiber, the mass of a digital fiber represents the mass of multiple actual fibers. If the digital fiber cross-section area is much larger than that of an actual fiber, the digital fiber bending rigidity is determined by 1) the number of actual fibers it represents and 2) friction between actual fibers. As such, numerical tests are employed to determine the effective bending rigidity of digital fibers.

In this research, a modified DEA approach is introduced for simulating ballistic penetration and impact using projectiles of arbitrary shape. A PC based numerical tool is presented for simulating impact of elastic deformable projectiles of arbitrary shape. A cluster based multi-thread parallel computing numerical tool is developed for simulating ballistic impact of real size fabric under projectiles of arbitrary shape. The DEA model is modified in following three aspects: (1) Take fiber-bending rigidity into consideration. (2) Combine tension and shear failure. (3) Enable simulating projectile of arbitrary shape. The effective digital fiber moment of inertia is numerically determined. A 3-D microscope is applied to measure the radius of FSP along the edge. The surface of the FSP is meshed into triangle elements. Contact forces applied to both FSP and fabric are calculated at each simulation step. The FSP is considered as a rigid body and its motion is determined by the resultant contact force. Fabric deformation and failure is calculated by means of the modified DEA. Ballistic strength of Kevlar KM2 fabric under FSP impact is evaluated. Numerical results are compared to high resolution experimental test data.

Research work in this dissertation presents:

1. Validation of explicit digital element dynamic relaxation approach in determining micro-geometry of 3-D woven fabrics

The DEA has been employed to determine the microgeometry of textile composite fabric preforms. For each fabric specimen, yarn denier number was measured using analytical scale. The external dimension, surface patterns and interior micro-geometries of ten 3-D fabrics of ten different weaving patterns are investigated and compared to DFMA simulation results. Accuracy of the DEA is discussed.

2. The combination of the DEA and FEM model

The DEA is combined with FEM for simulating textile ballistic perforation process against deformable projectile of arbitrary shape. First, the projectile surface is meshed into triangle elements. Second, the contact search method between fibrous fabric and solid body projectile is established. Third, the contact force applied to projectile is calculated and explained. Forth, the combined tension-shear failure algorithm is explained. Fifth, the explicit combined DEA and FEM algorithm is established. Simulation results from the combined DEA and FEM model is compared to the DEA model using spherical and cylindrical projectile. The combination of the DEA and FEM model is valid.

3. The modified DEA model

The previous DEA overestimate the impact strength of fabric against projectiles with sharp edges due to the neglecting of shear force. Shear force is determined by fiber bending rigidity. In this research work, a modified DEA approach incorporating fiber-bending rigidity is developed. The relationship between fiber bending rigidity and fiber area moment of inertia is explained. The effective digital fiber area moment of inertia is numerically determined.

4. Ballistic strength of textile fabrics against FSP

The modified DEA is developed for accurate modeling of ballistic impact process against FSP. First, the convergence of digital element mesh is analyzed on a single fiber under sharp edge RCC impact. Second, standard ballistic tests against FSP impact are simulated. The fabric size is 12'' by 12'', the total layer number ranges from 1 layer to 28 layers. The simulation results are compared to high-resolution experimental data. The modified DEA approach is validated.

Chapter 2 - Overview of ballistic impact analysis

In the history of body armor, various materials were used to protect human from injury in combats. Metal and ceramic shield served as early forms of body armor. During World War II, a flak jacket made of nylon was used as bulletproof vest. It is the first soft body armor attempted by military. In search of a lightweight and high strength material, simulation of ballistic impact and penetration is of high importance in military.

Fabric penetration resistance is determined by fiber physical properties, such as strength, modulus, density, thermal properties, and fabric structural geometry. In late 1960s, Du Pont invented the first bullet resistant fiber Kevlar, a synthetic fiber of high tensile strength used especially as a reinforcing agent in the manufacture of protective gear such as helmets and vests. Because of its high tensile strength-to-weight ratio, Kevlar remained popular for military use.

Since the 1960s, numerous experiments have been conducted to study the material properties of Kevlar. Numerical simulations provide insights for the design and development of textile body armor. An introduction of four common types of projectiles is given in the following section, followed by impact mechanics analysis of armor materials.

2.1 Projectile geometry

Bullet shape is an important factor in ballistic penetration and impact simulation. Early simulation methods were generally initiated using cylinder shape bullet. Four types of projectiles are frequently used in the tests: Sphere, Right Circular Cylinder (RCC), Fragment Simulating Projectile (FSP), and real bullets such as 9 mm caliber, the pictures of which are shown in Figure 2-1.



Figure 2-1 Four Common Types of Bullets

Sphere, RCC, and FSP bullets are made of one material while 9 mm caliber has a copper jacket and lead inside. Sphere, RCC, and FSP projectiles are primarily used in ballistic tests. RCC gained popularity in ballistic simulation in 1970s, the shape of which was idealized as rectangular viewed from the side. In an analytical model, the contact area between projectile and fabric can be calculated as the area of the end disk.

In the 2000s, bullet nose shape was taken into consideration by adding a nose shape factor into the empirical formulae. However, because empirical formulae are often formulated by curve-fitting test data, empirical formulae method is only applicable strictly within the limits of the test from which the data were acquired. In recent years, as the power of computer rises up, commercial FE code helped researchers gained more understanding of the impact mechanism. Sphere, FSP, and 9 mm caliber projectiles are often seen in the numerical simulations.

2.2 Ballistic fibers

Aramid fibers are a class of strong and heat-resistant synthetic fibers used in ballistic-rated body armor fabric. These fibers have extremely long chains oriental along the fiber axis, with a molecular mass usually between 2 and 6 million u. By strengthening intermolecular interactions, the length of the chain facilitates the transfer of load to polymer backbone, resulting in high impact strength. A brief review of ballistic fiber background is given in section 2.2.1, followed by the introduction of varies aramid fibers. The impact mechanics of Kevlar KM2 is discussed in detail.

2.2.1 Background

The first well-known bulletproof fabric used for making protection vest is made of silk. In 1881, physician George E. Goodfellow accidentally discovered that a silk handkerchief placed in the breast pocket of dealer Luke Short stopped the bullet from penetrating when was shot by a handgun. By putting 18 to 30 layers of silk fabric together, a piece of bulletproof fabric was made. At the end of 19th century, bulletproof vests were capable of stopping slow rounds from black powder handguns. However, the cost of the garment was out of reach for majorities.

During the World War I and World War II, the need for affordable and effective body armor became more and more urgent. In 1915, British Army Design Committee made the first

official attempts at commissioning body armor mainly used for bomber pilots, who were severely under-protection in the battle. Potential ballistic materials were steel, nickel, and silicon armor plate, interwoven layers of silk and cotton stiffened with resin. Those proposed materials largely hampered mobility of the wearers resulting in no practical use in the battle.

In 1943, a lightweight flak jacket made of nylon was produced by British company Wilkinson Sword. Unlike previously invented body armor, flak jacket was aimed to stop low velocity fragmentation. The development of aramid fibers went back and forth between lightweight flexible low ballistic strength textile and heavy and stiff high ballistic strength plate. After World War II, fiber-reinforced plastic and aluminum segments were woven into nylon vest to enhance mobility. However, flak jackets were unable to effectively stop bullets and fragments, resulting in limited use. On the other hand, in search of armor materials, which could effectively stop bullets and fragmentations, ceramic, boron carbide, silicon carbide, and aluminum oxide plate were all used for making bulletproof vest.

In 1973, DuPont introduced the epoch-making aramid fiber Kevlar, which is five times as strong as steel on an equal weight bases. It was the first organic fiber developed strong enough to be used in advanced composites and is composed entirely of aromatic polyamides. Unlike nylon and hard plate, the high-performance organic fibers are a combination of high strength, lightweight, durability, and protection. Because of the extraordinary material properties, organic fibers gained popularity in various of commercial application, such as military, aerospace, and automobile. To make Kevlar cloth, Kevlar yarns are woven in the simplest pattern, plain or tabby weave, which is merely the over and under pattern of threads interlace alternatively.

After 1985, soft body armor made of Kevlar was put to intensive use by police officers, validating the success and efficiency of Kevlar as ballistic material. However, experiments found

that, body armor made of Kevlar are capable of stopping handguns, not rifle and large fragments. The energy dissipation during the impact could cause life-threatening blunt trauma injuries in vital areas. In order to solve this problem, recent format of body armor highlights the trade-offs between force protection and mobility. Hard and small protective ceramic plates were used as inserts to protect the vital organs from higher-level threats.

In the following section, three types of organic fibers will be introduced.

2.2.2 Types of fibers

Three types of fibers will be introduced in this paragraph.

Kevlar

Kevlar is applicable to a variety of areas due to its excellent impact resistance. The most popular types of Kevlar are Kevlar 49 (composites grade) and Kevlar 29 (ballistics grade).

Kevlar 49 fabrics are developed specifically for composite reinforcement. By combining with Epoxy, Vinyl Ester or Polyester Resins to create a rigid laminate composite, Kevlar 49 maximized its physical properties. Common applications for Kevlar 49 fabrics include kayaks, canoes, high-speed boats, aircraft fuselage panels, pressure vessels, sporting equipment, and wind turbines.

Unlike Kevlar 49, Kevlar 29 fabrics are made of tough yarns built for ballistic protection. It is soft and often used in dry conditions. Typical applications include protective vests, gloves, as rubber reinforcement in tires and automotive hoses.

Different from the above two types of Kevlar; Kevlar KM2 is an evolution of the original Kevlar fabrics especially designed for military use, such as helmets and bulletproof vests. Numerous experiments and simulations are conducted by researchers to study material properties of Kevlar KM2 and its impact mechanism, such as stress-strain relationship, post-

ballistic impact residual yarn mechanical properties, and creep rupture of long-term failure behavior using both deterministic and statistical analysis.

Dyneema and Spectra

Ultra-High Molecular Weight Polyethylene (UHMWPE), also known as high-modulus polyethylene or high-performance polyethylene, is another synthetic fiber, which has long chemical chain of axis-oriented molecules. UHMWPE was introduced in the late 1970s by Dutch chemical company DSMunder. Dyneema and Spectra are an advanced form of UHMWPE. They are used as multi-filament fiber in yarn, in unidirectional sheets. Unlike Kevlar, Spectra fibers used in bulletproof vests are usually not woven. Instead, the strong polyethylene polymer filaments are spun into fibers and laid parallel to each other. Resin is used to coat the fibers, sealing them together to form a sheet of Spectra cloth.

Dyneema and Spectra are an advance form of Ultra High Molecular Weight Polyethylene. Similar to Kevlar fabrics, they are well known for high strength-to-weight ratio. The existence of extremely long molecular chains helps the transfer of load along axial direction. Different from Dyneema and Spectra, Kevlar derives its strength from strong bonding between relatively short molecules, when formed to fibers. However, the polymer chains of UHMWP material attain a parallel orientation greater than 95%.

Many thousands of individual fiber filaments are aligned in a 90-degree configuration to form laminated ballistic material. Fiber filaments were placed at right angles to one another and then laminated together. Each sheet is able to combine the unique strength of a fiber with the pliant thinness of the matrix design. Because of the lightness and flexibility, the laminated ballistic sheets appear semi-transparent.

M5 and other fibers

Other traditional ballistic materials are Twaron, Zylon, Technora, Vectran and M5. They obtain a material property similar to that of Kevlar. In 2014, researchers began to cast their eyes on graphene as a new material for body armour. Jae-Hwang Lee from University of Massachusetts is among the first researchers to perform ballistic tests to evaluate graphene's mettle. The experiments found that graphene sheets dissipated energy by stretching into cone shape and crack outward radially. According to Lee, though a single layer of graphene cracks under the ballistic impact, it performs twice as well as Kevlar.

2.2.3 Properties of Kevlar KM2

Continuous filament yarns comprised of fibers are widely used in fabrics as flexible protective materials. Kevlar KM2 is a special type of Kevlar designed for military use and a popular subject of ballistic research. Ballistic penetration and impact simulations provide insight into the impact mechanism of aramid materials. In this proposal, all simulations conducted by author used Kevlar KM2 fabric. Therefore, the impact mechanism of Kevlar KM2 is studied and presented below in detail.

2.2.3.1 Fiber strength

Fiber strength of Kevlar is a statistical distribution based on the presence of defects. A Weibull distribution is often used to characterize the strength of Kevlar yarns [3]. Statistical strength distribution can be affected by various factors. It was found that the strength of variation of aramid fibers is massively reduced in twisted yarns. Organic fibers like Kevlar KM2 also show non-linearity and strain rate dependence of tensile properties, and the viscoelasticity of which affects the Weibull strength distribution.

Because of peculiar “skin-core” physical structure of Kevlar KM2 [4], a bimodal Weibull distribution is commonly used for simulation. The bimodal Weibull distribution is given as [5]:

$$F(\sigma) = 1 - \exp\left(-\frac{L}{L_0}\left(\frac{\sigma}{\sigma_{01}}\right)^{m_1} - \frac{L}{L_0}\left(\frac{\sigma}{\sigma_{02}}\right)^{m_2}\right) \quad (2-1)$$

where $F(\sigma)$ is the failure probability, σ is the stress level of interest; σ_{01}, σ_{02} are the scale parameters and m_1, m_2 are the shape parameters. L is the length of yarn and L_0 is gage length at which the experimental data was generated. $\frac{L}{L_0}$ is the length-scale term, which is effected by gage length.

Because of the pre-exist tension in yarns caused by weaving process, the distribution of yarn strength is affected. Therefore, it is imperative to characterize the strength of yarns extracted from woven fabrics than yarns unraveled from a spool. The constitutive tensile response based on bimodal Weibull distribution is

$$\sigma = E \cdot \varepsilon \cdot \exp\left(-\frac{L}{L_0}\left(\frac{E \cdot \varepsilon}{\sigma_{01}}\right)^{m_1} - \frac{L}{L_0}\left(\frac{E \cdot \varepsilon}{\sigma_{02}}\right)^{m_2}\right) \quad (2-2)$$

Where σ and ε are the stress and strain respectively and E is the elastic modulus. $\sigma_{01}, \sigma_{02}, m_2$, and E is the set of Weibull parameters need to be determined by experimental methods. This distribution is mapped onto the model of fabric as a Monte Carlo simulation.

In 2013, Hudspeth et al. [6] investigated the degradation of aramid yarns recovered from soft-armor targets subjected to multiple ballistic impacts using deterministic analysis. Two-grain flat head and 9-mm ball round projectiles were used in the tests. The fabrics were comprised of 34 layers randomly lie in either 0° or 90° alignment with respect to the vertical direction. Shoot patterns are shown in Figure 2-2.



Figure 2-2 Shot Patterns [6]

Three yarns were pulled in a strategic pattern from weft and warp directions to analysis the effect of yarn-shot proximity. The pull out pattern and the shooting results are shown in Figure 2-3.

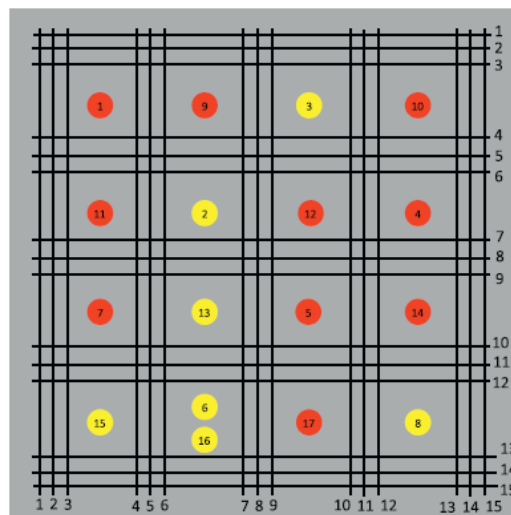


Figure 2-3 Yarn Pull out Pattern and Shooting Results [6]

Upon visual inspection, yellow circles represent locations where no penetration occurred to the last layer, and red circles represent locations where penetration happened to the last layer. Shooting results verified that yarn strength of aramid fibers is statistical distribution.

Mechanical properties of the pull out yarns were evaluated. It was found that tensile strength, failure strain, elastic modulus, and yarn toughness of the pull out yarns were similar to all tested yarns, regardless of yarn location, ply level, and penetrator size. When compared to native as-received spooled yarns, the strength of the pull out yarns was only slightly reduced by weaving, ballistic impact, and extracting. It is safe to conclude that ballistic damage on aramid fabrics is very localized.

2.2.3.2 Constitutional relationship of a single fiber

Based upon previous experimental research, it was found Kevlar KM2 fiber is linear elastic in axial direction and non-linear in transverse direction. However, many models [1][7] still assume a simple linear stress-strain relationship. In 2004 and 2005, Ming Cheng et al. [8][9] investigated the longitudinal and transverse mechanical properties of Kevlar KM2 fibers using deterministic analysis. The assumption was made, fiber failure happens at the link of highest strength. A brief review of their work follows.

The first step to achieve an accurate simulation for ballistic impact is to incorporate correct fabric material properties. A series of micro-measurement test systems are developed for direct mechanical properties measurement of a single fiber. The Cartesian coordinates of single fiber model is shown in Figure 2-4.

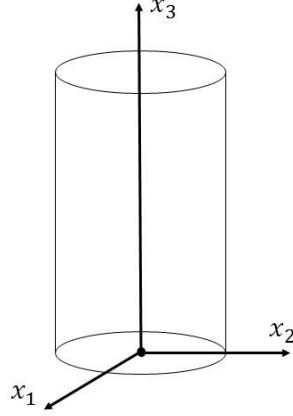


Figure 2-4 Cartesian Coordinates of Single Fiber Model [8]

Direction 1, 2, and 3 of a single fiber is shown in Figure 2-4. Direction 3 is normal to the plane of material isotropy. Assuming a Kevlar KM2 fiber is elastic within infinitesimal strain range; mechanical properties of the material can be described by five independent elastic constants [8]. The constitutional relationship of a single fiber in terms of five independent compliance constants [10] can be written as:

$$\begin{Bmatrix} \varepsilon_{11} \\ \varepsilon_{22} \\ \varepsilon_{33} \\ \varepsilon_{23} \\ \varepsilon_{31} \\ \varepsilon_{12} \end{Bmatrix} = \begin{bmatrix} S_{11} & S_{12} & S_{13} & 0 & 0 & 0 \\ S_{12} & S_{11} & S_{13} & 0 & 0 & 0 \\ S_{13} & S_{13} & S_{33} & 0 & 0 & 0 \\ 0 & 0 & 0 & 0.5S_{44} & 0 & 0 \\ 0 & 0 & 0 & 0 & 0.5S_{44} & 0 \\ 0 & 0 & 0 & 0 & 0 & S_{11} - S_{12} \end{bmatrix} \times \begin{Bmatrix} \sigma_{11} \\ \sigma_{22} \\ \sigma_{33} \\ \sigma_{23} \\ \sigma_{31} \\ \sigma_{12} \end{Bmatrix} \quad (2-3)$$

where S_{11} , S_{12} , S_{13} and S_{44} are:

$$S_{11} = \frac{1}{E_1} \quad (2-4)$$

$$S_{12} = -\frac{\nu_{12}}{E_1} \quad (2-5)$$

$$S_{13} = -\frac{\nu_{13}}{E_1} = -\frac{\nu_{31}}{E_3} \quad (2-6)$$

$$S_{33} = \frac{1}{E_3} \quad (2-7)$$

$$S_{44} = \frac{1}{G_{13}} \quad (2-8)$$

where E_i is the Young's elastic moduli in 1, 2, and 3 direction respectively, G_{13} is shear modulus in $x_1 - x_3$ plane, ν_{ij} is the Poisson ratios. When only normal load is applied in direction i , ν_{ij} is defined as the ratio of negative of the normal strain in direction j versus direction i .

Three types of experiments were conducted by Ming Cheng et al. to calculate the five independent compliance constants. They were longitudinal tensile tests, transverse compressive tests and torsional tests.

Longitudinal tensile tests

Figure 2-5 shows the stress-strain relationship of longitudinal tensile tests under quasi-static and high strain rate loading. The results of five tests are listed for clarity. The tests show Kevlar KM2 fiber is linear elastic until failure, and the Young's modulus of the fiber used was as 84.64GPa.

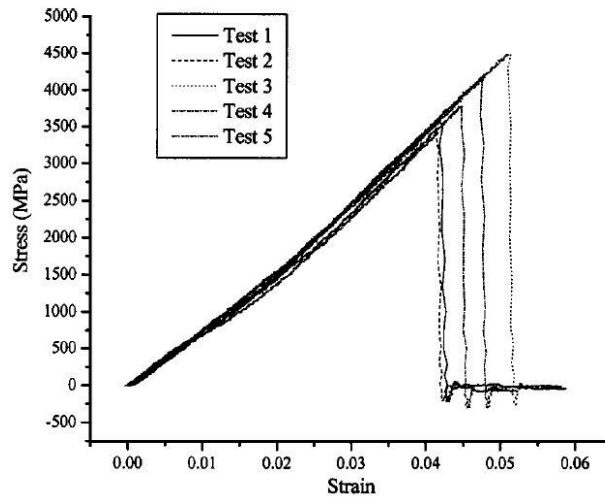


Figure 2-5 Stress Strain Relationship of Longitudinal Tensile Tests [8]

Transverse compressive tests

Transverse compressive tests were conducted under two conditions: without longitudinal tensile loading and with longitudinal tensile loading. In the first test, it was found that a large residual strain was left when the fiber was released from transverse compressive loading. The deformation remained as long as two month after the test. When the fiber was loaded again, the loading curve almost followed the previous path with minor deviation.

Results of test one is shown in Figure 2-6. Although the findings of test one showed significant evidence that the material properties of Kevlar KM2 is not linear in transverse direction, the inability to keep the fiber straight without applying load in longitudinal direction kept the researchers from obtaining accurate results.

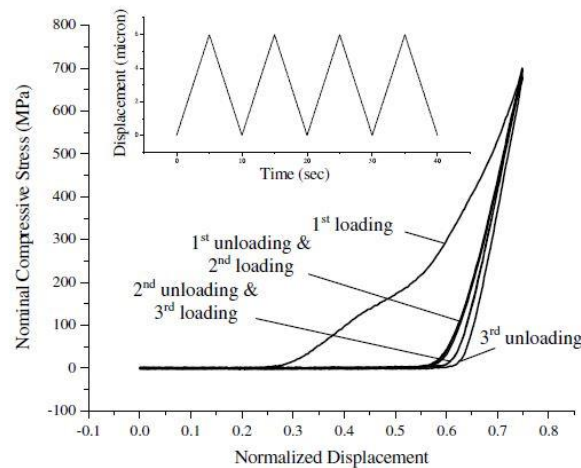


Figure 2-6 Stress Strain Relationship of Transverse Compressive Test without Tensile Loading [9]

Second tests were conducted to exam the stress-strain relationship under six nominal strains of different amplitude. Each strain had 4 loading and unloading cycles, which increased gradually during the test. The results are shown in Figure 2-7.

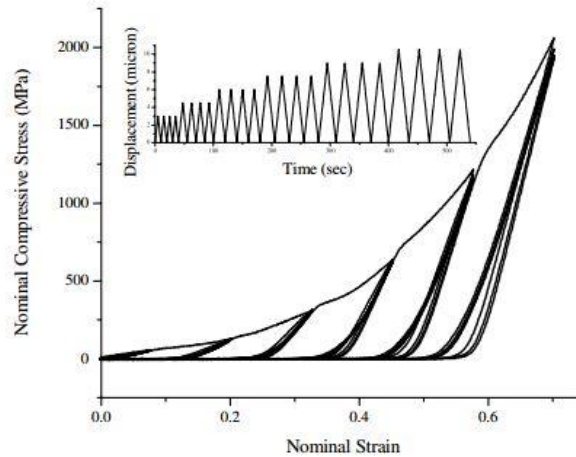


Figure 2-7 Stress Strain Relationship of Transverse Compressive Tests with Tensile Loading [9]

The results of test two generally agreed with the results of test one. Residual strain existed in between loading and unloading curve, resulting in energy absorption during the impact. Based on constitutional relationship of a single fiber described in 2.2.3.2, the transverse Young's modulus of Kevlar KM2 fibers was calculated as 1.34GPa.

2.2.3.3 Tribological properties of 2D-woven Kevlar KM2

In 1998, S. Rebouillat studied the tribological properties of woven para-aramid fabrics and their constituent yarns under different linear densities with different surface treatments, such as polysiloxane oil, hydrophobic paraffin or ester oil lubricant [11]. The experiments were carried out with a classical pin-on-disc tribometer with two different configurations: alternate sliding mode (ASM) and continuous sliding mode (CSM). Results show inter-yarn frictional coefficients of Kevlar 29 yarns range between 0.2 – 0.4.

In 2009, Z. Dong and C.T. Sun [12] investigated single yarn pull-out behavior of five styles of plain weave Kevlar fabrics. The result of a parametric study using finite element model shows that inter-fiber friction for parallel-fiber is around 0.3.

More recently, in 2012, Gaurav Nilakantan et al. evaluate ballistic performance of woven Kevlar KM2 fabrics considering yarn strength, friction, projectile impact location, and boundary condition effects [13]. Weibull strength distributions were mapped onto individual yarns. Similar conclusion was reached that ballistic performance increased when inter-yarn frictional coefficient increased from 0.0 to 0.4. The sliding energy due to frictional pullout of a single yarn from fabric weave dominated energy dissipation.

In 2016, Wang et al. studied the effect of the inter-fiber friction on fiber damage propagation and ballistic limit of 2-D woven fabrics under a fully confined boundary condition. Quoted from previous researches [11,14–16], the inter-fiber friction coefficient of Kevlar fibers is determined to be between 0.2 to 0.35. Wet fabric has a lower friction coefficient than dry fabric, which leads to lower fabric ballistic strength.

2.3 Ballistic impact strength of fabrics

Fabrics used in ballistic impact and penetration analysis are often made of textile material Kevlar due to its lightweight and extremely high tensile strength. However, textile performance is not only determined by fiber physical properties, but also by fabric architecture. Woven fabrics are the most common fabric structures used in ballistic impact analysis. Single layer woven fabric is placed on top of each layer to form multi-layer fabric. Examples of both are shown in Figure 2-8.

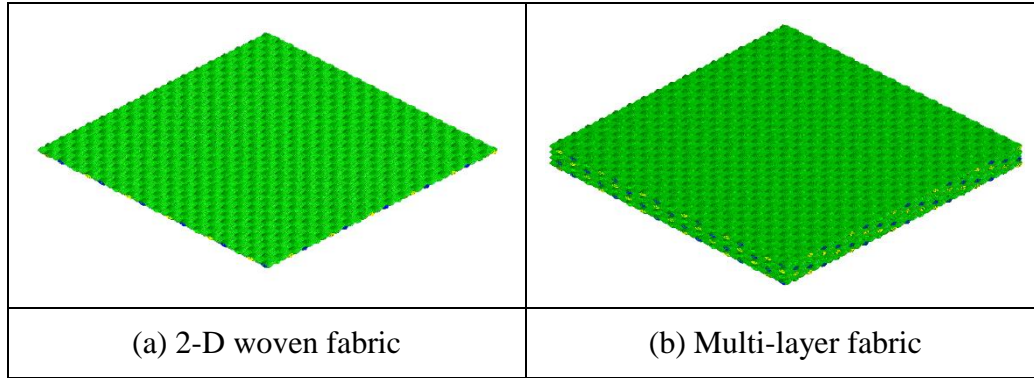


Figure 2-8 Fabric Structure

2.3.1 Homogenous model

Homogenous continuum model models the mechanical behavior of materials as a continuous mass. Assuming that the fibers of fabric completely fill the space they occupied, the microstructural behavior of fabrics is homogenized as an anisotropic continuum. The concept of homogenous fabric is popular among researchers in 1990s. Prior to Vinson and Zukas [17], a majority of ballistic impact of textile research was conducted on one-dimensional yarn bundles, fibers, and filaments.

In 1975, Taylor and Vinson proposed an analytical model, which simulates the transverse impact by treating textile fabric as flexible isotropic and homogeneous plate. The mechanical understanding of the fabric is limited to its density, weight per area, and it can elastically strain. The fabric was assumed to deform into the shape of a straight-sided conical shell through a stepwise procedure in time. The model aimed to determine the structural response of textile fabric under ballistic impact and made feasible to use computer in calculating strains, projectile position, forces, and decelerations as a function of time. The conical shell theory was established by observing the deformed fabric shape under projectile impact using mathematical methods.

Figure 2-9 shows the mathematical model of impacted textile fabric. In the figure U_{tot} is vertical displacement of the projectile, R_1 is radius of the projectile, and R_2 is transverse wave velocity U times time. The value of U changes with time.

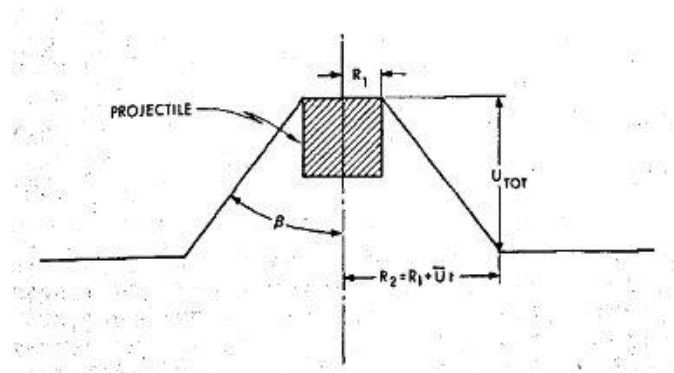


Figure 2-9 Mathematical Model of Impacted Textile Fabric [18]

In 1990, Taylor and Vinson [19] improved and expanded Vinson and Zukas' model by adding a thickness factor to the impact fabric in order to predict the behavior of multiple-layer target based on the behavior of a single-layer target. The concept of the approach is shown in Figure 2-10.

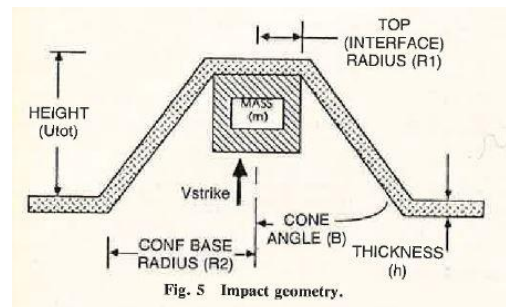


Figure 2-10 Multi-layer Model of Impacted Textile Fabric [19]

The improved multi-layer model was further categorized into two sub-models. One model assumed that every layer was affected as soon as the projectile strikes the first layer, as shown in Figure 2-11 (b). The other model assumed that only the layer in touch with the projectile is affected by the strikes and the layer in touch with the projectile has 100% compressibility, as shown in Figure 2-11 (b). Predicted geometries of the deflected fabric were relatively close to actual values obtained from high-speed videos, but large deformations of the projectiles during impact were not considered and no accurate measurements of striking and residual velocities were calculated.

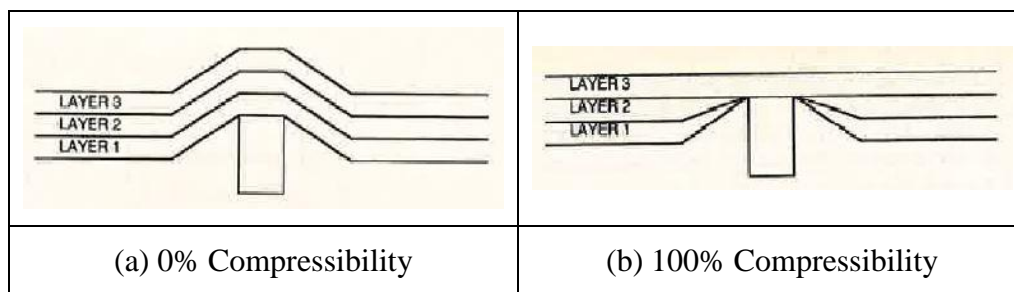


Figure 2-11 Multi-layer Model: [19]

Mathematical approach works with properties of its assumed isotropic fabric, which is immensely different from material properties of individual fibers. The simplification made by homogenous model captured the essence of the impact process, made it possible for early researchers to predict the ballistic impact process without computer aids. However, due to the lack of failure mechanisms such as yarn slippage in the fabric, fabric pullout at attachments and details of loading were not considered, these approaches are inherently limited.

2.3.1.1 Membrane model

Membrane model is an analytical model developed for ballistic impact of fibrous materials. The assumption is made that ballistic materials such as Kevlar, Spectra and Zylon

have the characteristic of membrane properties and fabric deforms into a cone shape during the impact.

In the 2000s, based on the pioneer work of Taylor and Vinson, Phoenix and Porwal [20] developed an analytical model for fibrous material of ballistic fabric. This model treated the fabric as 2D elastic membrane. Partial differential equations of the fabric were formulated to calculate a relative complete solutions of impact related parameters. geometry parameters related to the cone shape, reactive force on the projectile, areal density ratio, momentum exchange, velocity evolution during and after the impact, strain evolution, maximum strain concentration adjacent to the projectile, distance required to stop the projectile, energy absorbed in stopping projectile, residual velocity and V_{50} limit were calculated. An example of the membrane model is shown in Figure 2-12.

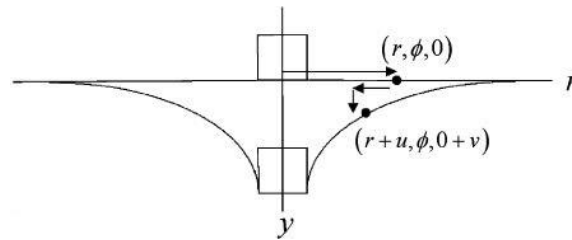


Figure 2-12 Membrane Model [20]

Due to large amount of computational resource and time required for simulating yarn level FE model of ballistic impact, Simons, Erlich, and Shockey [21], Lim, Shim, and Ng [22], and Silva et al. [23] formulated membrane models with shell element seeking computational efficiency, Erlich and Shockey's model implemented the shell elements of LS-DYNA3D FE code and used an orthotropic continuum formulation. Young's modulus in two orthogonal directions along the yarns was calculated. Pitch, thickness, areal density, force, and density were

also used for constructing the constitutive model. The purpose of membrane model is to provide guidance and possibility for full-scale tests of textile fabrics. The ability of membrane model producing valid results for ballistic impact simulation is limited.

Delamination, fabric architectural and material properties of fiber were not taken into consideration. The success of homogenous model in early times was based on the trade of simplicity of the model and relative accurate predictions of overall deformed fabric shape.

2.3.2 Yarn level model

Yarn level model models each yarn as a homogenous continuum. The microstructural behavior of yarn is homogenized as an anisotropic continuum. The assembly of solid yarns in a prearranged pattern forms the fabric. Yarn level models were aimed to capture yarn-to-yarn interaction and shed light on the impact mechanism of the fabric.

2.3.2.1 Roylance's model

In the early 1970s, Roylance, Widge and Tocci [24] proposed a pin-joint model shown in Figure 2-13. Yarns are defined by segments of orthogonal pins connected by nodes at the cross-over points to form a near net shape structure. Each fabric yarn and node was assigned a mass m . This technique used the dynamic stress-strain curve to predict the fiber's response upon impact and took viscoelastic response of fabric material into consideration [25]. Structural response is a function of material properties as well as structural geometry. In 1981, by taking strain intensification over time near the projectile impact point into consideration, Roylance and Wang [26] used the pin-joint model to perform numerical analysis of textile fabric impact. They found that the Kevlar panel, which is still considered the superior ballistic material, exhibited the best combination of penetration resistance and energy absorption rate.

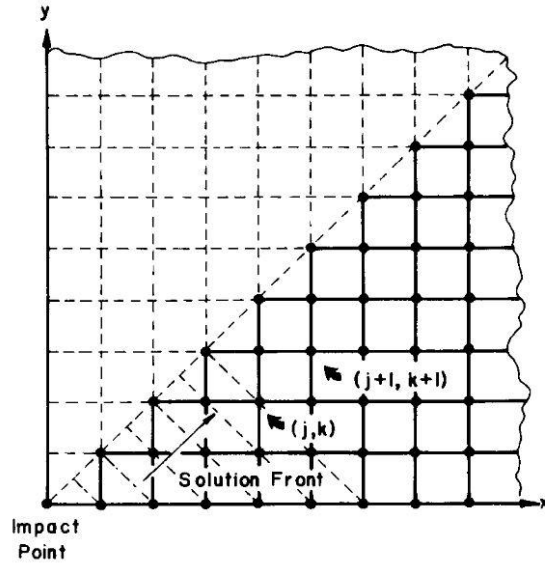


Figure 2-13 Roylance's Model [26]

By studying fabric impact mechanics through numerous of experiments, Cunniff [27] included projectile geometries and edge conditions into the Roylance model. In the late 1980s, Dent [28] and Prevorsek [29] noticed the effect of crimp interchange on woven fabrics. In 1994, Shim [30] and his coworkers incorporated viscoelasticity into formulation of the Roylance's model and identified yarn crimping as an important parameter.

In 1995, Roylance, Chammas, Ting, Chi and Scott [7] attempted to take yarn slippage and friction into consideration when reconstructing the model. In 1998, Ting, Ting J., Cunniff and Roylance [31] established a detailed model. This model models out-of-plane yarn undulations with inter-yarn elastic couplings at crossovers, as well as subdivision of yarn segments between crossovers to increase resolution near impact zone [20].

An illustration of the model representing the warp and fill fibers are shown in Figure 2-14. A transverse spring was inserted between the warp and weft fibers at crossover points to allow detailed analysis of the cooperative nature of wave propagation in fabrics. Spring stiffness was determined by fabric transverse stress-strain relations.

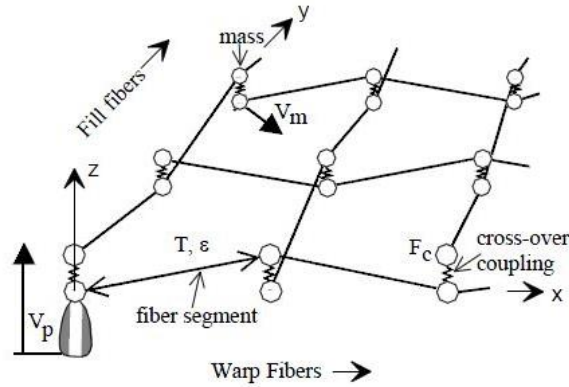


Figure 2-14 Improved Roylance's Model [31]

Though Roylance model was aimed to capture the essential physics of ballistic impact simulation and a considerable amount of detail were incorporated, this approach does not accurately represent the complexity of the fabric topology and micro-geometry of the yarn.

2.3.2.2 Finite element model

In recent years, computers become more and more capable of handling large quantities of calculation. As a result, researchers focused their attention on nonlinear explicit approach and FE algorithm using commercial FE code. AUTODYN, LS-DYNA and ABAQUS are three major FE tools used in textile fabric simulation. The approach relies on the selection of a geometric model for the fabric weave, coupled with constitutive models for the yarn behaviors [32]. Finite element model discretizes yarns into solid elements and takes the yarn-to-yarn and projectile-to-fabric friction into consideration.

In 1997, Shockey et al. [33] used DYNA3D to mesh fabric at yarn-structure hierarchy and modeled bullet penetration using solid body projectile. An 8-node hexahedron element mesh was adopted; a Tied Node with Failure (TNWF) algorithm for shell elements was used in the simulation.

Deformation of fabric structure, such as yarn crimp, friction between warp and weft yarns, and deformation and damage of yarn, are simulated using FE approach. As shown in Figure 2-15, Duan, Keefe, Bogetti, Cheeseman, and Powers [34–36] used LS-DYNA to investigate the influence of projectile-fabric friction and yarn-to-yarn friction. The mechanical behavior of juxtaposition of parallel fibers is implemented in the yarn constitution. Nine orthotropic elastic material data are used for the yarn continuum.

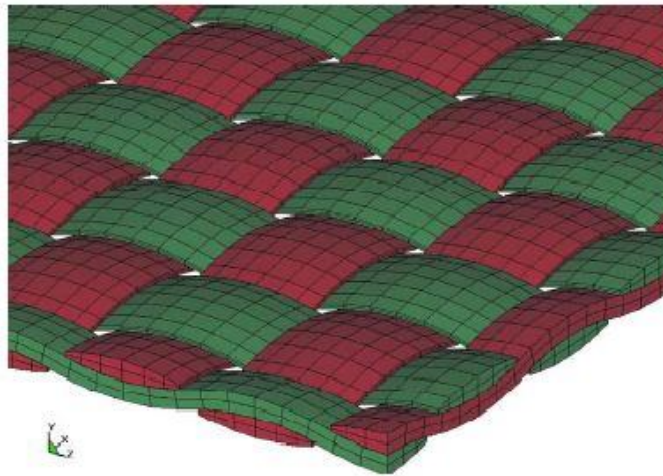


Figure 2-15 Yarn Level FE mesh Model [34]

Talebi, Wong and Hamouda [37] also used LS-DYNA to evaluate the nose angle effect of projectile in ballistic perforation of high strength fabric. The target fabric was meshed with a combination of 6 and 8 node elements at yarn level. Figure 2-16 illustrates the FE model of a projectile with nose angle of 75 °.

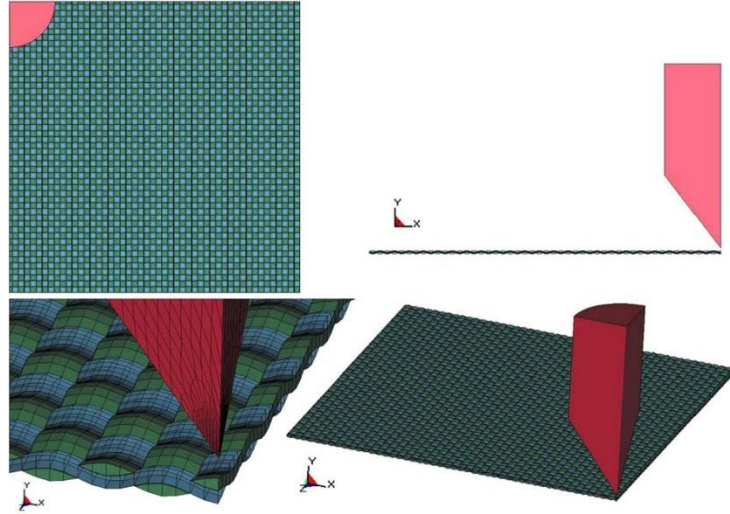


Figure 2-16 Talebi's Model [37]

Yen [38] developed a strain rate dependent lamina model based on continuum damage mechanics and implemented within LS-DYNA for modeling progressive failure behavior of plain weave composite layers. The ply-level material constitutive model was reported to be able to effectively simulate the fiber failure and delamination behavior under high strain-rate and high-pressure ballistic impact conditions.

Luan, Sun, and Gu [39] were among the first researchers to simulate FE 3-D angle-interlock models for ballistic impact strength test. A geometrical model of weft and warp yarns was obtained based on yarns' spatial geometrical relations. Figure 2-17 (a) shows the geometry model and, Figure 2-17 (b) shows the FE model with resin.

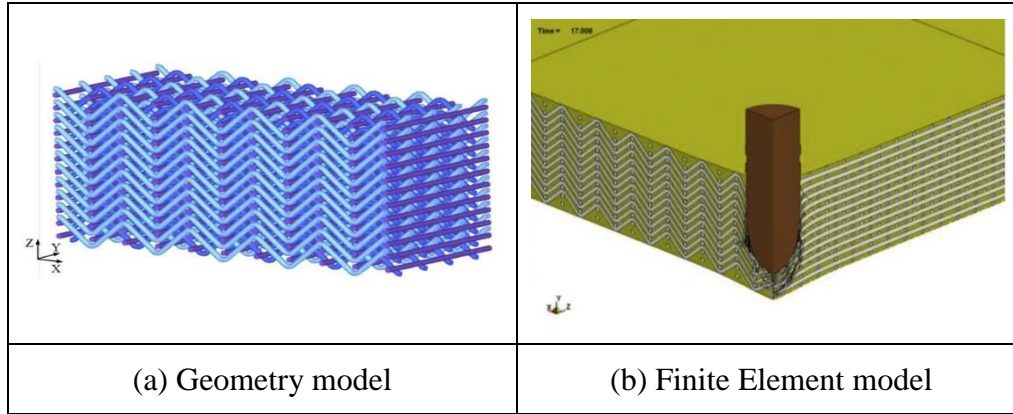


Figure 2-17 Luan Kun's Model [39]

Compared to previous models, Gu's model simulates interaction between the projectile and the fabric target more precisely in fabric target deformation, kinetic energy absorption, and strain wave distribution. However, impact interaction between the projectile and the fabric target at filament structure hierarchy was not modeled, leading to under-estimation of energy absorbed by fabric target.

Most yarn level FE ballistic model consumed excessive computational time and resources. The assumption was made that projectile and fabric target are symmetrical on XY and YZ plane during the impact process. Projectile deformation was not discussed.

2.3.3 Filament level model

The need for excessive computational time and resources on real scale fabric simulation is the bottleneck for current researchers. Most real scale FE yarn level models were formulated under the assumption that both fabric and projectile are symmetrical about x-z and y-z plane during simulation process. A quarter model was used to predict the impact behavior of the full size fabric. However, the search for a better scientific understanding of the mechanical response of ballistic materials has never stopped. Fiber level models have been developed in recent years.

Wang and Sun are the first researchers to study fabric mechanics at filament level. They noted that yarns are composed of multiple fibers [32] which have strongly directional material property [34]. A sub-yarn micro-scale model was developed in explicit digital element algorithm. The development of the digital element approach is given followed by a detailed convergence analysis and conclusion.

2.3.3.1 Digital element model

The concept of the digital element was first established by Wang and Sun [40–42]. In this approach, a fiber is made of digital chains connected by rod elements and frictionless pins. When the length of the rod element approaches zero, digital chains can move freely. Digital fibers are bundled to form a digital yarn; an assembly of yarn in prearranged orders forms the unit-cell. Fabric is created by repeating unit-cells in weft and warp direction.

As shown in Figure 2-18, digital fiber, digital yarn and contact elements are the three key concepts involved in the digital element approach. During the simulation process, one yarn is discretized into several fibers. The contact between digital fibers is calculated through the contact elements. Contact occurs at places where distance between two fibers is smaller than the fiber diameter. The two nodes in contact are defined as a contact pair.

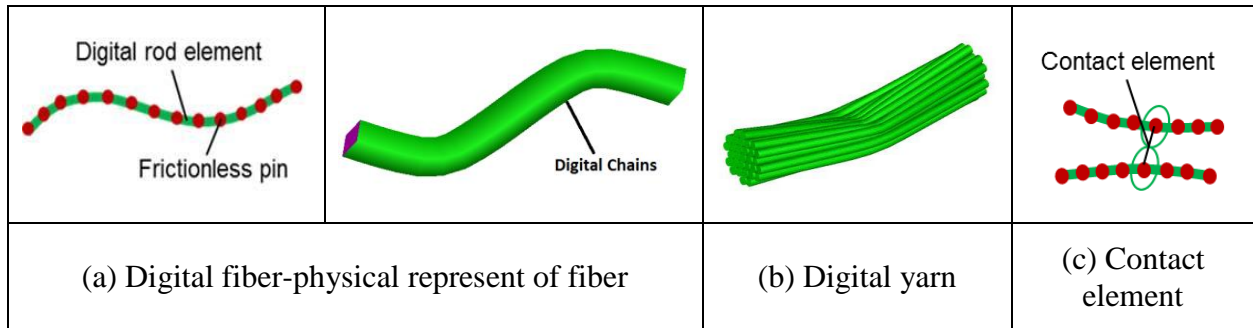


Figure 2-18 Digital Element Approach

The digital element approach was first modeled as a quasi-static structural mechanics problem with boundary conditions. However, because of difficulties in building up the original pattern of the topology and significantly large requirement of computer memory source, a static relaxation model was developed, which reduced computation time by 80%-90%. Recently, in order to further reduce the need for computer resource during calculation, a dynamic relaxation with periodic boundary condition algorithm is established [2].

Different from FE model, the digital element itself does not preserve physical properties; instead, the physical properties are imitated through digital fibers. This approach was attempted to solve the deficiency of flexible-armor numerical models by modeling at near filament level resolution.

2.3.3.2 Textile fabric impact of rigid body projectile

The digital element approach was first introduced in 2010 [1] for simulating impact and penetration of textiles. A set of basic procedures were established for simulation process. Unit-cell is the most basic and least volume consuming repeating structure of fabric. The fabric is an assembly of unit-cells. First, a piece of textile fabric is generated by digital element analyzer DFMA. By yarn discretization and fiber discretization, DFMA relaxes the unit-cell from its initial topology. When the unit-cell reaches its minimum potential energy state, it is determined to be fully relaxed. Then the relaxed unit-cell is assembled in weft and warp direction to form a piece of fabric. Therefore, fabric used for impact and penetration simulation is at the filament level and true to the initial state. Second, the size, position and material properties of the projectile are defined.

Sphere and cylinder are the only two projectile shapes available in digital element approach. As discussed in previous papers [1,43,44], the projectile is modeled as a non-

deformable rigid body particle. Spherical projectile is modeled as a node with radius r , while cylindrical projectile is comprised of a cylinder with front and end disk. When rigid body particle impacts the fabric, contacts between projectile and fabric are established accordingly with respect to its defined shape.

2.3.3.3 Convergence

Initial comparison between simulation results and experiment results focused on investigating convergence of the digital element approach by constructing models with varying number of fibers per yarn. Examples were presented with 1, 7, 14, and 19 digital fibers per yarn respectively. Figure 2-19 and Figure 2-20 show projectile displacement and energy loss with respect to time. Both displacement and energy loss of 14 and 19 fibers per yarn overlap each other. Therefore, the conclusion was made that in deterministic analysis, numerical results converge when the number of fibers per yarn increases.

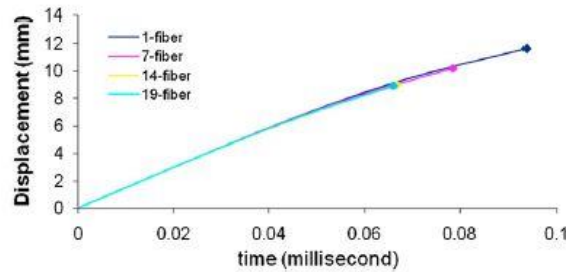


Figure 2-19 Projectile Displacement versus Time after Striking [1]

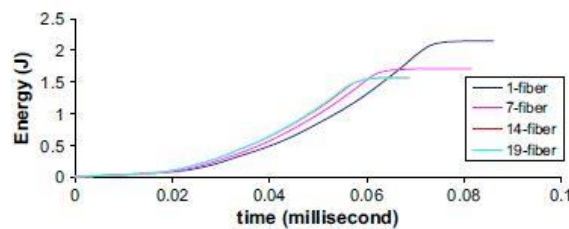


Figure 2-20 Projectile Energy Loss versus Time after Striking [1]

2.3.3.4 Elasto-plastic analysis

Several assumptions were made when establishing the convergence simulation described in 2.3.3.3. Contact between the fibers was considered elastic; contact force was calculated based on the linear elastic stress-strain relationship. However, as stated in Cheng's paper [8], Kevlar KM2 fiber is linear elastic in the longitudinal direction and non-linear elasto-plastic in transverse directions, resulting in a close prediction of the striking process but inaccurate prediction of the rebound process. Energy lost due to fiber transverse plastic deformation was not considered. As shown in Figure 2-21, displacement of the impact curve is almost symmetrical before and after the rebound for both circular and rectangular fixture. No energy loss was captured, but the experimental results showed otherwise. Fiber bending stiffness and air damping effect were also neglected in numerical simulation.

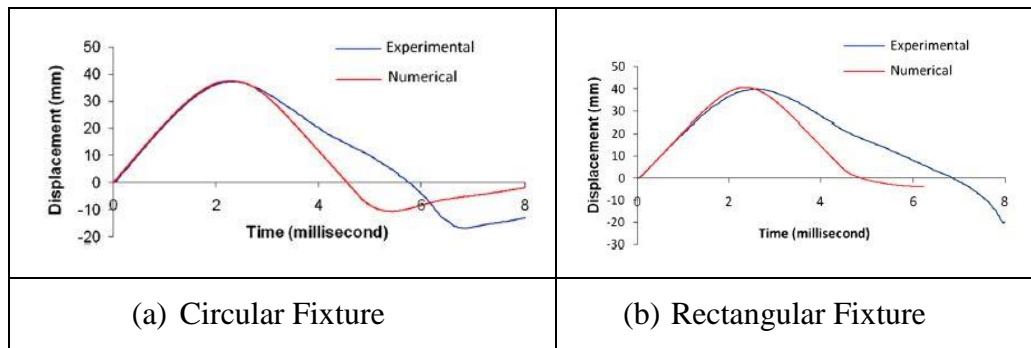


Figure 2-21 Comparison of Fabric Deflection in Impact Area (Elastic) [1]

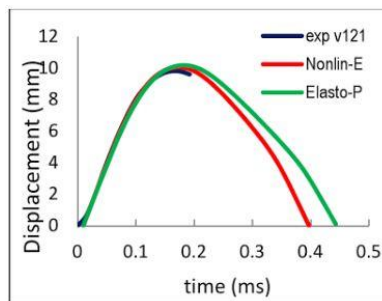


Figure 2-22 Comparison of Fabric Deflection in Impact Area (Plastic) [43]

Nonlinear elastic simulations and elasto-plastic simulations were conducted in this simulation. Because the transverse stress-strain relationship of Kevlar KM2 fiber is neither linear nor elastic, by studying the stress-strain relationship of Kevlar KM2 in transverse direction, following two equations were derived from curve fitting, and implemented in loading and unloading stages to account for energy loss due to transverse plastic deformation.

$$\bar{\sigma} = (6.9417\bar{\epsilon}^3 - 1.2208\bar{\epsilon}^2 + 0.5296\bar{\epsilon} + 0.0060) \times 10^9 \quad (2-9)$$

$$K = (18.666\bar{\epsilon}_{max}^2 + 7.0632\bar{\epsilon}_{max} + 0.0646) \times 10^9 \quad (2-10)$$

A set of numerical simulations were performed using non-linear elastic and elasto-plastic. As shown in Figure 2-22, two numerical examples were conducted using nonlinear and elasto-plastic simulations. Results showed that at rebound stage, displacement derived from elasto-plastic analysis were closer to experimental results than nonlinear elastic analysis, but still lower than experimental results. Discrepancies could be attributed to: lack of consideration of energy dissipation between the clamp and the edge of the fabric, fiber bending stiffness, and fiber damages. Therefore, the Weibull function was incorporated into the next set of simulations to investigate the effects of fiber friction coefficient on fabric penetration resistance.

2.3.3.5 Deterministic and statistical analysis

Researchers throughout the years conduct two types of impact analysis: deterministic analysis and statistical analysis. A deterministic mathematical model is meant to yield a single solution describing the outcome of given appropriate inputs. In deterministic ballistic simulation, yarn failure is based on a single strength and failure happens at location with the highest stress. On the contrary, a statistical model provides a distribution of possible outcomes. Yarn failure happens at fiber weakest link.

The strength of Kevlar is known to be statistically distributed due to the presence of defects and weak links along the fibers. Therefore, ballistic simulation results of textile fabrics using single deterministic fiber strength were compared to the results of statistical distributed fiber strength. In the simulations presented in section 2.3.3.3 and section 2.3.3.4, single deterministic fiber strength was assigned to all fiber elements, revealing that fiber failure always occurred at the point of highest stress, typically the impact point. However, in statistical simulations, a Monte Carlo process was used to assign a unique strength to each digital element following a bimodal Weibull distribution function. This allowed the numerical simulation to characterize Kevlar KM2 fiber strength in statistical simulation, which leads to a fiber failure at the weakest links.

A set of numerical simulations were conducted using deterministic and statistical approaches to investigate the effect of inter-fiber friction on fabric ballistic impact. Results showed that the fiber friction coefficient plays an important role in Weibull simulation in determining V_{50} . Different fiber friction coefficient yields different V_{50} . However, the effects of fiber friction coefficient on V_{50} decrease as strike velocity increase.

2.3.3.6 Conclusions

From the above three simulations, following conclusions are made:

1. The number of digital fibers per yarn affects the results of ballistic simulation of textile fabrics. However, when the number of digital fibers per yarn reaches 14 or above, continue increase of number of digital fibers per yarn has trivial effect on the results.

2. In elastic simulation, numerical simulation results derived from the digital element approach were in agreement with the experimental results in the loading stage. Discrepancies happened in the rebound stage.

3. In elasto-plastic simulation, simulation results agreed with the experimental results in loading stage. The time and displacement curve improved in the rebound stage. Energy loss due to the transverse deformation of fibers during the impact was captured.

3. In deterministic and statistical analysis, fiber friction coefficient affected the simulation results of V_{50} under low impact speed. When impact speed increased, the effect of fiber friction coefficient on determining V_{50} became trivial.

2.3.4 Other models

In 2005, Zohdi and Powell [45] proposed a model which considered the textile fabric to be a 2-D network of yarns. Yarns were comprised of micro-scale fibrils, which joined at the nodes to form a network. Illustration of the model is shown in Figure 2-23.

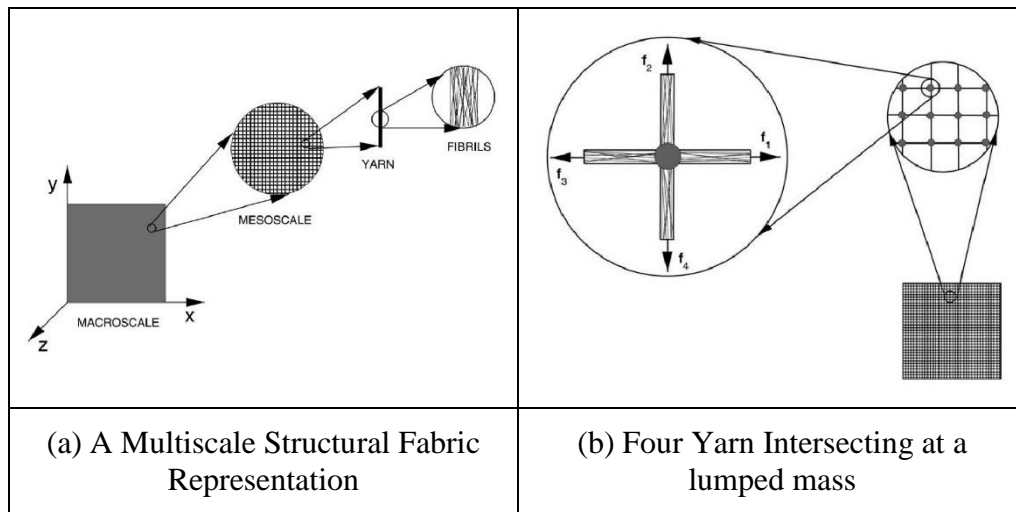


Figure 2-23 Zohdi and Powell's Model [45]

In 2011, inspired by DEA, Grujicic et al. [46] proposed a fiber-level model of simulating dynamic strength of Kevlar KM2 ballistic fabric using commercial FE software. First, a yarn-level geometrical model of the fabric was created. Second, each yarn is discretized into discrete

circular cross-section fibers bundled into a regular hexagonal close-packed configuration. Figure 2-24 shows the cross-sectional shape of various discretization patterns.

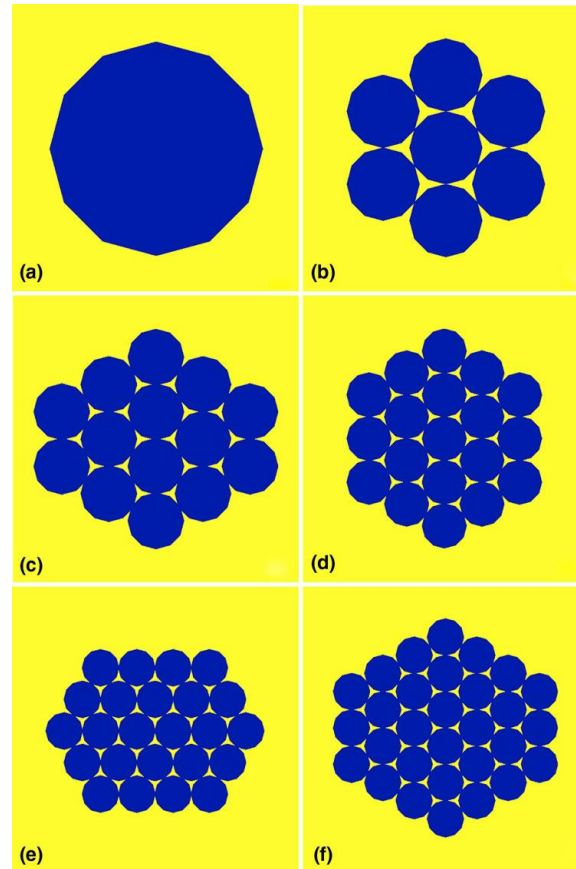


Figure 2-24 Various Cross-Sectional Shape of Discretization Patterns [46]

Each fiber is modeled as three-dimensional beam element with beam length chosen to match the fiber diameter. All simulations were obtained from commercial software ABAQUS/Explicit. The main objective of Grujicic and his co-workers' work is to extend the use of nonlinear dynamic digital element simulations [40–42] to the sub-yarn length scale and to compare results with Wang's [1] simulation results.

2.3.4.1 Hybrid

Most numerical simulations are only applicable for small-scale analysis. Some researchers resolve to single layer and a quarter of the fabric. Since fabric impact parameters are size dependent, small-scale analysis could fail to simulate the comprehensive of fabric failure. Therefore, computer capacity limitation becomes the major issue for projectile penetration and impact simulate.

Textile hybrid model is the result of a combination of two or more types of element mesh method. The purpose of hybrid model is to assign fine element mesh to the area of high interest, while coarse element mesh is assigned to the area of irrelevant. By doing that, the critical issue of computer resources and computational cost for modeling real scale fabric under projectile impact can be improved tremendously.

Numerical results based on full-scale fabric showed two important factors: (1) Stress wave travels along the principle yarns immediately after the impact. High yarn stress develops quickly from the impact center to a distance along principal yarns [47]. (2) The total number of fibers per yarn contributes significantly to memory use. However, increasing the total number of fibers per yarn beyond a certain value does little to increase the accuracy of the result. Based on the two observations, a yarn based hybrid mesh is developed by Dippolito, Wang et al. [47] in 2014. An example of hybrid model is shown in Figure 2-25.

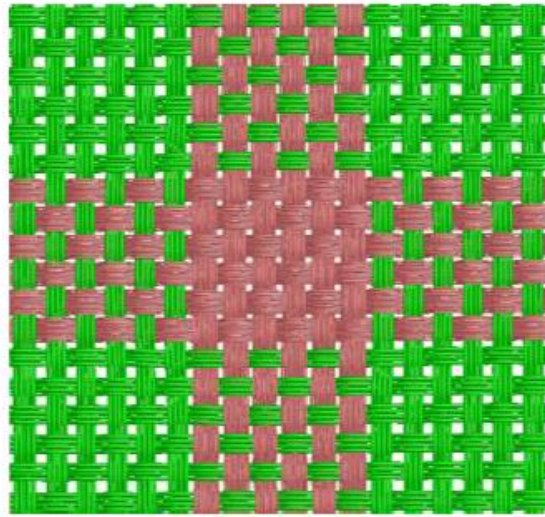


Figure 2-25 Hybrid Model [47] (The yarns in red are made of 19 fibers per yarn. The yarns in green have 4 fibers per yarn.)

2.4 Remarks

This chapter provides an overview of bullet geometry, ballistic fibers, and modeling methods of ballistic penetration and impact of textile fabrics. Sphere, RCC, and FSP are three common bullet types used in ballistic tests. However, due to limitation of modeling methods, the number of numerical simulations performed using RCC and spherical projectiles exceeds that of FSP. Bullet shape inevitably affects the ballistic impact outcome. Therefore, it is imperative to develop a ballistic model using arbitrary projectile shapes and accurately model the impact mechanism of both the fabric and projectile.

Soft body armor is made of fibrous textile fabric, while projectiles are deformable solid body. The difference between textile fabric and ballistic projectile serves as a challenge for researchers to model ballistic impact process. The subject of this research is to analyze ballistic strength of fabric using solid body projectile of arbitrary shape. A personal computer and cluster based numerical tool is developed to simulate ballistic penetration and impact of textile fabrics at

filament level. Organic aramid fiber Kevlar KM2 is the major material used in this research. Therefore, an overview of material properties of Kevlar KM2 is thoroughly discussed.

Digital element approach (DEA) was well established by Wang et al. [2,40–42,48,49]. In this approach, fabric is an assembly of unit-cells repeated in weft and warp direction, unit-cells are made of yarns in prearranged pattern. Yarns are further discretized into multiple fibers. The physical representation of a fiber is digital chain. The material properties of digital chain are modeled through rod element connected by frictionless pin. When the length of rod element approaches zero, full flexibility can be achieved.

The stress-strain relationship and strength distribution of Kevlar KM2 fiber are implemented in digital chain. When the distance between two nodes (frictionless pin) on two different fibers is smaller than fiber diameter, contact is detected. The contact force between two fibers is calculated using implemented material properties of Kevlar KM2.

The validation of the DEA is established in Chapter 3 -. 10 specimens of 10 different weaving styles and 2 material types are simulated and compared to microscopic pictures. The fabric later used in ballistic simulation is generated by the verified DEA. A detailed introduction of the combination of DEA and FEM approach is established in Chapter 4 -. This approach enabled ballistic impact simulation against deformable projectile with arbitrary shape. Numerical simulation derived from the combination of DEA and FEM approach is compared to the DEA approach. Chapter 5 - demonstrates a comprehensive understanding of bullet sharp edge radius and its edge effect on fabric ballistic strength. Fiber bending rigidity is incorporated into the modified DEA. The digital fiber effective area moment of inertia is numerically determined.

Real scale ballistic tests of multi-layer fabric against FSP projectile are simulated using the modified DEA in Chapter 6 -. The simulation results are compared to experimental results

provided by U.S. laboratory lab. Element length to fiber diameter ratio, digital fiber bending rigidity, number of digital fibers per yarn, and projectile radius are analyzed and discussed in detail to verify the modified DEA approach.

Chapter 3 - Validation of explicit DEA in determining micro-geometry of 3-D woven fabrics

3.1 Introduction

Textile fabrics have been widely used in non-traditional areas. For example, 2-D and 3-D woven and braided fabrics are used as composite preform. Various ballistic fabrics are used for soldier and police officer protection. As such, there is a need to develop a general numerical tool for fabric mechanics. The digital element approach was developed to determine fabric micro-geometry.

The concept of the digital element was originally established by Wang and Sun in 2000 [40,41] in order to determine fabric micro-geometry. In the original digital element model, it was assumed that each yarn was a flexible structural component with a circular cross-section, which was modeled as a frictionless pin-connected rod element chain. These rod elements are defined as “digital elements.” Using this digital element approach, the textile process was firstly modeled as a quasi-static structural mechanical problem with boundary conditions. A procedure similar to finite element analysis was adopted to simulate yarn movement during textile processes. Yarn cross-section deformation was, however, not considered. The concept of the multi-chain yarn was developed in 2003 [48]. In this modified model, a yarn was composed of multi-digital fibers. Each digital fiber was a flexible structural component with a circular cross-section that was modeled as a frictionless pin-connected rod element chain. The DEA was employed to simulate weaving and braiding processes and generate fabric micro-geometries with realistic yarn cross-sections.

The major obstacle of the application of the DEA to determine fabric micro-geometry was the huge amount of computer resource required for a full-scale textile process simulation. To

resolve the computer resource issue, a static relaxation algorithm was developed to replace step-by-step textile process simulation [49]. In the static approach, an initial fabric topology is established based upon weaving or braiding processes. Yarn is digitized into many digital fibers; tensile force is applied to the end of each fiber. The fabric deforms due to fiber tension until all non-equilibrium nodal force is relaxed. As such, textile micro-geometry is derived. Compared to full-scale textile process simulation, the static relaxation only requires 10-20% of computer resource.

Recently, a more efficient explicit dynamic relaxation algorithm with periodic boundary conditions was developed to determine the micro-geometry of 3-D textile fabrics [50]. In the new procedure, the unit-cell topology is generated based upon weaving patterns. Yarn is discretized into multi-digital fibers. A periodic boundary zone is added around the boundary zone through a mapping process. An initial yarn tension is assumed. During the relaxation step, the non-equilibrium nodal forces inside the unit-cell are calculated first. Then, nodal accelerations, velocities, displacements and positions are calculated. Nodal positions inside the periodic boundary zone are updated through a mapping process. The simulation continues until all nodal forces vanish. Because the material domain includes only one unit-cell, the computer resource is not an issue. This approach has been used to determine micro-geometries of various 3-D woven fabrics.

The objective of this research is to validate the digital element dynamic relaxation approach to determine the 3-D fabric micro-geometry. The external dimension, surface patterns, and interior micro-geometries of 10 actual 3-D woven fabrics in 10 different weaving patterns are investigated. The micro-geometry derived from microscope pictures is compared to the results derived from numerical simulation. Among the ten 3-D specimens, six consist of Nicalon

CG and four of glass fibers. Fabric thicknesses range between 3mm to 10mm. Plain and twist yarn structures are both used. These fabrics cover a broad range of weaving styles.

3.2 Modified fiber-to-fiber contact

In the DEA, distance between two fibers is modeled through the nodes on each fiber. If the distance between two nodes on two fibers is smaller than the fiber diameter, contact occurs. Because the distance between two neighboring nodes on the same digital chain (also called the length of the digital rod elements) is small, the assumption was made that the axial direction of the contact element aligns with the compressive force direction. However, if a longer length of the digital rod elements is adopted with a coarse mesh, the axial direction of the contact element does not accurately align with the compressive force direction, as shown in Figure 3-1 (a). The solid line between two fibers indicates the real direction of the contact force. The dashed line is the direction of the calculated contact force. Therefore, the direction of compressive forces between two digital chains is not perpendicular to two contacting digital elements, as shown in Figure 3-1 (b). As a result, both magnitude and direction of compressive forces are not calculated accurately. An artificial friction is inserted due to lateral component of the compressive force, which prevents relative sliding motion between digital chains even when the friction coefficient is assumed zero.

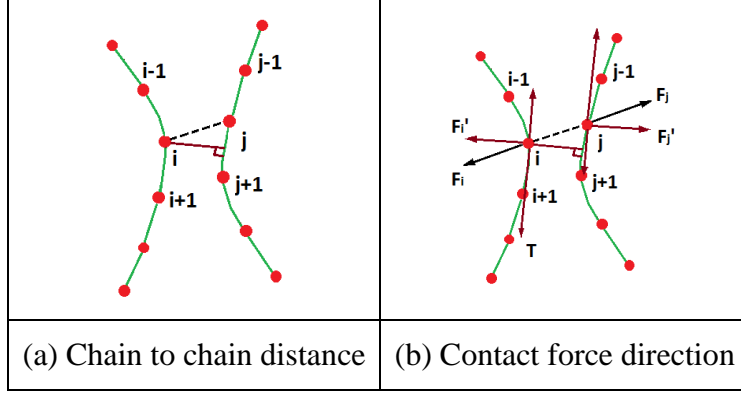


Figure 3-1 Modification of Contact Elements

Two modifications are made in order to minimize the effects of artificial friction. The assumption is made that the direction of the two contact elements is perpendicular to the tangential direction of each contacting element. If the distance between two neighboring nodes is smaller than the chain diameter, a contact element is inserted between the two nodes. However, as shown in Figure 3-2, the distance between two neighboring chains ij' reached the distance of the fiber diameter before the distance between node i and j , resulting in miscalculation of the fore-mentioned. An element coefficient is introduced to readjust the fiber diameter:

$$Element\ Coefficient = \frac{L_0}{d_0} \quad (3-1)$$

$$Diameter\ Coefficient = \sqrt{1 + \left(\frac{Element\ Coefficient}{2}\right)^2} \quad (3-2)$$

$$d_m = d_0 \times Diameter\ Coefficient \quad (3-3)$$

where L_0 is the original element length, d_0 is the original fiber diameter, and d_m is the modified fiber diameter. With application of this diameter modification, accuracy of contact element length can be achieved even under coarse mesh. Furthermore, multiplying the diameter coefficient to the original fiber diameter simplified the process of calculating the distance between two neighboring chains ij and saved computer memory while achieving the same

accuracy needed for simulation. In order to avoid contact distance miscalculation, a digital element length of 1/2 element diameter or less is recommended.

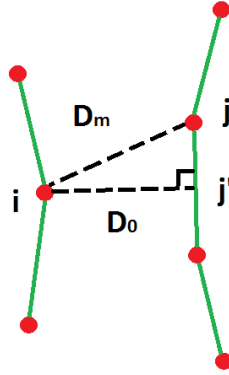


Figure 3-2 Modification of Diameter

3.3 Comparison between numerical and experimental results

In this section, the micro-geometries of 3-D woven fabrics derived from the numerical simulation are compared to that derived from experiment observation. Ten specimens, with different weaving patterns and topology shapes, are presented to validate the relaxation approach. Two types of fiber are used to weave these specimens: Nicalon CG and S-glass. Six of the ten specimens are made of Nicalon CG fibers and the other four specimens are made of S-glass fiber. The twisted yarns are used in one specimen and the plain yarns are used in the other nine specimens. Nine specimens have regular cuboids shape unit-cells, and one specimen has a sheared shape unit-cell. Thicknesses of these specimens range from 3mm to 10mm.

3.3.1 Experimental observation

When performing the simulation, the following three steps are involved in the experimental research:

1. Measure the actual denier numbers to verify yarn properties specified in the data sheets. Five to ten yarn segments are removed from each specimen and examined carefully. The actual denier numbers of each segment are calculated subsequently using analytical balance. The yarn's average cross-section area derived from the measured denier number is used in numerical simulation.

2. Exam the topology of each specimen by tracing yarn paths inside the fabric to verify the unit-cell topology specified in the data sheets. Length and width of the unit-cell are measured, and the weaving pattern is identified by disassembling the fabric section by section from the specimen edge.

3. Observe the fabric surface with a microscope and measure the fabric thickness. An average of 5-10 spots is randomly chosen from each specimen to calculate average fabric thickness using analytical balance. Interior microstructures of the specimens are also observed, and pictures are taken using Scanning Electron Microscope (SEM). Both microscopic images and thickness are compared to corresponding numerical simulation results.

Two types of fibers are used in the simulation: Nicalon CG and S-glass fiber. The given denier number of Nicalon CG and 1250S glass fibers (1250 yards/lb.) are 1800 and 3575 respectively. Corresponding yarn cross sections are calculated and listed in Table 3-1. The measured denier numbers are listed in Table 3-2. A comparison of Table 3-1 and Table 3-2 revealed that, for Nicalon CG fibers, the measured denier number is 10.46% greater than the given denier number specified in the datasheet. For 1250S and 250S glass fibers, the measured denier number is 3.40% and 2.36% greater than specified in the datasheet. Therefore, the cross-section area derived from the measured denier is used in numerical simulation.

Table 3-1 Given Fiber Properties

Type	Denier (g/9000m)	Density (kg/m ³)	Cross-Section Area(m ²)
Nicalon CG	1800	2550	7.843E-8
1250S Glass	3575	2460	1.613E-7
250S Glass	17874	2460	8.066E-7

Table 3-2 Measured Fiber Properties

Type	Denier (g/9000m)	Cross-Section Area(m ²)	Discrepancy
Nicalon CG	1988	8.66E-8	10.46%
1250S Glass	3697	1.668E-7	3.40%
250S Glass	18296	8.256E-7	2.36%

3.3.2 Fibers

Two types of fibers are used in this comparison: Nicalon CG and S-glass fiber. Nicalon CG fiber is a multi-filament silicon carbide-type fiber. The fiber is homogeneously composed of ultra-fine beta-SiC crystallites and an amorphous mixture of silicon, carbon, and oxygen. The fiber has excellent strength and modulus properties and retains its properties at high temperatures. Nicalon is also highly resistant to oxidation and chemical attack. Ceramic grade (CG) Nicalon offers the optimum mechanical properties and high-temp performance for most applications. S-glass is a modification of E-glass fiber having improved strength and other properties. The S-glass fiber reinforced composite materials also exhibit good impact resistance. 1800 denier yarns are used for Nicalon CG fabrics. 1250S glass fiber yarns (1250 yards/lb.) and 250S glass fiber yarns (250 yards/lb.) are used for S-glass fiber specimens. Corresponding yarn cross-sections are calculated. They are listed in Table 3-3. Density is also provided.

As aforementioned, the actual yarn denier is measured using an analytical balance. The measured denier number is listed in Table 3-4. For Nicalon CG fibers, the measured denier number is 10.46% greater than that specified in the datasheet. Correspondingly, the yarn cross section is recalculated. For 1250S and 250S glass fiber, the measured denier number is 3.40% and 2.36% greater than that listed in the datasheet, respectively. The cross-section areas are recalculated, which are listed in Table 2. These numbers are used in the numerical simulations later.

Table 3-3 Fiber Properties

Type	Denier (g/9000m)	Density (kg/m ³)	Cross-Section Area(m ²)
Nicalon CG	1800	2550	7.843E-8
1250S Glass	3575	2460	1.613E-7
250S Glass	17874	2460	8.066E-7

Table 3-4 Measured Fiber Properties

Type	Denier (g/9000m)	Cross-Section Area(m ²)	Discrepancy
Nicalon CG	1988	8.66E-8	10.46%
1250S Glass	3697	1.668E-7	3.40%
250S Glass	18296	8.256E-7	2.36%

3.3.3 Fabric weaving patterns and micro-geometries

Ten specimens are analyzed in the simulation: Six specimens are made of Nicalon CG fibers and four specimens are made of glass fibers. Simulated unit-cell topologies and specified micro geometries of Nicalon CG fibers are listed in Table 3-5, and the specimens that are made of glass fibers are listed in Table 3-6. Specimens 1-9 are made of plain yarns, and Specimen 10

has a twist rate on weft yarns. Specimens 1, 2, 7, 8, and 9 are orthogonal weave, and Specimens 3, 4 and 10 are layer-to-layer. The unit-cell of Specimen 5 is parallelogram due to the shift rate applied to the right boundary. Therefore, it is safe to conclude that the test specimens cover a broad range of 3-D weaving styles.

Table 3-5 Weaving Pattern and Microgeometry of Nicalon CG Specimens

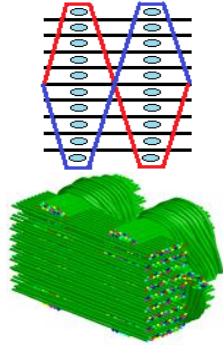
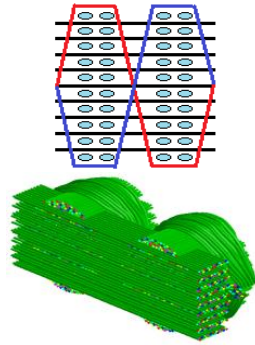
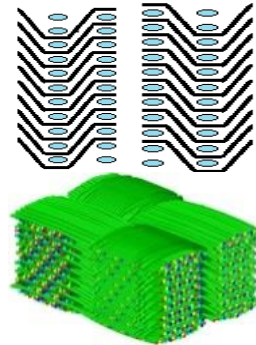
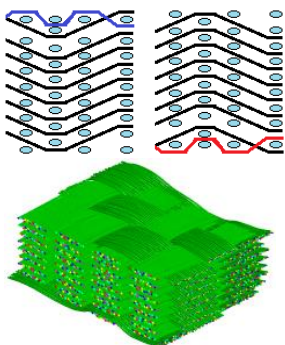
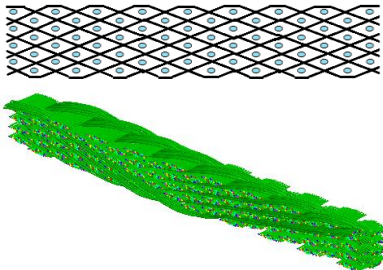
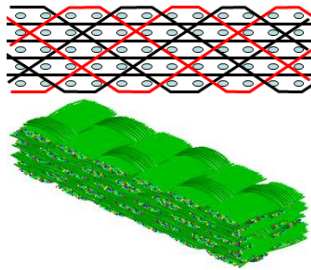
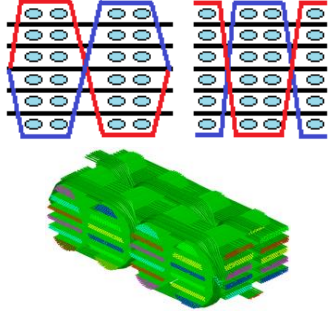
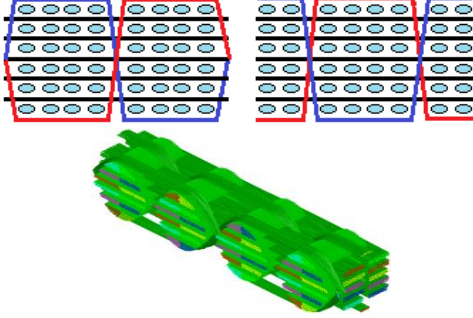
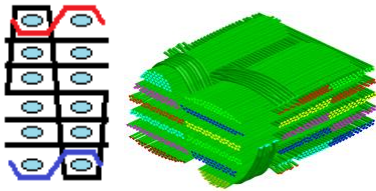
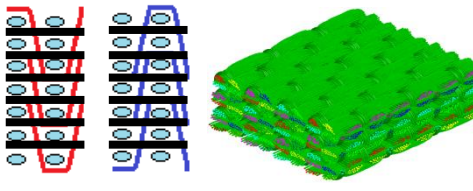
Specimen 1 Orthogonal weaving	Specimen 2 Orthogonal weaving	Specimen 3 Layer-to-layer weaving
		
Specimen 4 Modified layer-to-layer weaving	Specimen 5 Angle interlock weaving	Specimen 6 Modified interlock weaving
		

Table 3-6 Weaving Patterns and Microgeometries of S-Glass Fiber Specimens

Specimen 7 Orthogonal weaving	Specimen 8 Orthogonal Weaving
	
Specimen 9 Orthogonal weaving	Specimen 10 Layer-to-layer weaving(twisted yarns)
	

3.3.4 Comparison of micro-geometries

The microstructure of fabrics derived from numerical simulations is compared to actual fabrics using the following three criteria: surface appearance, interior yarn structures, and fabric thickness.

3.3.4.1 Surface appearances

Two typical specimens out of ten are shown in Figure 3-3 to illustrate surface appearances. Specimen 5 is made of plain weave and Specimen 10 is made of twisted yarn structures. The first picture on the left in Figure 3-3 is the microscopic image obtained from the actual specimen; the pictures on the right are the fiber level and yarn level numerical simulation

results. A comparison of the microscopic images reveals that, the numerical simulations closely resemble the actual structure.

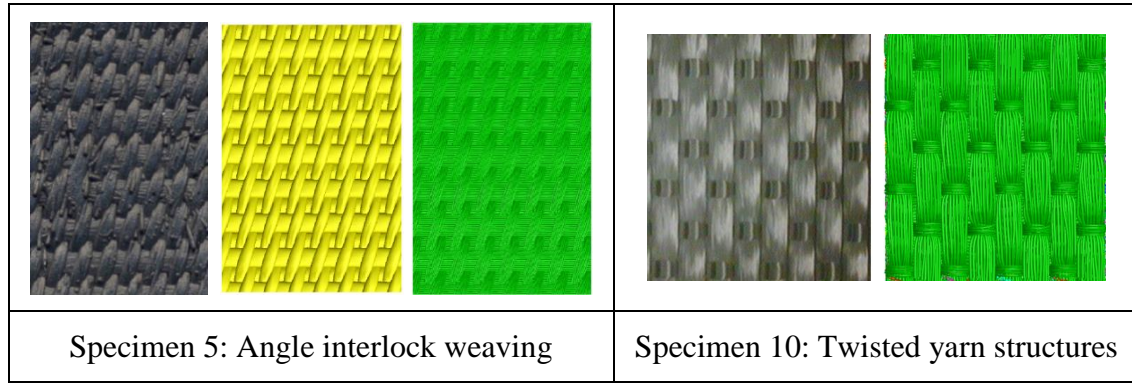


Figure 3-3 Comparison of Surface Appearances

3.3.4.2 Interior yarn structure

The interior cross-section of Specimen 2 and Specimen 5 are compared in Figure 3-4 and Figure 3-5. Images obtained from the microscope are shown in the upper position; the front and side view of numerical simulation results are placed below the microscope images. For warp sections comparison, the microscope picture captured voids between weaver and weft. However, the simulated unit-cell is full packed. One possible reason for this discrepancy is, in numerical simulation, the simulated unit-cell reaches its minimal energy state; however, in the dynamic weaving process, due to inter-fiber friction, each unit-cell reveals different energy state. The resemblance of numerical results and experimental results is still seen.

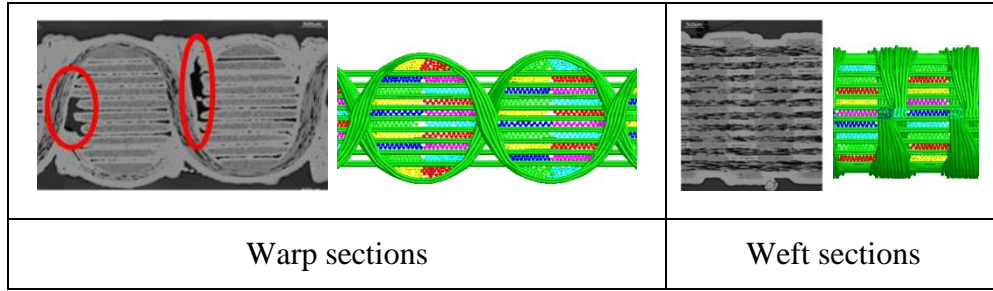


Figure 3-4 Comparison of Interior Microgeometry: Specimen 2

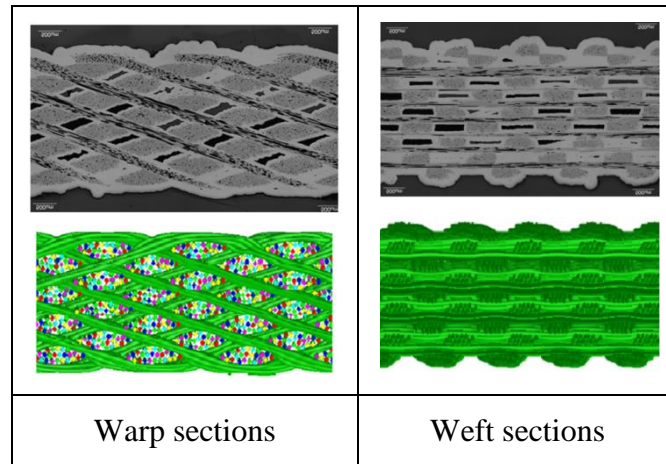


Figure 3-5 Comparison of Interior Microgeometry: Specimen 5

3.3.5 Comparison between fabric thickness

Fabric thickness of each specimen is measured and compared with numerical results. Comparison results are shown in Table 3-7. Numerical thickness of Specimen 10 is almost identical to its measured thickness. Numerical fabric thicknesses of Specimens 1-9 are approximately 5%-20% smaller than the measured fabric thicknesses. The discrepancy between the numerical results and experimental results occurred for two reasons. First, numerical simulation is performed under the minimum potential energy principle; when the change of minimum potential energy with respect to time step approaches zero, calculation stops. However, during the actual dynamic 3-D weaving process, fabric microgeometry is also affected by yarn

tension, weaving speed, and beat-up speed. Therefore, the actual fabric may not be able to reach the minimum potential energy state, resulting in a larger thickness. Second, since the weft yarns of Specimen 10 were made of twisted yarns, the cross-section deformation is more restrictive than the deformation of plain yarns. Twist rate played a more important role in determining fabric thickness than weaving kinetics in determining the fabric thickness.

Table 3-7 Comparison of Thicknesses

Specimen Number	Weaving Type	Fabric Thickness(m)		Discrepancy
		Measurement	Numerical	
1	Orthogonal	0.00382	0.00324	-15.18%
2	Orthogonal	0.00359	0.00330	-8.08%
3	L-to-L	0.00283	0.00255	-9.89%
4	Mod. L-to-L	0.00259	0.00243	-6.18%
5	Angle Interlock	0.00310	0.00274	-11.61%
6	Mod. Interlock	0.00341	0.00299	-12.32%
7	Orthogonal	0.00730	0.00597	-18.22%
8	Orthogonal	0.00789	0.00637	-19.26%
9	Ortho weave with stuffer	0.00657	0.00551	-16.13%
10	Orthogonal (Twisted yarn)	0.00879	0.00864	-1.71%
Average	-	-	-	-11.86%

3.3.6 Fabric thickness discrepancy analysis

1. Refer to Figure 3-4, in the numerical simulation, the fabric microstructure is the one, which makes the potential energy a minimum value. However, the 3-D weaving process is a dynamic process. The fabric micro-geometry is also affected by the weaving speed, beat-up speed and yarn tension. The micro-geometry of actual fabric may not be the one that reaches the minimum potential energy state. Therefore, actual fabrics are usually thicker than the fabrics derived from numerical simulation.

2. Specimen-10 is made of twisted yarns. The cross-section deformation of twisted yarn is more restrictive than that of plain yarn. Twist rate plays a more important role than the weaving kinetics to determine fabric thickness. The fabric derived from numerical simulation is only slightly (1.71%) thinner than that of the actual fabric.

3.4 Conclusion

The objective of this research is to analyze the effectiveness of the digital element dynamic relaxation approach to determine 3-D fabric micro-geometry. The external dimension, surface patterns and interior micro-geometries of ten 3-D fabrics in ten different weaving patterns are investigated and compared to the DEA simulation results, qualitatively and quantitatively, in order to evaluate the accuracy of the DEA simulation. Among the ten 3-D specimens, six consist of Nicalon CG and four of glass fibers. Fabric thicknesses range between 3mm to 10mm. Plain and twist yarn structures are both used. The following conclusions can be reached [51]:

1. Surface patterns derived from numerical simulation are compared to the surface pattern of the actual specimens, revealing that simulated surface appearances closely resembled the actual fabric surface.

2. Simulated results correctly predicted the actual interior micro-geometry patterns. Cross-section images of the simulation results match the microscope pictures taken from the specimens.

3. Results showed that fabric thicknesses derived from numerical simulation are generally thinner than actual fabric thicknesses. For nine specimens made of plain yarn, the numerical results are 5% -20% thinner than measured fabric thickness. For the specimen made of twisted yarn, the discrepancy is less than 2%. One possible reason for the difference between specimens made of twisted yarns and plain yarns in thickness is: yarn cross-section deformation of twisted yarns is more restricted than plain yarns; therefore, the numerical simulation is more stable.

4. DEA is an accurate fiber level approach for simulating textile fabrics.

Chapter 4 - Combined DEA-FEM model

4.1 Previous version of DEA

Sphere, RCC, and FSP projectiles are most common shape bullets used in standard ballistic tests. The previous version of DFMA is only capable of simulating ballistic impact of textile fabric using rigid body spherical and cylindrical projectiles only. FSP and real bullets are not modeled. The subject of this research is to simulate ballistic perforation process using projectile of arbitrary shape. Projectile elastic deformation is simulated using combined FEM and DEA model. The method of determining contacts between textile fabric and solid body is established. Contact forces are calculated accordingly.

Ballistic impact of textile fabrics using rigid body spherical and cylindrical projectiles is performed using the previous DEA and combined DEA-FEM separately. Numerical results from the modified DEA approach are compared to results from the previous DEA.

Ballistic impact of textile fabrics using deformable body projectile with arbitrary shape is simulated. The purpose of this simulation is to test the feasibility of the combined DEA-FEM approach in simulating solid body elastic deformable projectiles and validate the need to transfer personal computer (PC) based code to parallel cluster based code for real scale multilayer soft-armor analysis.

In this chapter, first, the method of generating arbitrary shape projectile with triangle surface mesh is explained. Second, the contact search and contact force calculation between fibrous textile fabric and solid body projectile is generated. Third, the combined explicit DEA and FEM algorithm is established. Fourth, ballistic impact of rigid and elastic deformable solid body projectile is performed and compared to previous the DEA approach. Solid conclusions are reached.

4.2 Ballistic impact to fabric using rigid body projectile of arbitrary shape

The most common ballistic test performed in labs is a V_{50} evaluation. V_{50} is the velocity at which there is a 50% probability the target will be penetrated by projectile. Fragment simulators, spherical, RCC and FSP projectile, made of hard steel, are often used in ballistic tests, projectiles normally ranging in weight from 2 grains to 64 grains.

In the previous DEA, only spherical and cylindrical projectiles can be simulated. Fabric ballistic strength under RCC and spherical projectile impact has been thoroughly analyzed in previous researches. The modified DEA enabled simulation of ballistic impact using projectile of arbitrary shape. The simulation steps are: 1. Use commercial FEM package to generate FE meshed projectile, and output nodal and element information. 2. Translate projectile mesh information into DFMA readable format, and identify projectile mesh surface. 3. Establish contacts between projectile surface and fabric. 4. Calculate the fabric stress and deformation. 5. Calculate the contact force applied to projectile, and resultant velocity, displacement and rotation.

4.2.1 Generate projectile with arbitrary shape

4.2.1.1 Element type

The FE meshed projectile is created and meshed by commercial FE software using 8-node element, as shown in Figure 4-1. This element is comprised of 8 nodes, 12 lines, and 6 faces. Each node has 6 degrees of freedom: translations in the nodal x , y , and z directions and rotations about the nodal x -, y -, and z -axes. A node number is assigned to each node in counter clockwise direction from bottom to top face. One node is shared by 4 or 8 elements.

The Roman numbers I to VI represent six faces. Face I is comprised of Nodes 1, 4, 2, and 3. As such the vector direction of $\overrightarrow{41} \times \overrightarrow{21}$ points outward and is normal to surface $I24$.

Similarly, Face II is comprised of Nodes 5, 6, 8, and 7. Face III is comprised of Nodes 5, 1, 6, and 2. Face IV is comprised of Nodes 7, 6, 3, and 2. Face V is comprised of Nodes 8, 7, 4, and 3. Face VI is comprised of Nodes 8, 4, 5, and 1.

Since the four nodes consisting of each face are not necessarily on the same plane, each face is discretized into two adjacent triangles. The contact between fabric and solid body projectile is established through the triangle surfaces.

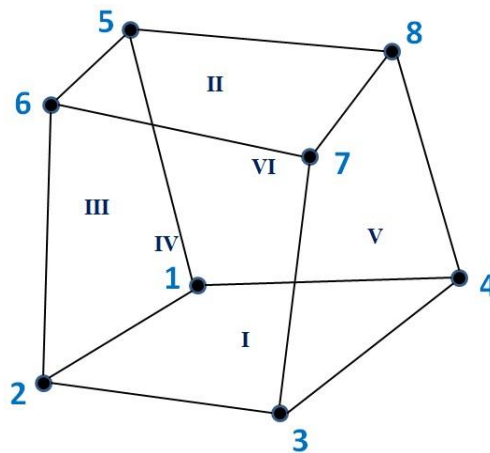


Figure 4-1 8-Node Element

4.2.1.2 Meshed method

Figure 4-2 shows four examples of typical bullet shapes meshed by ANSYS using element type solid73. In order to eliminate the effect of mesh pattern on calculating projectile deformation, a mapped mesh symmetrical about x - y or y - z plane is adopted for all types of projectile. Assume the projectile initial speed is along y -axis. For spherical bullets, the mesh pattern is symmetrical about x - z , x - y and y - z plane. For RCC and 9 mm caliber, the mesh pattern is symmetrical about y - z and x - y plane. For FSP, the mesh pattern is symmetrical about x - y plane. Considering computational time and resource, the projectile surfaces in direct contact with fabric

have a finer mesh than the surfaces not in direction contact with fabric. Sphere and RCC bullets are used in the DEA for ballistic impact simulation. FSP and real bullets like 9mm caliber are often used in constitutive FE model.

Simulation results from the previous DEA are compared to results from the modified DEA approach using rigid body and deformable spherical and cylindrical projectiles in section 4.4.3.

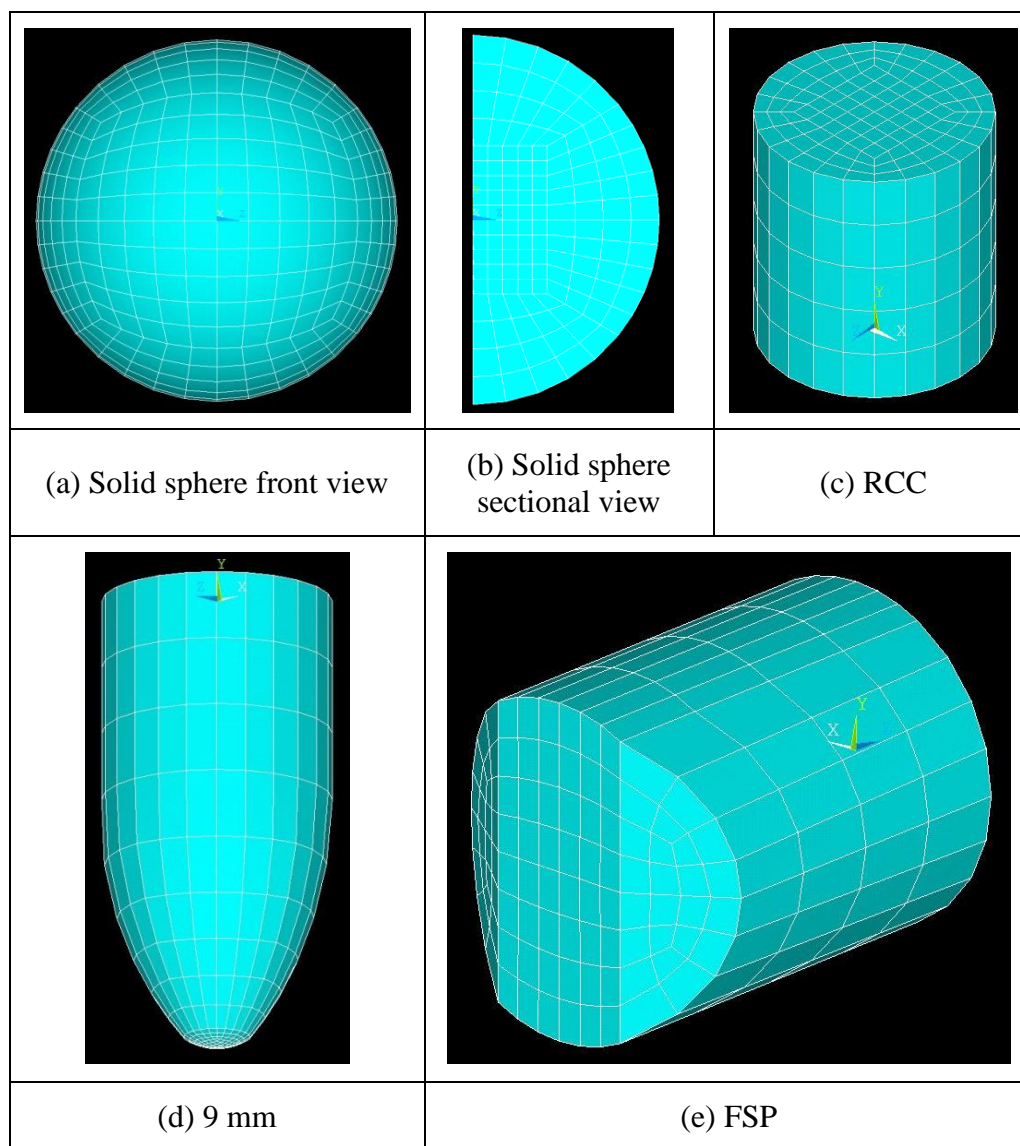


Figure 4-2 ANSYS Meshed Solid Body

4.2.1.3 Generate projectile surface

When projectile encounters the fabric, a node-to-surface contact algorithm is established between projectile surface and the fabric. Therefore, in preparation for contact calculation, projectile surface is identified and saved before simulation. Projectile failure due to impact is not considered at this stage.

Meshed projectile is comprised of 8-node elements, 8-node elements are comprised of 8 nodes, 6 faces, and 12 triangular surface elements. One node of the projectile is shared by four or eight elements. Likewise, one face of an element is shared by adjacent elements. If the face is not shared by other elements, this face belongs projectile surface. Only projectile surfaces are in contact with the fabric. Figure 4-3 shows the only projectile surface.

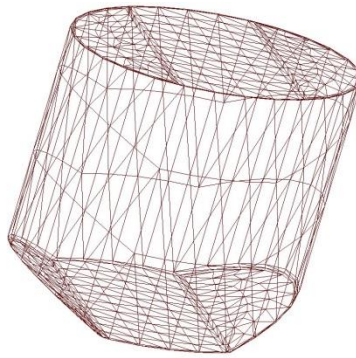


Figure 4-3 Solid Mesh FSP

4.2.2 Contact search

In the DEA, physical representation of a fiber is digital fiber. Digital fiber is composed of rod element and free pin, which are the basic components of the fabric. Free pin is modeled as a

node, the radius of which equals to the size of the digital fiber radius. Therefore, contact between the fabric and the solid body projectile can be modeled as node to surface contact.

During textile relaxation process, approximately 80%-90% of the computing time is spent on contact search. The size of a single layer 19 fibers-per-yarn 1 in. by 1 in. plain weave fabric is 41,463KB. In real scale simulation, the fabric dimension is up to 12 in. by 12 in. and 28 layers. It is imperative to establish a computer resource friendly and time-efficient contact search method.

Because the projectile size is comparably small compare to that of the fabric, less than 1/10 of the total fabric is in physical contact with the projectile. Thereby a contact domain defined by projectile position is created and updated every 50 steps. Only the nodes inside the contact domain are used in projectile-to-fabric contact search. On loop exit, the nodes in possible contact with each projectile surface are defined.

For spherical and cylindrical shape rigid body projectiles used in the previous DEA, contact domain serves as the smallest search entity. However, for meshed solid body projectile, to save the most time spend on contact search, contact domain is further divided into several sub cubes. The search method is explained in following paragraphs.

Contact domain is shaped as a cube, the size of which is determined by projectile boundaries. As shown in Figure 4-4, because the size of the projectile surface triangle is significantly small compared to the contact domain, the contact domain is divided into several sub cubes to facilitate contact search. The size of the cube, denoted as a , ranges from 1.2 to 1.5 times the largest fiber diameter. As such, one node is only in possible contact with another node of the same cube or its surrounding cubes.

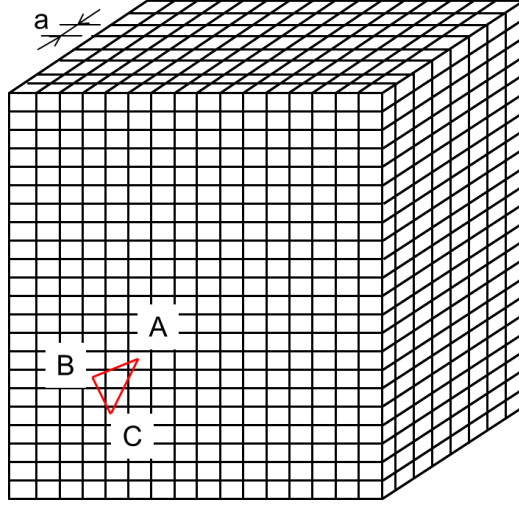


Figure 4-4 Contact Search

Contact between fabric and solid body projectile can occur as node-to-surface contact, node-to-line contact, or node-to-node contact. Node-to-surface contact is the most common contact between projectile and fabric. Therefore, only node-to-surface contact is considered during the contact search.

As discussed in section 4.2.1 and section 4.2.1.3, FE projectile is comprised of 8-node elements. Each element has 6 surfaces, warped and plain. In order to establish node-to-surface contact between fabric and projectile surfaces, the surface comprised of the projectile surface is further divided into two triangles, and each triangle has its own outward normal.

An example is shown in Figure 4-4. Triangle ABC belongs to the projectile surface. A , B , and C are the corner nodes of triangle ABC . To determine which cubes are in possible contact with triangle ABC , first, locate the cubes each corner node belongs to. The cubes are expressed as $C_1(N_{x1}, N_{y1}, N_{z1})$, $C_2(N_{x2}, N_{y2}, N_{z2})$, and $C_3(N_{x3}, N_{y3}, N_{z3})$, with N_x , N_y , and N_z denoted as cubic numbers in x, y, and z direction. Second, minimum and maximum cubic numbers of C_1 , C_2 and C_3 are calculated in each direction. The cubes inside the x, y, and z boundary of C_1 , C_2 , and

C_3 are defined as the possible contact regions of triangle ABC . During the contact search, only nodes in the same cubes as the triangle and the adjacent cubes are calculated.

Among the three types of contact, node-to-surface contact is typically counted first. As such, if one node is determined to be in contact with the surface, it is excluded from the node-to-line contact search. Likewise, a node-to-line contact search is taken place after node-to-surface contact search. Only nodes that are in contact with neither the surface nor the line are searched in the node-to-node contact search. Three contact search methods are established and discussed in following sections.

4.2.2.1 Node to surface contact

As shown in Figure 4-5, point P is a node on the fabric, and triangle element ABC belongs to the projectile surface. When node P encounters triangle ABC , a virtual node O is generated to represent the physical point upon which the contact force is applied. Line PO is perpendicular to plane ABC , the shortest distance between node P and plane ABC .

In order for point P to be in contact with triangle element ABC , two conditions must be satisfied: 1) the distance between node P and the plane defined by element ABC must be smaller than the radius of the digital fiber, and 2) point O must be located on the triangular element.

Distance l_c between point P and the plane can be calculated as:

$$l_c = n_1(x_p - x_A) + n_2(y_p - y_A) + n_3(z_p - z_A) \quad (4-1)$$

where n_1 , n_2 , and n_3 are the x , y , and z components of the normal vector \vec{n} . Let vector \vec{r}_1 be a vector from point A to point B and \vec{r}_2 be a vector from point A to point C . The normal vector of triangle ABC can be calculated as $\vec{n} = \frac{\vec{r}_1 \times \vec{r}_2}{|\vec{r}_1 \times \vec{r}_2|}$. The direction of \vec{n} is determined using the right hand rule and should always point to outwards direction.

If the distance is smaller than the digital fiber radius, the location of point O must be verified. This can be accomplished with the following procedure: 1) divide triangle ABC into three sub-triangles: BCO , ACO , and ABO . 2) Calculate the area of each sub-triangle a_1 , a_2 , a_3 , and the area of triangle ABC , denoted as a . 3) If $a_1 + a_2 + a_3 = a$, node O is inside triangle ABC signifying that node P and triangle ABC are in contact. Otherwise, node O is outside triangle ABC , signifying that there is no contact between node P and triangle ABC . This latter case will be discussed in the next sub-section.

If there is a contact between node P and triangle ABC , contact force F_{PO} will be calculated and be distributed proportionally onto nodes A , B , and C , as such $F_A = \frac{a_1}{a} F_{PO}$, $F_B = \frac{a_2}{a} F_{PO}$, $F_C = \frac{a_3}{a} F_{PO}$, and $F_A + F_B + F_C = F_{PO}$. The direction of F_A , F_B , and F_C is the same as the direction of F_{PO} .

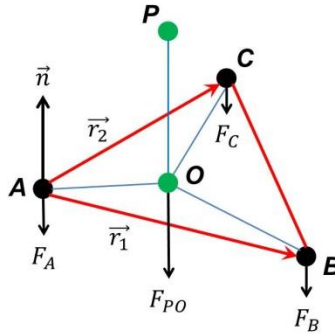


Figure 4-5 Node to Surface Contact

4.2.2.2 Node-to-line contact

As shown in Figure 4-7, assume node P contacts with the plane defined by triangular element ABC . However, the contact point is outside the element. As discussed in the previous subsection, no contact is defined between node P and the surface element. However, it is still

possible for the node to contact the intersection line between the element ABC and ABD , indicating contact between the node and projectile. As such, a node-to-line contact requires to be defined.

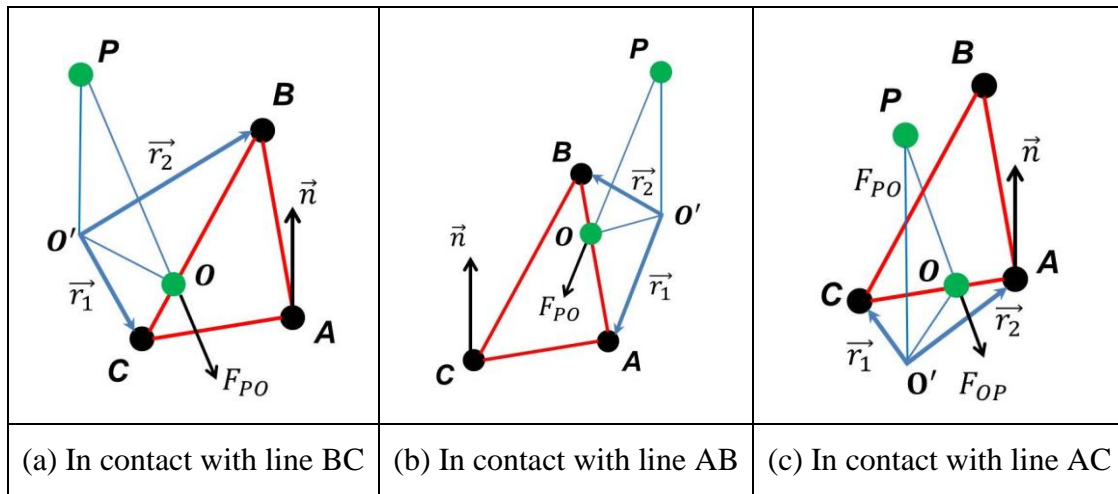


Figure 4-6 Node to Line Contact

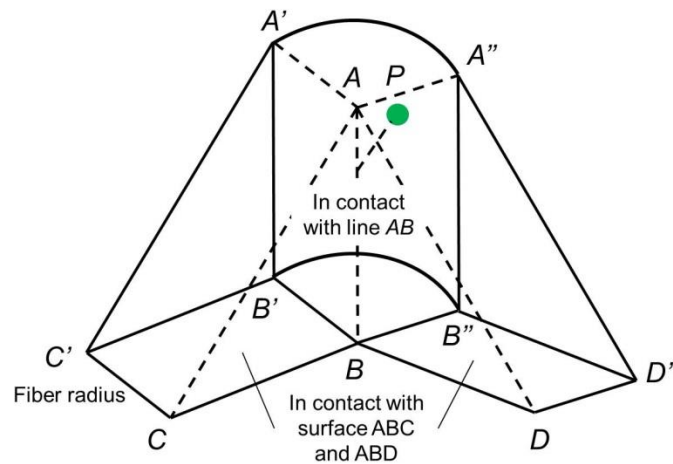


Figure 4-7 Contact between Node and the Intersection Line

In order for point P to be in contact with one of the three sides of the triangular element ABC , three conditions must be satisfied: 1) the distance between node P and at least one of the lines

defined by element boundary AB , BC and CA must be smaller than the radius of the digital fiber, 2) point O must be located inside segments AB , BC or CA , and 3) node P does not contact adjacent elements. Therefore, only nodes that are not in contact with triangle surface elements are looped again for searching node-to-line contacts.

First, derive vector $\overrightarrow{O'A}$, $\overrightarrow{O'B}$, and $\overrightarrow{O'C}$. If the direction of $\overrightarrow{O'A} \times \overrightarrow{O'C}$ is the same as the outward normal of the plane \vec{n} , node P is in possible contact with line AC . Likewise, if the direction of $\overrightarrow{O'C} \times \overrightarrow{O'B}$ is the same as the outward normal of the plane \vec{n} , node P is in possible contact with line BC . If the direction of $\overrightarrow{O'B} \times \overrightarrow{O'A}$ is the same as the outward normal of the plane \vec{n} , node P is in possible contact with line AB . These three situations are shown in Figure 4-6 (a), (b), and (c) respectively. Upon determining to which line node P belongs, the distance between the line and node P is calculated and then compared to the digital fiber radius. If the distance is smaller than the digital fiber radius, one needs to find contact point O . If point O is inside the corresponding segment (AB , BC or CA), a node-to-line contact will be established. Contact force is would be applied to point O in the direction of vector \overrightarrow{PO} , which is distributed proportionally to the two end nodes of the corresponding segments.

4.2.2.3 Node to node contact

Refer to Figure 4-6 again. Assume that contact point O is outside segments AB , BC , and CA . It is still possible to contact three corners of the triangle element. As such, node-to-node distance is calculated and then compared to the fiber radius. If the node-to-node distance is smaller than the fiber radius, the node is in contact with the triangle corner node, so force would only be applied to the corner node. Similarly, only nodes only nodes that are in contact with neither elements nor lines are looped for searching node-to-node contacts.

4.2.3 Contact calculation

Three types of forces are applied to the nodes: tension induced force, contact induced force, and friction force. Tension induced force exists within one fiber, while the remaining forces occur between two fibers or fibers and a projectile. Tension induced force and contact induced force have been introduced in the doctoral thesis of Huang [52]. A review of tension induced force and contact induced force are given in section 4.2.3.1 to 4.2.3.3. Projectile to fiber contact induced force and friction force are discussed in detail in section 0 and 4.2.3.3.

4.2.3.1 Tension induced nodal force

Tension induced nodal force occurs inside one fiber. Length of the rod element changes when forces are applied to the two ends of the rod element in longitudinal direction.

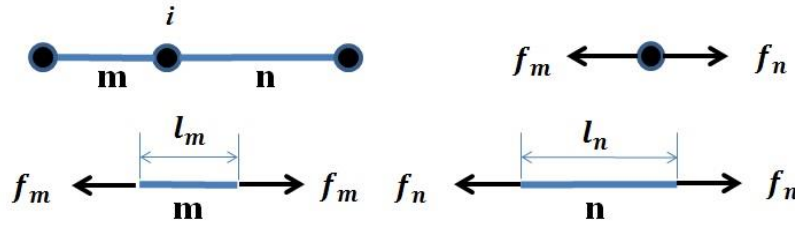


Figure 4-8 Tension Induced Force

As shown in Figure 4-8, node i is connected by two rod elements m and n , and the tension applied to node i is denoted as f_m and f_n .

$$f_m = E_L A \frac{l_m - l_0}{l_0} \quad (4-2)$$

$$f_n = E_L A \frac{l_n - l_0}{l_0} \quad (4-3)$$

where E_L is the modulus of the fiber in longitudinal direction, l_m is the length of the rod element m , l_n is the length of the rod element n , l_0 is denoted as the original length of the rod elements

before deformation, and A is the cross-sectional area of the fiber. The total tension induced force applied to node i is $F_i = f_m - f_n$.

4.2.3.2 Contact induced nodal force

Contact induced nodal force occurs between two fibers and a projectile and fiber. Two types of contact-induced force were involved in the simulation for this research: elastic contact and elasto-plastic contact. Elastic contact, commonly assumed when calculating contact induced force, is applicable for most textile materials. Elasto-plastic contact is designed especially for Kevlar KM2 fabric material, which is often used in ballistic impact simulation.

Elastic

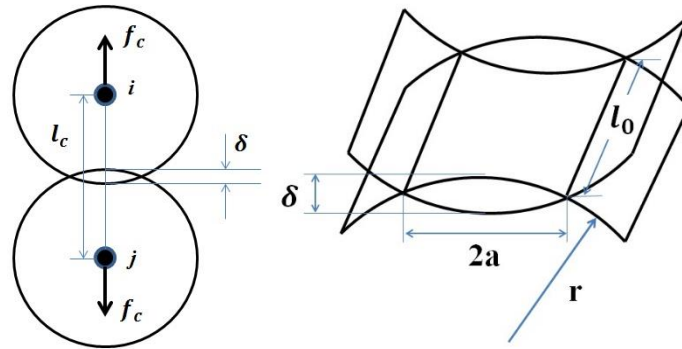


Figure 4-9 Elastic Contact Induced Force

Hertz contact theory [53] is adopted for elastic contact. As shown in Figure 4-9, i and j are two nodes on two separate fibers, and l_c is the distance between node i and j . When l_c is smaller than the total radius of the fiber to which node i and j belong, node i and j are in contact. Contact force between them is denoted as f_c .

$$df_c = k_c d\delta \quad (4-4)$$

where δ is the difference between l_c and the total radius of node i and j , k_c is contact stiffness, which can be calculated as

$$k_c = \frac{E_T A_c}{l_c} = \frac{2E_T a l_0}{l_c} \quad (4-5)$$

where E_T is the fiber modulus in transverse direction, A_c is the penetrated area between node i and node j , and defined as $2al_0$. l_0 is the original length of the element. When $\delta \ll r$, length of a can be calculated

$$a = \sqrt{r^2 - \left(r - \frac{\delta}{2}\right)^2} = \sqrt{r\delta - \frac{\delta^2}{4}} = \sqrt{r\delta} \quad (4-6)$$

where r is the radius of the fiber.

Substitute Equation (4-6) into Equation (4-5).

$$k_c = \frac{E_T A_c}{l_c} = \frac{2E_T \sqrt{r\delta} l_0}{l_c} \quad (4-7)$$

Substituting Equation (4-7) into Equation (4-4) and integrating Equation (4-4) with respect to δ , the total contact force can be described as

$$f_c = \int_0^\delta \frac{2E_T \sqrt{r\delta} l_0}{l_c} d\delta = \frac{4E_T \sqrt{r} l_0}{3l_c} \delta^{3/2} \quad (4-8)$$

Elasto-Plastic

In 2005, Chen et al. [8] investigated mechanical properties of a single Kevlar KM2 fiber using deterministic approach, and found that Kevlar KM2 fibers are linear elastic in the axial direction and non-linear elasto-plastic in the transverse direction. The stress-strain relationship of Kevlar KM2 fiber under transverse compression load was derived and studied by Wang et al.[43]. As shown in Figure 4-10, the black line is derived from experimental results, the green, blue, and red line are generated by Wang using curve fitting. The green curve was used in linear elastic contact calculation. The blue and red curve were used for elasto-plastic contact calculation. Large residual stress can be found between loading and unloading stage. Therefore,

in the modified DEA approach, Kevlar KM2 fibers were modeled as linear elastic in longitudinal direction and elasto-plastic in transverse direction [43]. In the loading stage, the stress can be expressed as

$$\bar{\sigma} = (6.9417\bar{\epsilon}^3 - 1.2208\bar{\epsilon}^2 + 0.5296\bar{\epsilon} + 0.0060) \times 10^9 \quad (4-9)$$

The slope of the unloading path can be expressed as:

$$K = (18.666\bar{\epsilon}_{max}^2 + 7.0632\bar{\epsilon}_{max} + 0.0646) \times 10^9 \quad (4-10)$$

Equations (4-9) and (4-10) were used to calculate transverse compression between digital fibers.

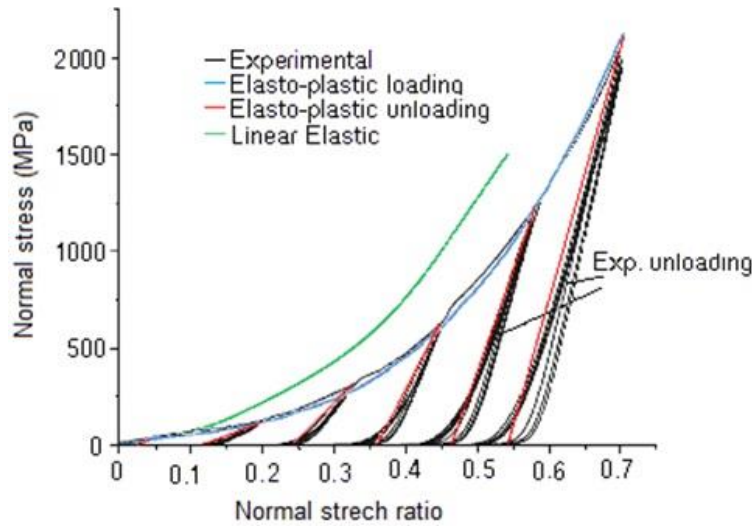


Figure 4-10 Transverse Nominal Stress and Strain Curve of Kevlar KM2 Fibers [43]

4.2.3.3 Friction force

Frictional forces are common between fibers and between fibers and projectile. It plays a critical role in simulating impact and penetration process. Friction coefficient varies in dry and wet conditions. Therefore, friction coefficient is designed to be assessable by users. Friction can be calculated as

$$\vec{F}_s = k_s \vec{U}_s \quad (4-11)$$

$$k_s = \mu k_n \quad (4-12)$$

where k_s is friction stiffness, \vec{U}_s is relative tangential displacement, \vec{F}_n is the normal force between contact elements, and μ is the friction coefficient.

If the calculated friction force $|F_s| > \mu F_n$, sliding occurs and $\vec{F}_s = \mu F_n \cdot \vec{U}_s$. If $|F_s| \leq \mu F_n$, sticking occurs, $\vec{F}_s = \mu \vec{k}_n \cdot \vec{U}_s$, and the kinetic friction coefficient and static friction coefficient are assumed to be identical.

When two nodes contact for the first time, no relative sliding occurs; friction force increases in subsequent steps. \vec{U}_s is determined by relative tangential displacement in the previous time step. As shown in Figure 4-11, node i and j initially comes into contact at step n . At step $n+1$, node i' and j' continue to be in contact. This process is called “sticking”. When two nodes stick together for two or more steps, frictional force is generated. Assume the position vector between i and j when they first come into contact is \vec{v}_0 , the position vector between i' and j' at any following steps is \vec{v}' . We can derive the following:

$$\vec{u} = \vec{v}' - \vec{v}_0 \quad (4-13)$$

$$\vec{u}_n = (\vec{u} \cdot \vec{v}') \frac{\vec{v}'}{|\vec{v}'|} \quad (4-14)$$

$$\vec{u}_s = \vec{u} - \vec{u}_n \quad (4-15)$$

By normalizing \vec{u}_s , the position vector of frictional force can be obtained.

\vec{v}_0 used in Equation (4-13) remains unchanged if node i and j are continuously in contact with each other, \vec{v}_0 is reset only after node i and j falls out of contact.

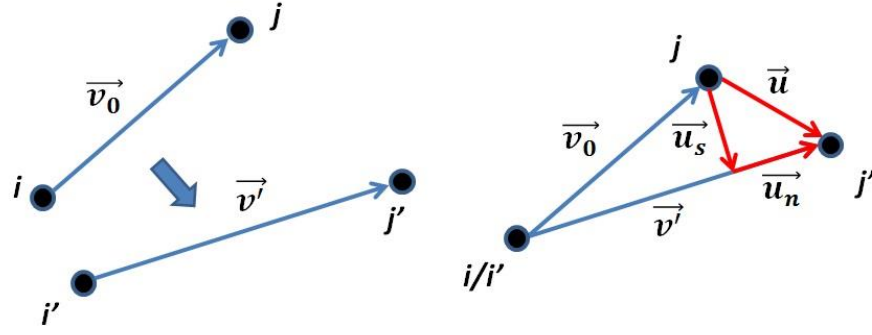


Figure 4-11 Friction Force

4.2.4 Failure algorithm

Fibers and matrix are the two major materials of textile composites. Compared to matrix, the weaving pattern and material properties of fiber take up a majority of the impact strength. As a result, fiber failure is the most common failure in textile impact simulation. In material design, fibers are mainly used to sustain loads along the fiber direction, thus the fiber strength and stiffness are regarded as the most important properties when considering fiber failure.

In the DEA, one fiber is simulated as a digital chain. The digital chain is made of rod element and frictionless pin. The length of the rod element changes when fiber is under loads along the fiber direction. Thus, stress of the rod element can be calculated as:

$$\varepsilon = E \frac{l - l_0}{l_0} \quad (4-16)$$

where E is the longitudinal modulus of the fiber, l_0 is the original length of the rod element, and l is the current length of the element.

When ε is bigger than the yield strength, the element is considered to have failed. If the elements on both sides of the node fail, the node is exempt from the calculation.

4.2.5 The explicit algorithm

In a single degree system, the relationship between mass, spring elements and viscous damper can be expressed as [54]:

$$(r_i)_e - (k_{ij})_e \times (u_i)_e - c(\dot{u}_i)_e = (m_{ij})_e \times (\ddot{u}_i)_e \quad (4-17)$$

where $(r_i)_e$ is the external force of element e applied to node i , $(k_{ij})_e$ is the element stiffness matrix, and $(u_i)_e$ is the relative displacement of element e with respect to the original position. Thus $(k_{ij})_e \times (u_i)_e$ is also known as the internal force. During each time step, element stiffness matrix of each element and the corresponding internal forces of each node are calculated, and then the nodal forces of each element are assembled into a global force vector. A central difference explicit direction integration algorithm is employed to calculate nodal velocity, acceleration, and displacement of the fabric, as well as the FE meshed projectile.

$$(a_i)_n = \frac{(F_i)_n}{m_i} \quad (4-18)$$

$$(v_i)_{n+1/2} = (v_i)_{n-1/2} + (a_i)_n \Delta t \quad (4-19)$$

$$(u_i)_{n+1} = (u_i)_n + (v_i)_{n+1/2} \Delta t \quad (4-20)$$

where i is the node number; n is the number of steps; m , F , a , v , and u represent nodal mass, force, acceleration, velocity, and displacement respectively. In every iteration, a Δt smaller than critical time step is used to maintain conditional stability. For FE meshed projectile, the internal nodal forces are calculated element by element and distributed onto each node. No global stiffness matrix is generated.

Seven simulation steps are involved in the modified DEA model:

1. Generate and mesh the projectile with detailed geometry using commercial FE software. Translate element and nodal information into DFMA readable format.

2. Identify projectile mesh surfaces and discretize each surface into two sub-triangle contact units.
3. Search contacts between fibers and save the contact pairs for fiber-to-fiber contact force calculation.
4. Search contacts between projectile surface and fabric and save contact pairs for projectile-to-fabric contact force calculation.
5. Calculate fabric stress and deformation. If the rod element strength is bigger than yield strength, the element is considered broken and exempted from further calculation.
6. Calculate the contact force applied to projectile and resultant velocity and nodal displacement and rotation.
7. Repeat step 2 to 6 until the perforation process is finished.

4.3 Ballistic impact to fabric using deformable projectile of arbitrary shape

An explicit nonlinear dynamic approach combining DEA and FEM is initiated. In this approach, projectile is modeled as an elastic deformable solid body. The explicit DEA is implemented to model fabric at filament level; while the deformation of arbitrary shape projectile is modeled using FEM. This approach is aimed to provide insights into high-speed ballistic perforation and serve as a solid foundation for bullet deformation modeling. The method of calculation projectile internal force and deformation is explained in following section.

4.3.1 Mass lumping

Direction mass lumping and variational mass lumping are two standard methods used to construct mass matrix for FEM dynamic analysis of structures. The mass matrix of a structural FEM model emerged as the discrete operator that converts nodal accelerations to inertia nodal forces [55]:

$$f_i = M \cdot \ddot{u} \quad (4-21)$$

where f_i is internal force, for a discrete dynamic system M denotes the constant masses in time. In the framework of the Direct Stiffness Method (DSM), the construction of M is realized through standard FE procedure: calculate element mass matrix in local coordinates; transform element mass matrix to global coordinates; merge the globalized element mass matrices using an element-by-element loop to form global master mass matrix M .

The preceding steps of deriving global stiffness matrix K is largely parallel that of global master mass matrix M . A notable difference with the stiffness matrix is the possibility of converting M to a diagonally lumped mass matrix (DLMM) using direction mass lumping method. The advantages of DLMM are: can be stored as a vector; none zero entries, and easy to invert in space, which significantly simplified computations related to M^{-1} .

Explicit time integration is used in modified DEA approach in calculating projectile nodal velocity, acceleration, and displacement. Therefore, it is imperative to convert the master mass matrix into a lumped mass matrix. Master mass matrix obtained from the same shape function used for obtaining stiffness matrix is also called consistent mass matrix (CMM), and is defined by the choice of kinetic energy functional and shape functions. A large amount of mass diagonalization schemes starts from the CMM. In this research, mass diagonalization method Hinton-Rock-Zienkiewicz (HRZ) lumping was adopted to formulate the diagonal mass matrix.

In modified DEA approach, three translational Degree of Freedom (DOF) and three rotational DOF are contributed to the projectile motion. Assume the element CMM can be written as

$$m_e = \begin{bmatrix} m_{11} & m_{12} & m_{13} & & m_{16} & m_{17} & m_{18} \\ m_{21} & m_{22} & m_{23} & \dots & m_{26} & m_{27} & m_{28} \\ m_{31} & m_{32} & m_{33} & & m_{36} & m_{37} & m_{38} \\ & \vdots & & \ddots & & \vdots & \\ m_{61} & m_{62} & m_{63} & & m_{66} & m_{67} & m_{68} \\ m_{71} & m_{72} & m_{73} & \dots & m_{76} & m_{77} & m_{78} \\ m_{81} & m_{82} & m_{83} & & m_{86} & m_{87} & m_{88} \end{bmatrix} \quad (4-22)$$

Firstly add up the diagonal entries of CMM relative to translational DOF and set to D . Secondly, add up the entries of both translational DOF and rotational DOF and set to S . Third, apportion S to DLMM on dividing the CMM diagonal entries by D . Fourth, set the non-diagonal entries to zero. This procedure is expressed in equations from (4-23) to (4-25).

$$D = \sum_{i=0}^8 \sum_{i=0}^8 m_{ii} \quad (4-23)$$

$$S = \sum_{i=0}^8 \sum_{j=0}^8 m_{ij} \quad (4-24)$$

$$m_e = \text{diag}[\frac{S}{D} m_{ii}] \quad (4-25)$$

HRZ lumping method is convenient to implement and applicable to a broad range of element when a CMM is available, and retaining non-negativity. DLMM yields more reasonable results under the condition that the element has only translational freedoms. If rotational freedoms exist in the system the results can be poor compared to customized templates.

4.4 Validations

The previous DEA successfully simulate ballistic impact and penetration of textile fabrics. The DEA models the fabric as an assembly of yarns; yarns are made of fiber bundles. In contrast to other well-established models, this approach models the textile relaxation process at the filament level and is computer resource friendly.

Projectile deformation is seldom discussed in previous literature. However, a bullet deforms or disintegrates under high-speed impact. In the previous DEA, projectile is treated as a rigid body or a particle, as such only spherical and cylindrical shaped projectiles can be simulated. The combined DEA and FEM approach models projectile of arbitrary shape as deformable solid body. The example projectiles presented in the simulations below were all generated and meshed using commercial software ANSYS. The FEM is integrated in explicit algorithm to calculate projectile deformation during each time step.

In this section, two types of simulations were performed using the combined DEA and FEM solver. In the first set of simulations, ballistic impact is simulated using rigid body projectiles. The objective of this simulation is to validate the approach in simulating ballistic impact of arbitrary shape projectile. In order to have the same numerical precondition as the DEA, both spherical and cylindrical projectiles are modeled as rigid bodies. No projectile deformation occurred during the impact event.

In the second set of simulations, ballistic impact is simulated using solid body deformable projectiles. The objective of this simulation is to evaluate the accuracy and capacity of the code in simulating ballistic impact of deformable arbitrary shape projectile. Projectile internal force and deformation are calculated. Each projectile is simulated four to five times using different material properties. For each test, the modulus was 10 times smaller than the previous test. Simulation details are discussed below.

4.4.1 Material properties and projectile geometry

The fabric material and projectile properties used in this simulation are listed in Table 4-1 and Table 4-2. The fabric, 2-D plain weave, is a 1 in. \times 1 in. rectangular fixed in all four boundaries.

Table 4-1 Material Properties of Kevlar KM2

Type	E11 (Pa)	E22 (Pa)	Strength (Pa)	ρ (kg/m³)
Kevlar KM2	8.46e10	1.34e9	3.8e9	1440

Projectile is initially positioned at the center of the fabric, with an initial velocity of 50 m/s directed towards the fabric. Projectile geometry and material properties provided by ARL (Army Research Lab).

Table 4-2 Projectile Geometry

Projectile type	Diameter (m)	Mass (kg)	Density (kg/m³)	E11(Pa)	E22(Pa)	Height (m)	v
Sphere	0.00556	0.000692	7689	2.09e11	2.09e11	-	0.3
RCC	0.0034	0.0002592	7689	2.09e11	2.09e11	0.0037	0.3

4.4.2 Ballistic impact simulation using rigid body projectile

Ballistic impact of textile fabrics using rigid body spherical and cylindrical projectiles is simulated using the modified DEA approach. Simulation results from the modified DEA approach are compared to results from the previous DEA.

4.4.2.1 Mesh convergence check

The total nodes of the fabric and the mesh density of the projectile affect computational time spent on the dynamic FE impact simulation. In general, the higher mesh density of the projectile, the more accurate the results will be. As the total number of nodes in projectile increases, the simulation result converges. One of the objectives of this simulation is to find the least number of nodes of projectile, which produces smallest discrepancy, comparing to the well-

published results from the previous DEA. Projectiles with different mesh densities were simulated.

Table 4-3 shows the simulation results of FE meshed spherical projectile using the modified DEA approach. The total nodes of FE meshed projectiles ranged from 53 to 2248 nodes with a corresponding total element varying from 32 to 2037. The maximum projectile force and bounce back velocity calculated during simulation are compared to results from the previous DEA, and the discrepancies and projectile details are listed below.

Table 4-3 Simulation Results for FE Spherical Projectiles

Test #	Simulation time (min)	# of elements	# of nodes	Max. projectile force(N)	Discrepancy	Rebound speed (m/s)	Discrepancy
1	13	32	53	793.51	-22.5%	37.29	-2.97%
2	88	256	321	950.12	-7.20%	38.54	0.284%
3	234	649	779	992.13	-3.10%	38.42	-0.028%
4	318	864	997	990.37	-3.27%	38.55	0.314%
5	925	2037	2248	994.45	-2.87%	37.95	-1.26%

Results of the maximum projectile force shows that, for spherical projectile, when the total number of nodes increases, the modified DEA simulation results more closely resembled the previous DEA results. However, when the total number of nodes reaches 779 or more, the simulation results between the modified DEA and the previous DEA approach are almost identical. The deviation of the bounce back speed is much smaller compares to the results of maximum projectile force. Approximately 2.7% improvement is noted between Test 1 and Test 2 on rebound speed. However, as the total number of nodes exceeded 779, the discrepancy

between the rebound speeds derive from the modified DEA and the previous DEA approach became bigger.

Figure 4-12 shows the calculation time steps-projectile force curve. The red curve is derived from the previous DEA; other curves are derived from the modified DEA approach. Discrepancies between the modified DEA and the previous DEA approach are observed in Test 1 and 2 before and after the projectile reaches maximum force. The results from Test 3, 4, and 5 overlapped each other and closely matched the blue curve.

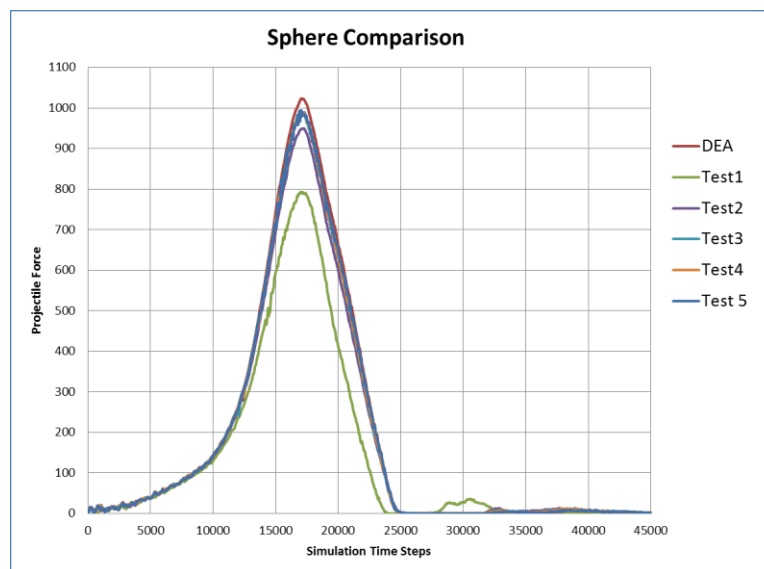


Figure 4-12 Projectile Force Comparison for Spherical Projectile

Table 4-4 shows the simulation results of FE meshed cylindrical projectile using dynamic FE approach. Similarly, simulated maximum projectile force and rebound speed are compared to results obtained from the DEA.

Table 4-4 Simulation Results for FE Cylindrical Projectiles

Test #	Simulation time (min)	# of elements	# of nodes	Max. projectile force(N)	Discrepancy	Rebound speed (m/s)	Discrepancy
1	35	96	171	345.62	-3.91%	34.64	-0.99%
2	115	324	484	354.04	-1.57%	35.22	0.67%
3	296	768	1045	356.08	-1.00%	35.09	0.29%
4	667	1500	1926	353.95	-1.59%	34.92	-0.20%

Likewise, similar conclusions can be reached for cylindrical projectiles test results. Table 4-4 showed that discrepancies of both maximum projectile force and rebound speed decrease when the number of elements in projectile increases. The variation of the number of elements has a smaller effect on predicting rebound speed than it does on predicting maximum projectile force. However, the mesh density of cylindrical projectiles has significantly less effect on simulation results than spherical projectiles. Less than 0.8% improvement on rebound speed is observed between Test 1 and Test 4.

Figure 4-13 shows the diagram of simulation time steps versus the projectile force. The blue curve is the projectile force from the previous DEA; other curves are from the modified DEA approach. Discrepancies between the modified DEA and the previous DEA approach were visible in Test 1. As mesh density increased, the simulation results of Test 3 to 5 closely match results from the previous DEA.

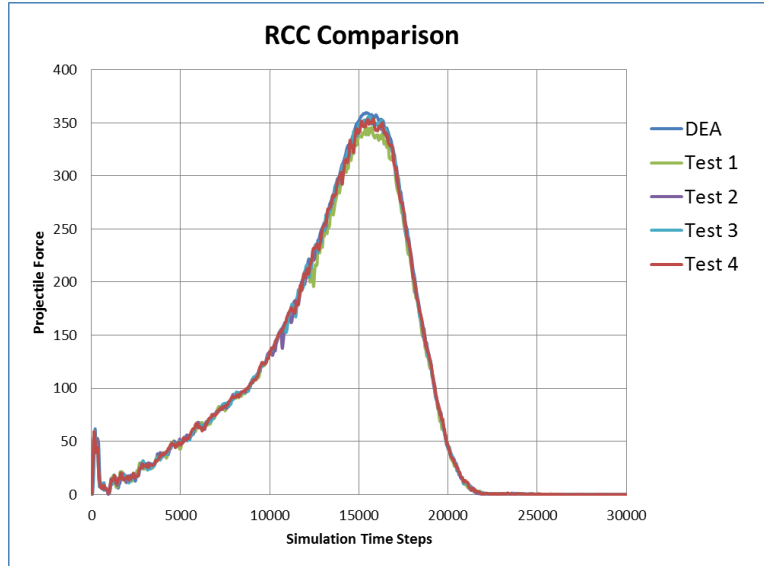


Figure 4-13 Projectile Force Comparison for RCC Projectile

From the above two sets of simulation described, following conclusions are reached:

1. Simulation results of the modified DEA approach using spherical and cylindrical projectiles closely resemble the results of the previous DEA. The modified DEA approach successfully replicates the results from the previous DEA and is capable of simulating ballistic impact of textile fabrics using rigid body projectiles of arbitrary shape. The numerical maximum projectile force and bounce back speed diagram with respect to time match closely that of the previous DEA.
2. General speaking, the increase of mesh density improves simulation results. However, when the projectile total number of nodes reached 1000, the improvement of mesh density on simulation results became trivial, occasionally leading to slightly less accurate results than projectiles with coarser mesh.
3. Mesh density has a greater effect on spherical projectiles than cylindrical projectiles.

4. Because higher mesh density consumes significantly more computational time, a total number of nodes between 500 and 1000 is recommended for time-efficient simulation.

5. The PC based modified DEA approach analyzer provides guidance for simulation of deformable and real shape bullets. To simulate large-scale textile fabrics, it is imperative to transfer the PC based code to cluster code.

4.4.3 Ballistic impact simulation using deformable projectile

Dynamic FE approach is designed to simulate ballistic impact of textile fabrics using elastic deformable projectiles, and provide insights for high-speed bullet perforation process and failure mechanism of real bullets. Ballistic impact of textile fabrics using sphere, RCC and FSP projectiles is simulated to test the code capability. The purposes of this simulation are 1. Verify simulation results from the dynamic FE approach using deformable projectiles. Test the ability of the dynamic FE approach code in simulating solid body deformable projectiles of arbitrary shape. 2. Predict the elastic deformed projectile shape due to impact. 3. Evaluate the limitations of the PC based code and provide valid results for transforming into a cluster code.

The fabric, spherical and RCC projectiles used in this simulation are the same as section 4.4.2. Fabric material and projectile dimensions are listed in Table 4-1 and Table 4-2. The simulation results of spherical and RCC projectile obtained from the dynamic FE approach are compared to simulation results obtained from the previous DEA.

Ballistic impact of textile fabrics using FSP projectile is simulated for the first time to test the capability of the DEA-FEM solver and provide insights for ballistic deformation simulation. No numerical data has been obtained from the previous DEA. The feasibility of the dynamic FE approach and further research work are discussed.

For each type of projectile, 4 to 5 tests are simulated with different material properties, the modulus of which decreased gradually by a multiple of 10. The E_{11} and E_{22} of each test are listed below.

Table 4-5 Projectile Modulus

Test #	1	2	3	4	5
E_{11}	2.09e11	2.09e10	2.09e9	2.09e8	2.09e7
E_{22}	2.09e11	2.09e10	2.09e9	2.09e8	2.09e7

All projectiles are generated and meshed with 8-node solid elements. Based on the conclusions derived from section 4.4.2, the projectile total node used in this simulation is approximately 700.

4.4.3.1 High modulus projectile simulation results

Spherical and RCC projectiles are made of steel and commonly used in ballistic test. The modulus of steel in longitudinal and transverse direction is 2.09e11. Because of the high modulus, the deformation of spherical and RCC projectiles during low speed ballistic tests is negligible. Therefore, numerical results from Test 1 are compared to results from the DEA to validate the dynamic FE approach. The calculation time steps versus projectile force curves are shown below.

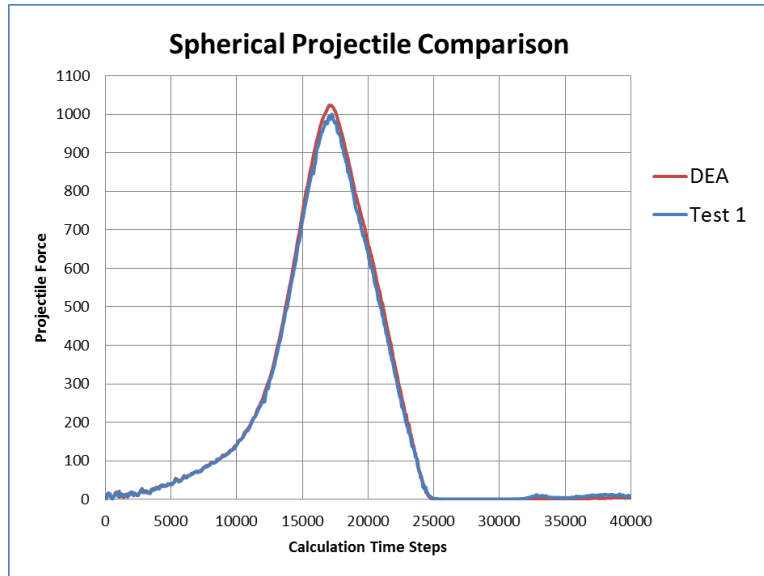


Figure 4-14 Spherical Projectile Comparison

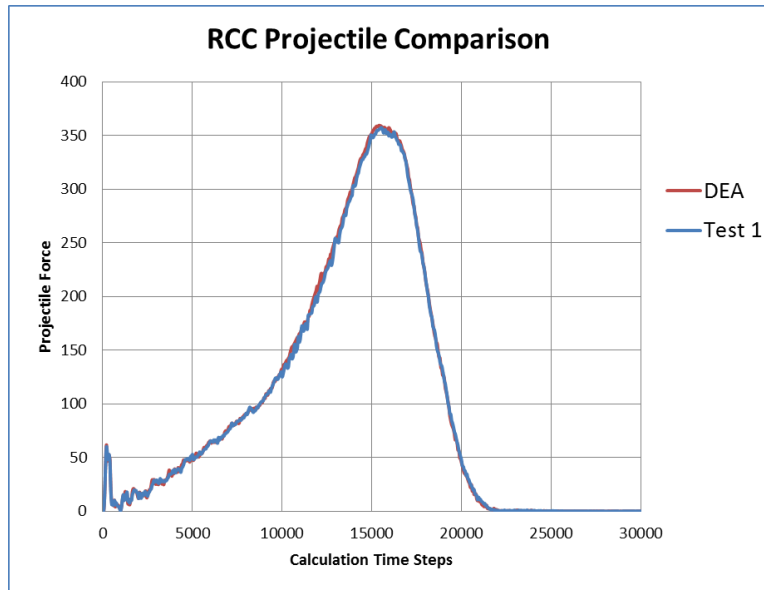


Figure 4-15 RCC Projectile Comparison

Figure 4-14 and Figure 4-15 shows the numerical results from the previous DEA and the dynamic FE approach. Total force applied to the projectile is calculated every time step. Red curve is derived from the previous DEA, and blue is derived from the dynamic FE approach. Simulation results of deformable solid body spherical and RCC projectiles from the dynamic FE

approach closely resemble the simulation results from the previous DEA. The dynamic FE approach of simulating ballistic impact using deformable projectiles is successfully validated.

4.4.3.2 Low modulus projectile simulation results

Ballistic impact of textile fabrics using projectiles with variable modulus is simulated by the dynamic FE approach. The purpose of the simulation is to compare deformation of projectiles made of different materials and their effect on projectile force.

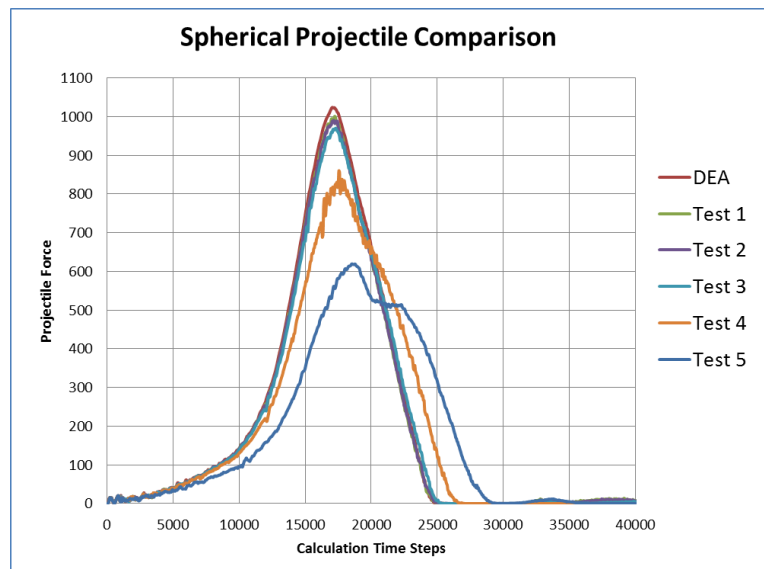


Figure 4-16 Spherical Projectile with Different Modulus Comparison

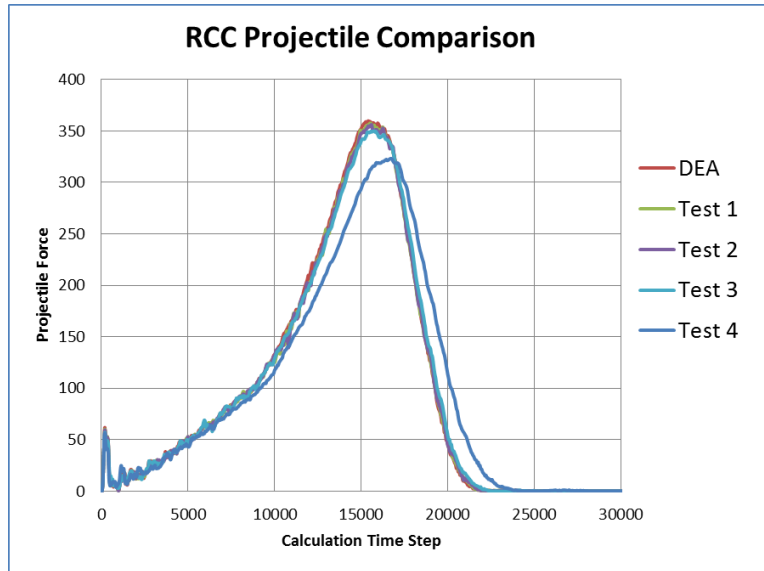


Figure 4-17 RCC Projectile with Different Modulus Comparison

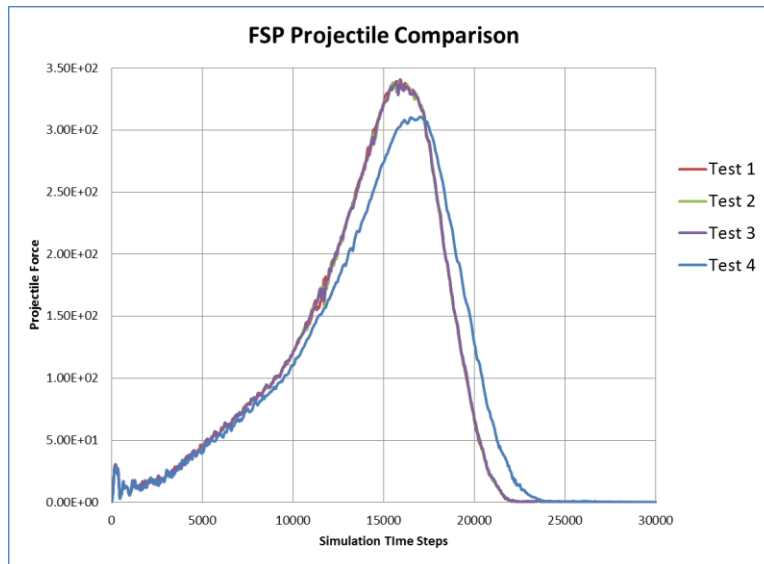


Figure 4-18 FSP Projectile with Different Modulus Comparison

Figure 4-16 and Figure 4-17 show the simulation results of spherical and RCC projectile with different modulus. The red line is derived from the previous DEA. One can see, as the projectile modulus decreases, the projectile force decreases. Simulation results of Test 1 to Test 3 are similar to the simulation results of the previous DEA. Simulation results of Test 4 and 5

differ from the results of the DEA by more than 10%. Figure 4-18 shows the numerical results of FSP projectile. The shape of FSP is similar to the shape of RCC with two symmetrical 35 ° cuts on each side of the front nose. The numerical maximum projectile force of FSP was slightly lower than that of RCC. No numerical data is obtained from the previous DEA using FSP projectile. The simulation results obtained from the dynamic FE approach using FSP with varied material modulus followed the same pattern as that of spherical and RCC projectile. The dynamic FE approach successfully simulates ballistic impact of textile fabrics using deformable projectiles of arbitrary shape. However, comparison between numerical results and experimental results needs to be made to further validate the approach.

4.5 Conclusion

The combined DEA and FEM solver are developed to evaluate ballistic strength of textile fabric using deformable projectiles of arbitrary shape. This approach models the textile fabric at filament level and the projectile as solid body of arbitrary shape. Projectile deformation is predicted using dynamic FEM solver. The following conclusions are reached:

1. The DEA successfully incorporated material properties of Kevlar KM2. Simulation results of spherical and cylindrical projectiles closely matched experimental results.
2. Spherical and cylindrical projectiles are generated and meshed with different mesh densities. The simulation results from the combined DEA and FEM solver match the simulation results from the previous DEA approach.
3. Mesh density has great influence on computational time, but not necessarily leads to results that are more accurate. A total projectile node between 500 and 1000 is estimated to be most time efficient.

4. The combined DEA and FEM solver is capable of simulating ballistic impact using rigid body projectiles with arbitrary shape.

5. Deformable spherical, RCC, and FSP projectiles are simulated using combined DEA and FEM approach to test the code strength. This approach is capable of simulating ballistic impact using deformable projectiles of arbitrary shape. Due to the lack of experimental data, no comparison is made between numerical results and experimental results. Further validation of ballistic impact of textiles using deformable projectiles is required.

6. Although PC based code is convenient for systematic monitoring and vision inspection, due to limited computer resources, no real-size model can be simulated. It is imperative to transform the PC based code to cluster code.

Chapter 5 - Modified DEA

In this chapter, a modified digital element approach (DEA) is introduced to determine the ballistic limit of multi-layer Kevlar KM-2 fabric soft armors against fragment simulating projectiles (FSP). The previous version of the DEA assumed that the digital fiber is fully flexible and its bending rigidity is negligible. Shear force was thus neglected. It was found that fabrics could fail due to shear force when projectiles with sharp edge(s), such as FSP, were applied in numerical simulation. Therefore, numerical tests are conducted to determine the effective bending rigidity of digital fibers. A combined tension-shear failure model is incorporated into the DEA.

5.1 Previous version of the DEA

In the previous iteration of the DEA, numerical results overestimated the ballistic limit of 2-D woven fabric against projectiles with sharp edges, such as the right RCC and FSP. It was found that fibers fail along the sharp edge due to shear force. The digital fiber was assumed fully flexible and the bending rigidity was assumed negligible. As such, shear force was not captured by numerical simulation.

The DEA model is modified in this research project in two aspects: (1) consideration of fiber bending rigidity, and, (2) modification of failure criteria for digital fibers.

5.2 Modified DEA Formulation

5.2.1 Shear force and bending rigidity relations

In the modified version, the free pin, connecting two adjacent elements at node i , is replaced by a torsional spring as shown in Figure 5-1. Assume the element length is l_0 , the angle between two elements θ_i , the torsional rigidity of the spring is K_t , and the moment at node i is M_i . Q is the shear force applied to the element.

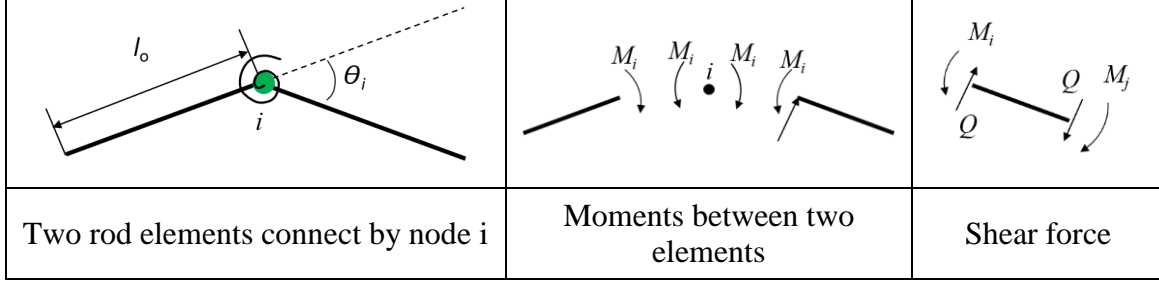


Figure 5-1 Shear Force Calculation

The moment M_i can be calculated as:

$$M_i = K_t \theta_i \quad (5-1)$$

The curvature of the fiber can be derived as:

$$\kappa_i = \frac{\theta_i}{l_0} \quad (5-2)$$

As such, the moment and curvature relation can be derived as:

$$M_i = K_t l_0 \kappa_i = K_b \kappa_i \quad (5-3)$$

The bending rigidity of the shear force can be calculated as:

$$Q = (M_i - M_j)/l_0 \quad (5-4)$$

where κ_i is the radius of curvature of two adjacent elements, M_i is the moment, I is the digital fiber area moment of inertia, E is the longitudinal fiber modulus, Q is the shear force. Maximum shear stress in a circular cross-section beam is:

$$\tau_{max} = \frac{4Q}{3A} \quad (5-5)$$

5.2.2 Fiber strength and failure criterion

Kevlar KM2 fabrics are used for both numerical simulations and real scale standard ballistic tests. Single fiber tests have been conducted to determine the Weibull distribution of fiber strength. In order to examine possible fiber damage due to the weaving process, weft and

warp yarns were taken from an actual fabric. It was found that fibers from the warp yarns are slightly weaker than fibers from weft yarns. As such, warp fiber strength is applied for the numerical simulation using Weibull distribution as discussed in 2.2.3.1.

Fiber failure is detected, when:

$$\left(\frac{\sigma}{\sigma_u}\right)^2 + \left(\frac{\tau}{\tau_u}\right)^2 > 1 \quad (5-6)$$

where σ_u is fiber tensile strength, τ_u is fiber shear strength. An experimental tensile strength, calculated by Dr. Lease at Kansas State Mechanical Testing Laboratory from as received Kevlar KM2 shoot packs with variable areal densities, is assigned to each element utilizing Monte Carlo process, following a bimodal Weibull distribution function. Sanborn B. and Weerasooriya T. [56] investigated the effect of strain rate and fiber pre-twist on failure strength at Army Research Lab (ARL). Using the experimental data obtained from ARL, Wang determined the saturated strength ratio and solved for shear strength. Shear stress 0.7672GPa is used in all simulation presented in this paper [57].

Fiber bending rigidity is directly related to shear force. If bending rigidity is known, the shear force applied to fiber can be determined based on force equilibrium.

5.2.3 Effective bending rigidity of the digital fiber

The process of discretization models textile relaxing process at near fiber level and allows changes to yarn cross-section shape. As shown in Figure 5-2, assume elliptical cross-section yarn shape, a digital yarn is discretized into 25 digital fibers. However, a real yarn is composed of hundreds of actual fibers. By comparing the 25 digital mesh model, with actual fiber model, one can see a digital fiber represents a small bundle of actual fibers. The number of actual fibers a digital fiber represents equals to the number of actual fiber per yarn divided by the number of digital fiber per yarn.

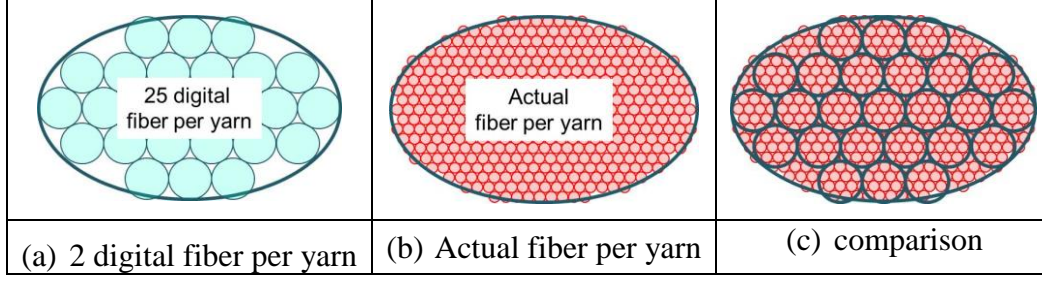


Figure 5-2 Comparison between 19-d Fibers and Actual Fibers per Yarn

Digital fiber bending rigidity is related to inter-fiber friction. If inter-fiber friction is negligible, each actual fiber inside the digital fiber can bend freely. The moment of inertia of the digital fiber should be the summation of all actual fibers represented by the digital fibers. The bending rigidity of the digital fiber can be calculated as:

$$K_b = nI_a E = I_0 E \quad (5-7)$$

where n denotes the number of actual fibers that a digital fiber represents. $I_a = \pi d_a^4 / 64$ denotes the moment of inertia of an actual fiber, d_a is the diameter of the actual fiber, and E is the actual fiber modulus. I_0 is defined as the effective modulus of a digital fiber when the friction coefficient equals zero.

If the friction is large enough to stop the relative motion between actual fibers, the digital fiber can be approximately modeled as a solid unity with a circular cross section as shown in Figure 5-3. The digital fiber cross-section area is equal to the summation of all actual fiber cross-section areas. As such, the bending rigidity of the digital fiber can be approximated as:

$$K_b = \frac{\pi d_d^4}{64} E = I_\infty E \quad (5-8)$$

where d_d denotes the diameter of the digital fiber. I_∞ is defined as the effective moment of inertia of the digital fiber if inter-fiber friction is large enough to prevent inter-fiber relative motion in the axial direction.

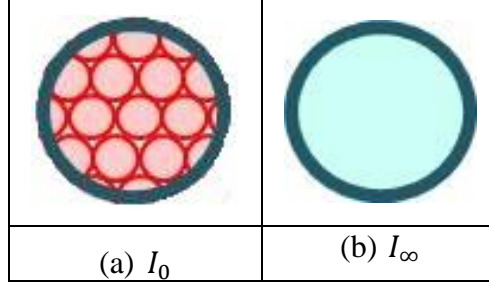


Figure 5-3 Digital Fiber Area Moment of Inertia

Generally speaking, I_∞ is much greater than I_0 . The I_∞/I_0 ratio is equal to the ratio between the digital fiber cross-section area and the actual fiber cross-section area, which is also equal to n , the number of actual fibers that a digital fiber represents, i.e.:

$$\frac{I_\infty}{I_0} = \frac{A_d}{A_a} = n \quad (5-9)$$

where A_d denotes the digital fiber cross-section area and A_a the actual fiber cross-section area. When the number of actual fibers per yarn equals to the number of digital fibers per yarn, $I_0 = I_\infty$. In the real situation, friction exists, so the digital fiber effective moment of inertia should be larger than I_0 . On the other hand, there are relative movements between fibers. As such, the digital fiber effective moment of inertia should be smaller than I_∞ . Therefore, we assume the effective moment of inertia can be derived from the following equation with two variables:

$$I = \left(\frac{\mu}{k_2}\right)^{k_1} I_\infty + \left[1 - \left(\frac{\mu}{k_2}\right)^{k_1}\right] I_0 \quad (5-10)$$

where μ is the inter-fiber friction coefficient and k_1 and k_2 are two variables which will be determined by a numerical test in the next sub-section. The effective moment of inertia I_e and the friction coefficient μ relation is shown in Figure 5-4. When $\mu=0$ and $I = I_0$, each actual fiber acts independently; when $\mu = k_2$, $I = I_\infty$. Therefore k_2 represents the inter-fiber friction coefficient that stops relative fiber movement. k_1 represents the shape of the curve.

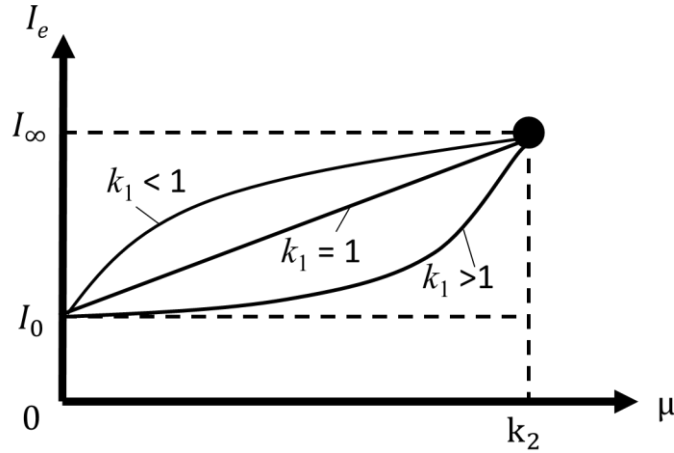


Figure 5-4 Effective Moment of Inertia and Friction Coefficient Relation

5.3 Estimate effective moment of inertia

The digital fiber effective moment of inertia I_e is determined by two variables k_1 and k_2 . In this section, numerical tests are performed to determine the value of the two variables. A circular cylinder projectile impacts a single 0.4 k Kevlar KM-2 yarn. On each end, a small mass is applied to provide stability. The mass is constrained by a friction surface parallel to yarn alignment. The maximum friction of each mass is 10N. Fibers are constrained from spreading laterally during the impact event. The simulation setup is shown in Figure 5-5.

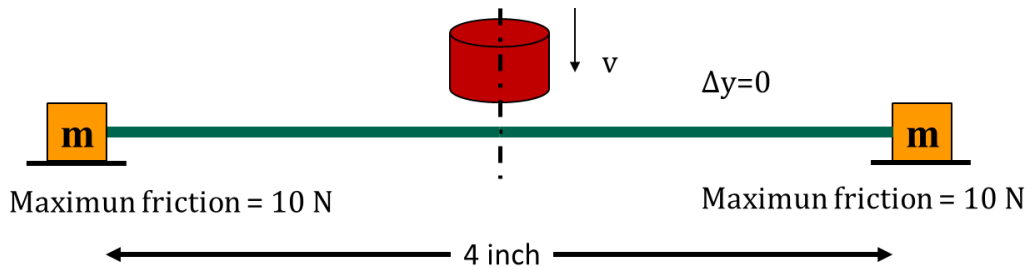
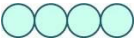
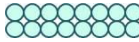
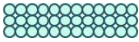






Figure 5-5 Single Yarn Model

No initial stress exists prior to the impact. The cylindrical projectile has a diameter of 0.00556m, height 0.0037m, weight 5e-5kg, with edge radius 50 μ m. To increase fiber failure due to shear force, the tensile strength used in this simulation is 7.76e9Pa, double the strength of Kevlar KM2. The shear strength used in this simulation is 1.92e8Pa, 1/4 of the actual shear strength. The yarn cross-section shape for 4- to 196-digital fibers per yarn is designed to be the same only varied in number of digital fibers; as such, the number of fibers in x direction is always 4 times the number of fibers in y direction in all test examples. The cross-section yarn shapes depicted are displayed in Table 5-1.

Table 5-1 Single Yarn Cross-section Shape

						
4-d	16-d	36-d	64-d	100-d	144-d	196-d

d: digital fiber per yarn.

The V_{50} of 4- to 196-digital fibers per yarn is calculated using digital fiber area moment of inertia I_0 and I_∞ . When $I = I_0$, the effect of inter-fiber friction on relative motion between fibers is insignificant, which leads to low digital fiber bending rigidity and high V_{50} . When $I = I_\infty$, inter-fiber friction stops relative motion between fibers, resulting in high digital fiber bending rigidity and low V_{50} . Simulation results are listed in Table 5-2.

Table 5-2 V_{50} of a Single Yarn Impacted by Cylindrical Projectile using I_∞ and I_0

Fiber #	4-d	16-d	36-d	64-d	100-d	144-d	196-d
I_0	255	215	185	155	135	125	115
I_∞	45	45	55	78	85	95	95

unit: m/s, $\mu=0.3$.

However, as aforementioned, it is impossible to use an actual fiber or yarn model to simulate ballistic impact due to computer resource limitation. The impact strength of a 64-digital fiber per yarn model is simulated using $I_e = I_0$ under different inter-fiber frictions to estimate k_2 . When μ increases until a critical value, relative motion between fibers decreases, resulting in a higher digital fiber bending rigidity and a lower impact strength. If μ reaches the critical value, the inter-fiber relative movement is limited. The impact strength ceases to decrease. The critical value is defined as $k_2 = \mu$. Numerical results are listed in Table 5-3. When μ reaches 1 or above, impact strength remains constant. As a result, k_2 is assumed to be 1.

Table 5-3 V_{50} of 64 Digital Fiber per Yarn Model using I_0

μ	0.3	0.5	0.7	1	2
Impact strength (m/s)	155	147	143	125	125

Then, the impact strength of 4- to 196-digital fibers per yarn is numerically derived using $k_2 = 1$ and $k_1 = 1.4, 1.2, 1$, and 0.8 . The purpose of these simulations is to estimate k_1 . When $k_1 = 0.8$, the impact strength for all amounts of digital fibers within a yarn model approaches the same; impact strength fluctuates around the dashed line. Therefore, k_1 is estimated to be 0.8 . The result is shown in Figure 5-6.

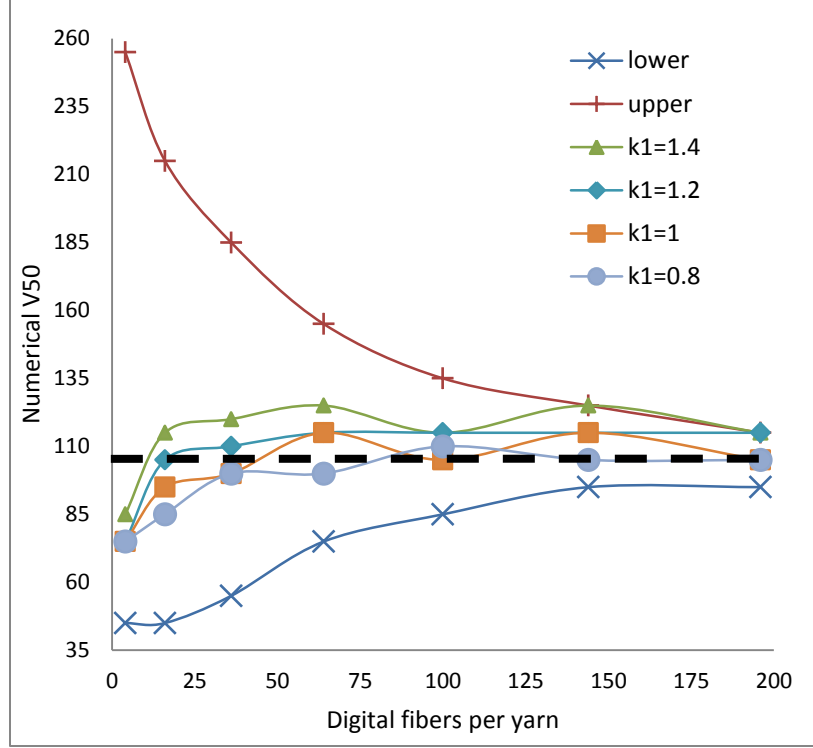


Figure 5-6 V_{50} of 4- to 196-digital Fibers per Yarn

5.4 Conclusion

The relationship between shear force and fiber bending rigidity is explained in this chapter. Digital fiber effective bending rigidity is derived by means of actual fiber bending rigidity and inter-fiber friction coefficient. Digital fiber effective bending rigidity is numerically calculated using 4- to 196-fibers per yarn model. Following conclusions can be reached from the above results:

1. Impact limit derived from I_0 is always higher than that derived from I_∞ because I_0 is much smaller than I_∞ . Smaller effective moment of inertia results in a smaller shear force and higher impact strength. As such, the impact strength derived from I_0 represents an upper bound and the impact strength derived from I_∞ represents a lower bound as shown in Figure 5-6.

2. As the number of digital fibers per yarn increases, impact strength derived from I_0 (Upper bound) decreases; inversely, impact strength derived from I_∞ (Lower bound) increases. The two curves approach gradually with an increase in the number of digital fibers. If the number of digital fibers approach the number of actual fibers, $I_0 = I_\infty$. The upper bound and lower bound converges.

3. The simulated V_{50} for all fibers per yarn using $k_2 = 1$ and $k_1 = 0.8, 1, 1.2, \text{ and } 1.4$ is in between the upper bound and lower bound. When k_1 decreases, the simulated V_{50} decreases. The black dashed line in Figure 5-6 indicates the V_{50} using 400 digital fibers per yarn. When $k_1 = 0.8$, the simulated V_{50} for all number of digital fibers per yarn model approaches the same and fluctuates around the V_{50} of actual number of fibers per yarn. Therefore, k_1 is estimated to be 0.8.

Chapter 6 - Numerical simulation

Experimental results of 14 standard sets of Kevlar KM2 shoot packs with varied areal densities are received from the United States test labs. Seven shoot packs are tested using RCC projectile, and 7 shoot packs are tested using FSP projectile. Real scale impact simulations using RCC projectile were performed and verified by the digital element approach. However, simulation results of FSP projectile have not been compared.

In this chapter, the modified DEA is applied to estimate ballistic limit of multi-layer Kevlar KM2 fabric soft armor against FSP. A 3-D microscope is applied to measure the radius of FSP along the edge. Numerical results are compared to high-resolution experimental test data.

6.1 Convergence analysis

Near fiber-level simulation is achieved in the DEA by discretizing one yarn into multiple digital fibers. The number of digital fibers per yarn is a user-defined parameter, which can be up to that of actual fibers per yarn. Refer to section 3.2, a digital element length of 1/2 element diameter or less is recommended for numerical simulation. therefore, number of digital fiber per yarn and digital element length combined determines the digital mesh density. However, considering computer resource, result accuracy, and time-efficient calculation, presumably each yarn is numerically determined to discretize into 19 fibers [1,44] in standard deterministic and statistic ballistic impact simulation. The convergence of digital element length has never been discussed. In this section, the convergence issue is analyzed and discussed in detail on a single yarn to investigate the effect of digital element length on fabric V_{50} .

6.1.1 Single fiber

The DEA approach models fiber as short rod elements connected by pins. When the length of short rod elements reaches zero, fully flexibility is reached. Presumably, the shorter the

rod element length, the more accurate the result. However, the number of rod elements heavily effects computer recourses needed for calculation. In search of a balance between time-efficient calculation and accurate results, the element length to fiber diameter ratio is analyzed by simulating ballistic penetration and impact process using single fiber per yarn with two different element lengths to fiber diameter ratio. Different from previous convergence analysis [1,44], this study evaluates the ballistic strength of a single fiber with different element length to fiber diameter ratio. Fiber bending stiffness, shear stress, and shear stress failure are considered.

The fiber simulated in this section is 4 inch (0.1016 m) long, made of Kelvar KM2 with both ends fixed. The fiber diameter is 50 μm . As discussed in 3.2, the fiber-to-fiber contact force calculation is effected by element length. Long element length caused by coarse mesh will lead to inaccurate results. For periodic boundary relaxation of the unit-cell, element length equals to fiber radius. Thus, element length to fiber diameter ratio 0.5 and 0.125 are adopted to explore the effect of element length on single fiber ballistic strength. A spherical projectile is used to impact fiber center at the speed of 100 m/s. The weight and diameter of the projectile are 5e-06 kg and 0.00556 m respectively. The numerical results verified the convergence of the DEA approach at filament level. Details are discussed below.

Fiber element stress is recorded 7 times during calculation to observe the movement of stress wave and compare results with different element length.

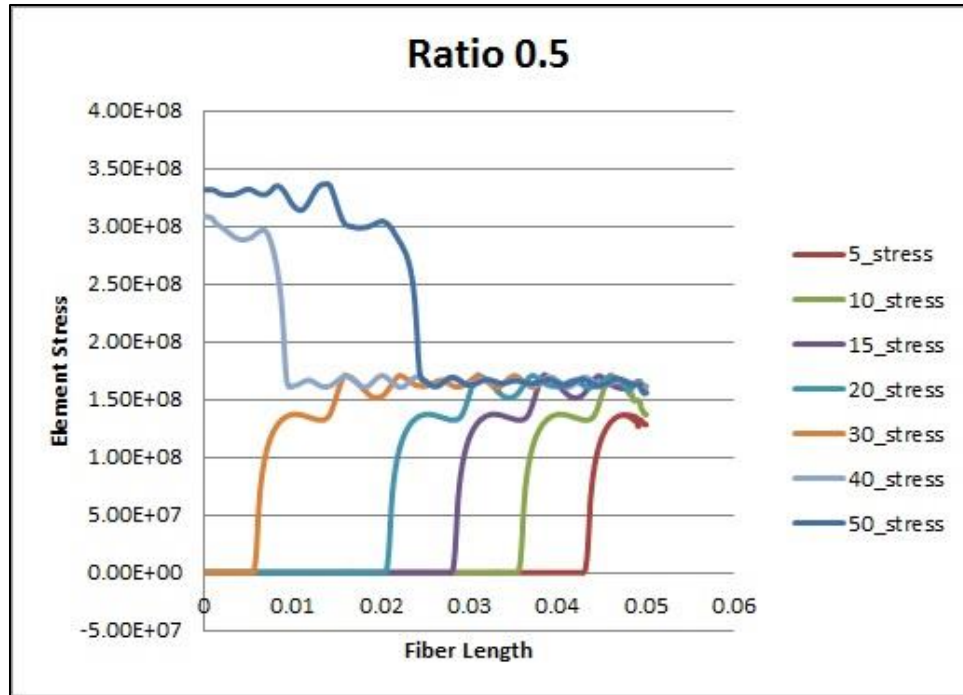


Figure 6-1 Fiber Stress of Element Length/ Fiber Diameter=0.5

Figure 6-1 shows the fiber stress of Element Length/ Fiber Diameter=0.5 fiber along fiber length starting from left end to fiber center. Only the element stress of fiber left half is plotted due to symmetry. The stress wave travels outward from fiber center to fixed fiber edge. The element stress is recorded every 5 or 10 steps. It is observed that the wave front is initiated at step 5 and is slightly lower than the rest. The stress wave reaches the edge between step 30 and step 40 and the magnitude of which doubled afterwards, continuing travel in opposite direction.

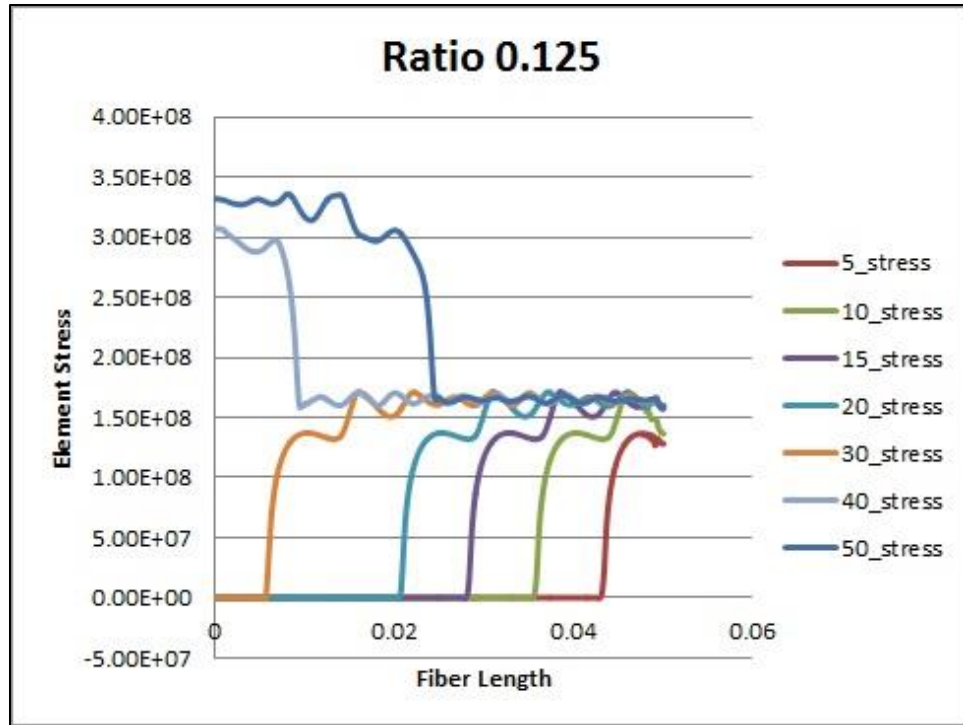
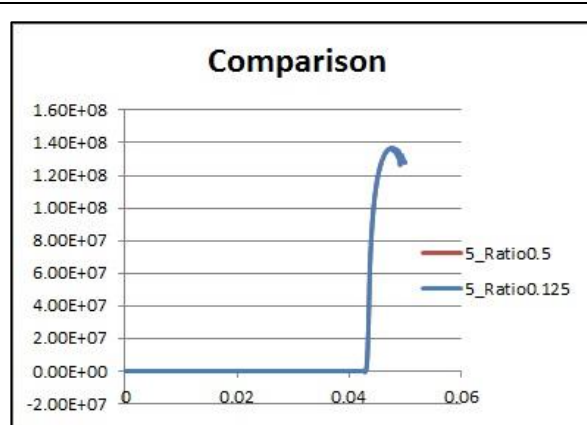
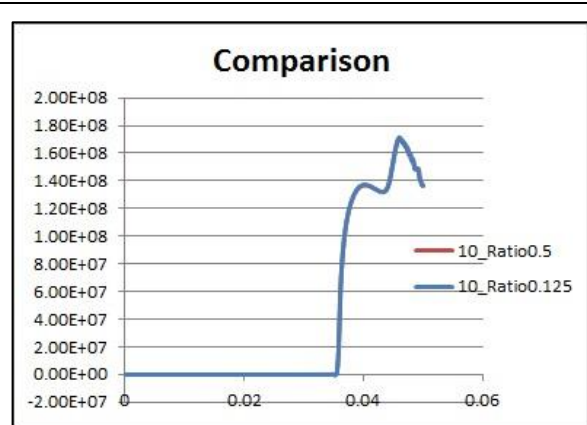


Figure 6-2 Fiber Stress of Element Length/ Fiber Diameter=0.125

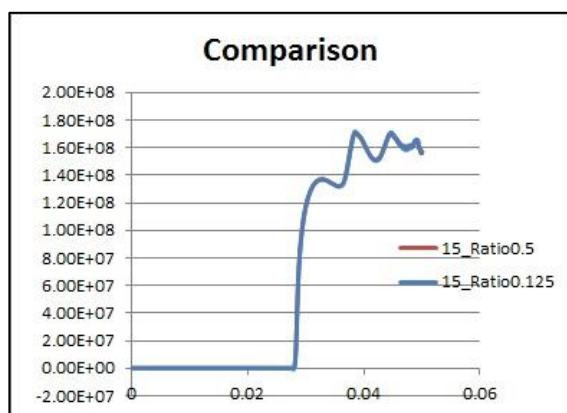
Figure 6-2 shows the element stress of ratio Fiber Stress of Element Length/ Fiber Diameter=0.125 fiber along fiber length starting from left end to fiber center. The element stress wave is recorded at the same time as previous examples, which produces almost identical results as the element stress of Fiber Stress of Element Length/ Fiber Diameter=0.125 fiber. Further comparisons between these two fibers at each step are shown Figure 6-3.



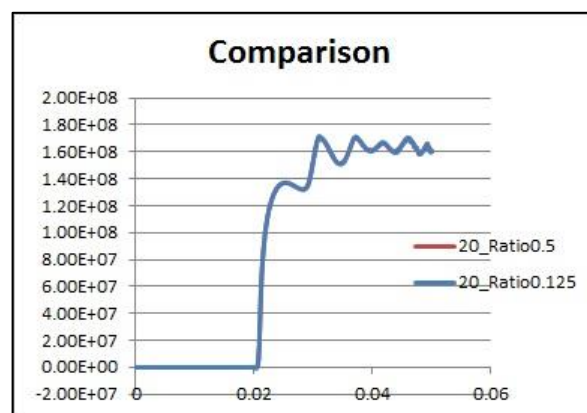
Step 5



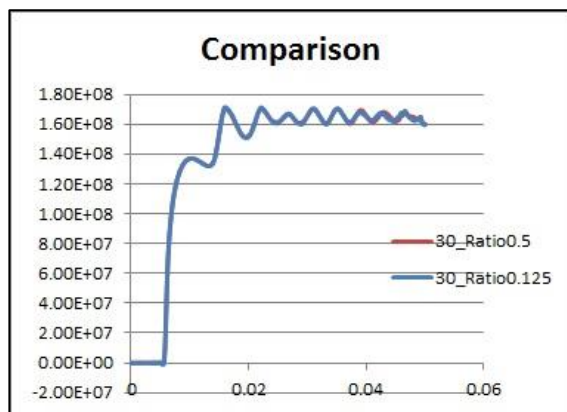
Step 10



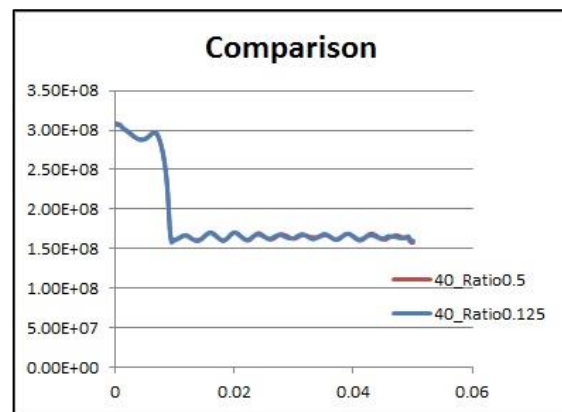
Step 15



Step 20



Step 30



Step 40

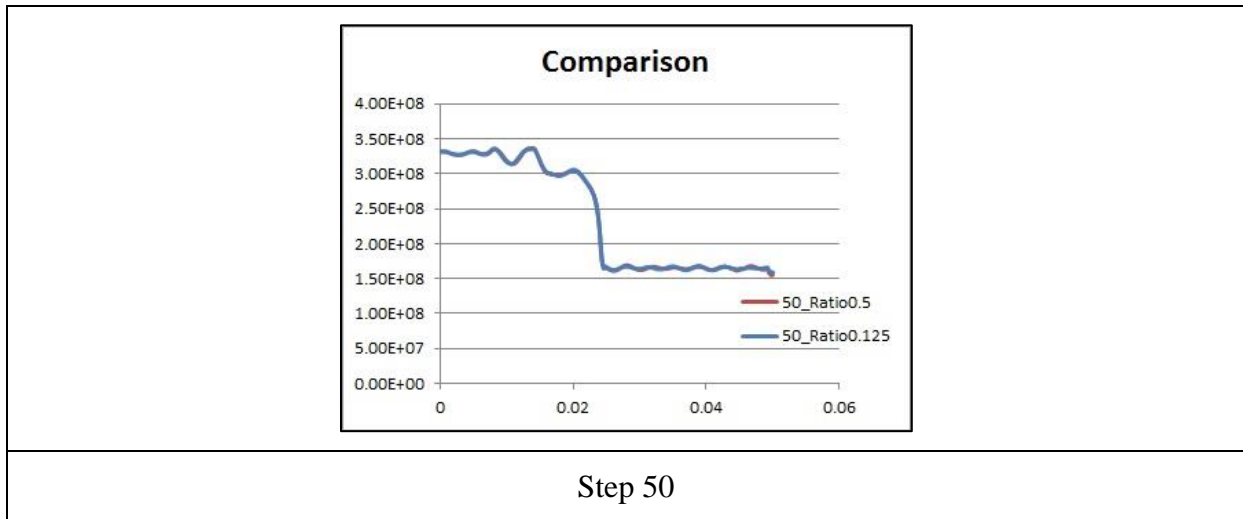


Figure 6-3 Element Stress Comparison between Ratio 0.5 and Ratio 0.125 Fiber

The two stress curves displayed in Figure 6-3 during each step is perfectly matched. The red curve and blue curve overlapped each other, thus only one curve can be observed.

The time versus projectile force curve is also developed and compared.

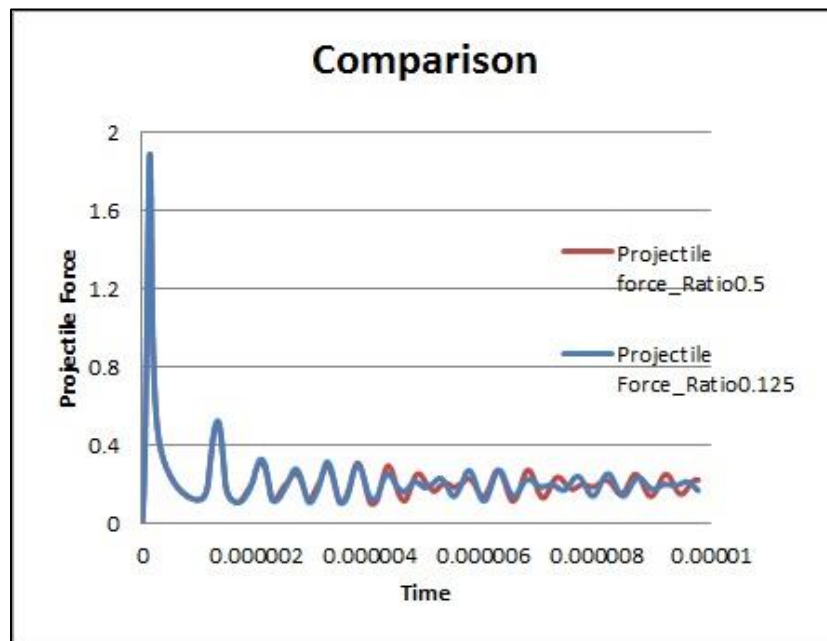


Figure 6-4 Projectile Force Comparison between Ratio 0.5 and Ratio 0.125 Fiber

6.1.2 Conclusion

Convergence check of ballistic strength evaluation is performed on a single fiber. Fiber element stress and resultant fiber to projectile force of a single fiber with different element length to fiber diameter ratio are derived and compared at multiple stages. An element length equals to fiber radius is used to ensure correct fiber-to-fiber contact calculation. An element length equals to 1/8 fiber diameter is used to produce supposable results that are more accurate. Following conclusions are reached: (1) Fiber stress plots at different stages for element length equals to 1/2 fiber diameter match perfectly that of the fiber stress plots for element length equals to 1/8 fiber diameter. (2) The fiber length versus projectile force plot of above-mentioned two sample fibers also resembles closely. (3) Ballistic strength of a single fiber converges when the element length reaches fiber radius or below. (4) The improvement of simulation result accuracy is trial when element length equals to half of fiber diameter and below. The element size equals to fiber radius is sufficient and accurate for ballistic strength simulation using spherical projectile.

6.2 Ballistic strength of multi-layer fabrics against FSP

6.2.1 Edge radius measurement

Projectile edge radius plays a significant role in estimating V_{50} in terms of high shear stress during the impact event. Fabric strength varies under the same projectile impact with different edge radius. It is critical to accurately model projectile geometry in detail. The front nose of FSP is comprised of 3 types of edges, numbered 1, 2, and 3 in Figure 6-5. Leica DVM2500, which uses the modular Leica Application Suite (LAS) and Leica MAP software package, is adopted to perform image analysis and real-time enhancement of projectile edge surface field and depth field.



Figure 6-5 FSP Projectile Edges

Figure 6-6 demonstrates the 3D view and corresponding radius profile of FSP edge 1 to edge 3 with micron scale. A smooth transaction between two surfaces can be observed for all three edges. Radius of curvature of edge 1 is approximately three times smaller than that of edge 2 and 3. As shown in Figure 6-6, the radius of curvature of edge 1, 2, and 3 is estimated to be 50 μm , 150 μm , and 150 μm respectively. The measured edge radius is used in FSP impact simulation presented in this paper.

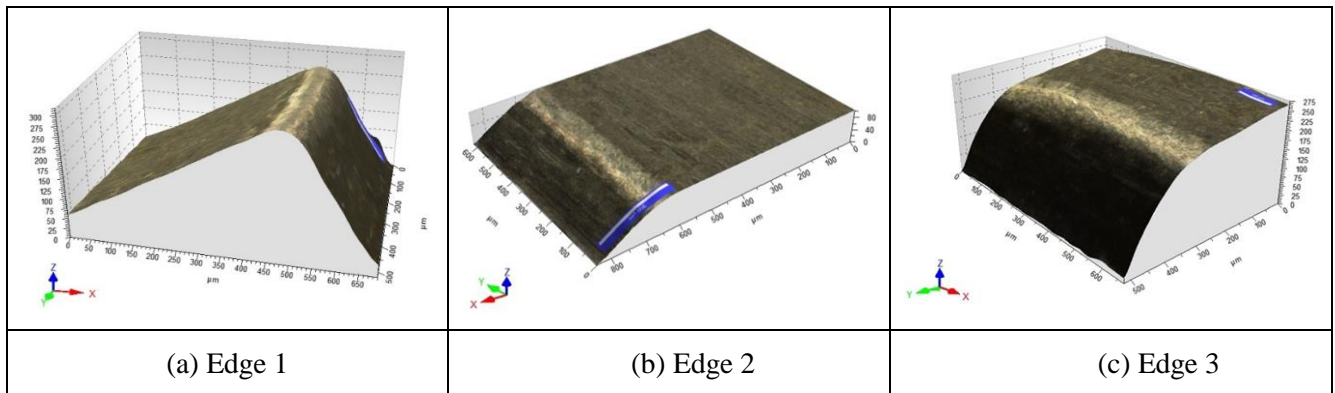


Figure 6-6 3D View and Radius Profile of FSP Edges

6.2.2 Numerical results

Experimental results of 7 standard sets of Kevlar KM2 shoot packs impacted by 17 grain FSP are received from the United States test laboratory. The striking and residual velocities were obtained using Doppler Radar. The fabric size of all specimens is 15'' by 15'', with 12'' by 12'' rectangular opening. In numerical simulation, it is assumed that the inter-fiber friction coefficient is 0.3. Number of layers ranges from 4 layers to 28 layers. The comparison between experimental set-up and numerical set-up is illustrated in Figure 6-7.

6.2.2.1 Comparison between experimental and numerical set-up

In the ballistic tests, one fabric was shot 16 times, under the condition that one shot should not be too close to prior shots. The failed fibers caused by prior shots are served as free boundaries. However, in the numerical simulation, one fabric is impacted only once at fabric center. No fabric damage prior to the impact. As such, for the experimental method, the accumulated stress wave bounced back from boundaries is higher than that of numerical simulation. Besides, for fabrics with low V_{50} , the penetration process takes longer time than fabrics with high V_{50} . Therefore, two conclusions are reached: 1) the experimental method could underestimate fabric ballistic strength due to bounced back stress wave. 2) the effect of fabric boundary on stress wave is lower for fabrics with high V_{50} .

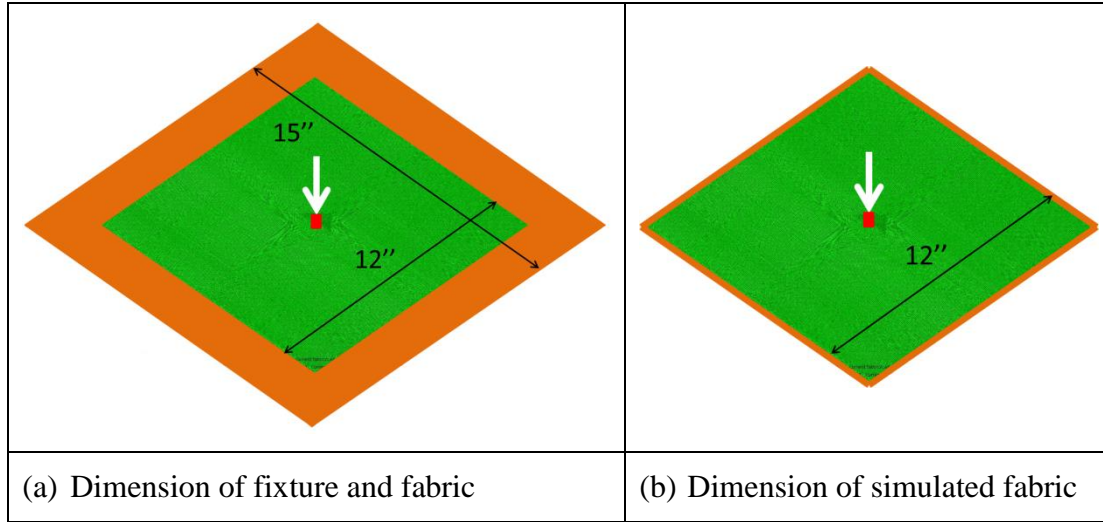


Figure 6-7 Comparison between Experimental and Numerical Set-up

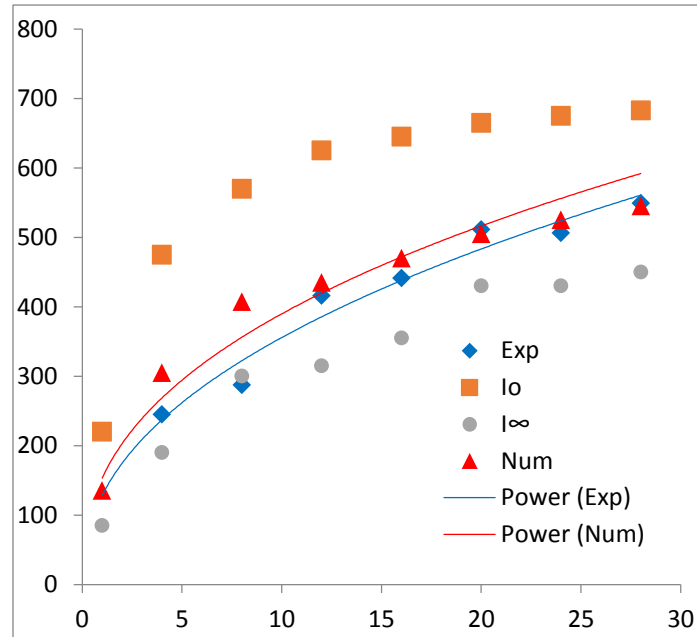
6.2.2.2 Simulation results

Refer to section 5.2, the effective bending rigidity of the digital fiber is modeled in three ways: 1) assume inter-fiber friction stops relative movement between actual fibers, the digital fiber behaves as an unity, the digital fiber area moment of inertia is denoted as $I = I_{\infty}$, 2) assume the effect of inter-fiber friction on relative motion between actual fibers is insignificant, the actual fibers move freely, the digital fiber area moment of inertia is denoted as $I = I_0$, 3) the digital fiber area moment of inertia is numerically determined as $I = \mu^{0.8}I_{\infty} + (1 - \mu^{0.8})I_0$ ($k_2 = 1, k_1 = 0.8$). Numerical results under above three conditions are listed in Table 6-1.

Table 6-1 Fabric V_{50} of Impacted by FSP

Method	1	4	8	12	16	20	24	28
I_0	220	475	570	625	645	665	675	683
I_∞	85	190	300	315	355	430	430	450
$k_1 = 1, k_2 = 0.8$	135	305	407	435	475	505	525	545
Exp.	-	245	287	416	441	511	506	549

$\mu=0.3$, unit: m/s.

Figure 6-8 Fabric V_{50} Impacted by FSP

As shown in Figure 6-8, for $I = I_\infty$, the V_{50} derived from numerical simulation of 4- to 28-layer fabric are lower than that of the experimental V_{50} except for 8-layer fabric, for $I = I_0$, the V_{50} calculated from numerical simulation of 4- to 28-layer fabric are higher than that of the experimental V_{50} . The experimental V_{50} of 8-layer fabric is notably lower than that of 12-layer fabric, which indicates a possible error in the experiment handling. The V_{50} calculated from I_∞ is

noted as the ballistic strength lower bound, the V_{50} calculated from I_0 is noted as the ballistic strength upper bound. The experimental V_{50} falls in between the upper bound and lower bound of V_{50} .

For 12- to 28-layer fabric, the simulated V_{50} matches the experiment V_{50} perfectly with the experimental V_{50} . However, for 4- and 8-layer fabric, the simulated V_{50} using $k_1 = 1, k_2 = 0.8$ is higher than that of the experimental V_{50} . The discrepancy is possibly caused by the difference between experimental and numerical set-up illustrated in **Error! Reference source not found..** Therefore, it is safe to conclude the modified DEA approach successfully predict ballistic strength of multi-layer fabrics against FSP projectile.

6.3 Conclusion

The objective of this research is to estimate ballistic strength of textile fabric using FSP. First, the modified DEA with combined tension-shear failure model is established. The effective digital fiber bending rigidity is numerically determined. Second, filament level contact search method between solid body projectile and textile fabric is explained. This method enables simulating ballistic impact of textile fabric using projectile of arbitrary shape. Third, ballistic simulation of real scale multi-layer fabric is performed using measured edge radius. This simulation analyzed the effect of digital fiber bending rigidity on fabric V_{50} and verified the modified DEA approach. Numerical results are compared to high resolution experimental data. The following conclusions are reached:

1. Fabric shear force plays a significant role in estimating fabric ballistic strength against projectile with sharp edge(s). The same projectile with different edge radius produces

different fabric V_{50} . For projectile with sharp edges, failure mechanism shifted from tension to shear dominant. It is critical to determine fiber shear stress.

2. The effective digital fiber bending rigidity is modeled under two conditions: 1) assume inter-fiber friction stops relative movement between fibers, the digital fiber area moment of inertia is expressed as $I = I_{\infty}$, 2) assume the effect of inter-fiber friction on relative motion between fibers is insignificant, each fiber acts independently, the digital fiber area moment of inertia is expressed as $I = I_0$. When $I = I_0$, the numerical V_{50} produces the upper bound, when $I = I_{\infty}$, the simulated V_{50} produces the lower bound. When the number of digital fiber per yarn approach actual fiber per yarn, simulation results using I_{∞} and I_0 converged.

3. Digital fiber area moment of inertia coefficients k_1 and k_2 are numerically determined. When $k_1 = 1$, $k_2 = 0.8$, the simulated V_{50} for a single yarn with different number of digital fibers stays close to the V_{50} of actual fibers per yarn model. The number of digital fiber per yarn has relatively small effect on yarn V_{50} . Coefficients $k_1 = 1$, $k_2 = 0.8$ are applicable for Kevlar KM2 fabric.

4. The ballistic simulation of real scale multi-layer fabric impacted by FSP is performed using three different digital fiber bending rigidity. The experimental V_{50} is in between the simulated upper bound and lower bound of V_{50} . The numerical results simulated using coefficients $k_1 = 1$, $k_2 = 0.8$ matches the experimental results closely. The modified DEA approach successfully estimated the ballistic strength of real scale multi-layer fabric against FSP.

5. The modified DEA has broad applications and implications for understanding how practical protective structures respond to projectiles with different geometries. This approach does not only provide guidance to experimental research and manufactural production, but also

verifies real scale multi-layer ballistic tests results against types of projectiles, offering a broad platform for solid body impact and penetration simulation of textile fabrics.

References

- [1] Wang Y, Miao Y, Swenson D, Cheeseman BA, Yen CF, LaMattina B. Digital element approach for simulating impact and penetration of textiles. *Int J Impact Eng* 2010;37:552–60. doi:10.1016/j.ijimpeng.2009.10.009.
- [2] Huang L, Wang Y, Miao Y, Swenson D, Ma Y, Yen CF. Dynamic relaxation approach with periodic boundary conditions in determining the 3-D woven textile micro-geometry. *Compos Struct* 2013;106:417–25. doi:10.1016/j.compstruct.2013.05.057.
- [3] Nilakantan G, Keefe M, Gillespie JW. Modeling the Material and Failure Response of Continuous Filament Fabrics for use in Impact Applications. *Texcomp 9 – Int Conf Text Compos* 2008.
- [4] Wang YXYM. Experimental and theoretical study on the strain rate and temperature dependence of mechanical behavior of Kevlar fibre. *Compos Part A Appl Sci Manuf* 1999;30:1251–7.
- [5] Koichi Goda HF. The evaluation of the strength distribution of silicon carbide and alumina fibres by a multi-modal Weibull distribution. *J Mater Sci* 1986;21:4475–80.
- [6] Hudspeth M, Agarwal A, Andrews B, Claus B, Hai F, Funnell C, et al. Degradation of yarns recovered from soft-armor targets subjected to multiple ballistic impacts. *Compos Part A Appl Sci Manuf* 2014;58:98–106. doi:10.1016/j.compositesa.2013.12.004.
- [7] Roylance D, Hammas P, Ting J, Chi H, Scott B. Numerical modeling of fabric impact. *Asme-Publications-Ad* 1995.
- [8] Cheng M, Chen W, Weerasooriya T. Mechanical Properties of Kevlar® KM2 Single Fiber. *J Eng Mater Technol* 2005;127:197. doi:10.1115/1.1857937.
- [9] Cheng M, Chen W, Weerasooriya T. Experimental investigation of the transverse mechanical properties of a single Kevlar® KM2 fiber. *Int J Solids Struct* 2004;41:6215–32. doi:10.1016/j.ijsolstr.2004.05.016.
- [10] Kaw AK. *Mechanics of Composite Materials*. Boca Raton: CRC Press; 1997.
- [11] Rebouillat S. Tribological properties of woven para-aramid fabrics and their constituent yarns. *J Mater Sci* 1998;33:3293–301. doi:10.1023/a:1013225027778.
- [12] Dong Z, Sun CT. Testing and modeling of yarn pull-out in plain woven Kevlar fabrics. *Compos Part A Appl Sci Manuf* 2009;40:1863–9. doi:10.1016/j.compositesa.2009.04.019.

- [13] Nilakantan G, Gillespie JW. Ballistic impact modeling of woven fabrics considering yarn strength, friction, projectile impact location, and fabric boundary condition effects. *Compos Struct* 2012;94:3624–34. doi:10.1016/j.compstruct.2012.05.030.
- [14] Briscoe BJ, Motamedi F. Role of interfacial friction and lubrication in yarn and fabric mechanics. *Text Res J* 1990;60:697–708.
- [15] Briscoe BJ, Motamedi F. The ballistic impact characteristics of aramid fabrics: The influence of interface friction. *Wear* 1992;158:229–47. doi:10.1016/0043-1648(92)90041-6.
- [16] Bszhenov S. Dissipation of energy by bulletproof aramid fabric. *J Mater Sci* 1997;32:4167–73.
- [17] Vinson JR, Zukas JA. On the ballistic impact of textile body armor. *J Appl Mech* 1975;42:263–8. doi:10.1115/1.3423564.
- [18] Vinson JR, Zukas JA. On the Ballistic Impact of Textile Body Armor. *J Appl Mech* 1975;42:263–8.
- [19] Jack R, Vinson JR, William J. Modeling ballistic impact into flexible materials. *AIAA J* 1990;28:2098–103.
- [20] Leigh Phoenix S, Porwal PK. A new membrane model for the ballistic impact response and V50 performance of multi-ply fibrous systems. *Int J Solids Struct* 2003;40:6723–65. doi:10.1016/S0020-7683(03)00329-9.
- [21] Simons JW, Erlich DC, SHOCKEY DA. finite element design model for ballistic response of woven fabrics. 19th Int. Symposium Ballist., 2001, p. 1415–22.
- [22] Lim CT, Shim VPW, Ng YH. Finite-element modeling of the ballistic impact of fabric armor. *Int J Impact Eng* 2003;28:13–31. doi:10.1016/S0734-743X(02)00031-3.
- [23] Silva MAG, CISMASUI C, Chiorean CG. Numerical Simulation of Ballistic Impact on Composite Laminates. *Int J Impact Eng* 2005;31:289–306.
- [24] Roylance D, Wilde A, Tocci G. Ballistic Impact of Textile Structures. *Text Res J* 1973;43:34–41. doi:10.1177/004051757304300105.
- [25] Roylance D. Wave Propagation in a Viscoelastic Fiber Subjected to Transverse Impact. *J Appl Mech* 1973;40:143. doi:10.1115/1.3422914.
- [26] Roylance D, Wang SS. Influence of fibre properties on ballistic penetration of textile panels. *Fibre Sci Technol* 1981;14:183–90. doi:10.1016/0015-0568(81)90010-5.

- [27] Cunniff PM. An Analysis of the System Effects in Woven Fabrics under Ballistic Impact. *Text Res J* 1992;62:495–509.
- [28] Dent R, J.G. D. Projectile Impact with Flexible-Armor with Crimp Interchange. 1988.
- [29] Prevorsek DC. Spectra Composite Armor: Dynamics of Absorbing the Kinetic Energy of Ballistic Projectiles. 34th Int. SAMPE Symp., 1989, p. 1780–9.
- [30] Shim VPW, Tan VBC, Tay TE. Modelling deformation and damage characteristics of woven fabric under small projectile impact. *Int J Impact Eng* 1995;16:585–605. doi:10.1016/0734-743X(94)00063-3.
- [31] Philip Cunniff, Ting C, Ting J, Roylance D. Numerical characterization of the effects of transverse yarn interaction on textile ballistic response. 30th Tnternational SAMPE Tech Conf 1998:1–13.
- [32] King MJ, Jearanaisilawong P, Socrate S. A continuum constitutive model for the mechanical behavior of woven fabrics. *Int J Solids Struct* 2005;42:3867–96. doi:10.1016/j.ijsolstr.2004.10.030.
- [33] Shockey D a, Giovanola JH, Simons JW, Erlich DC, Kolpp RW, Skaggs SR. Advanced armour technology: application potential for engine fragment barrier for commercial aircraft 1997.
- [34] Duan Y, Keefe M, Bogetti TA, Cheeseman BA. Modeling friction effects on the ballistic impact behavior of a single-ply high-strength fabric. *Int J Impact Eng* 2005;31:996–1012. doi:10.1016/j.ijimpeng.2004.06.008.
- [35] Duan Y, Keefe M, Bogetti TA, Cheeseman BA, Powers B. A numerical investigation of the influence of friction on energy absorption by a high-strength fabric subjected to ballistic impact. *Int J Impact Eng* 2006;32:1299–312. doi:10.1016/j.ijimpeng.2004.11.005.
- [36] Duan Y, Keefe M, Bogetti TA, Powers B. Finite element modeling of transverse impact on a ballistic fabric. *Int J Mech Sci* 2006;48:33–43. doi:10.1016/j.ijmecsci.2005.09.007.
- [37] Talebi H, Wong S V., Hamouda AMS. Finite element evaluation of projectile nose angle effects in ballistic perforation of high strength fabric. *Compos Struct* 2009;87:314–20. doi:10.1016/j.compstruct.2008.02.009.
- [38] Yen C. A Ballistic Material Model for Continuous-fiber Reinforced Composites. *Int J Impact Eng* 2012;46:11–22.
- [39] Luan K, Sun B, Gu B. Ballistic impact damages of 3-D angle-interlock woven composites

- based on high strain rate constitutive equation of fiber tows. *Int J Impact Eng* 2013;57:145–58. doi:10.1016/j.ijimpeng.2013.02.003.
- [40] Wang Y, Sun X. Determining the geometry of textile preforms using finite element analysis. *Proc. Am. Soc. Compos.*, College Station, TX: 2000, p. 485–92.
 - [41] Sun X, Wang Y. Geometry of 3-D braiding rectangular preform with axial yarns. 46th Int. SAMPE Symp., Long Beach Convention Center, CA: 2001, p. 311–9.
 - [42] Wang Y, Sun X. Digital element simulation of textile processes. *Compos Sci Technol* 2001;63:311–9.
 - [43] Miao Y, Yu J, Wang Y, Yen C, Swenson D, Cheeseman B. Energy loss due to transverse plastic deformation of fibers in textile fabric impact processes. *Am. Soc. Compos. 25th Tech. Conf.*, Dayton, Ohio: 2010.
 - [44] Wang Y, Miao Y, Huang L, Swenson D, Yen CF, Yu J, et al. Effect of the inter-fiber friction on fiber damage propagation and ballistic limit of 2-D woven fabrics under a fully confined boundary condition. *Int J Impact Eng* 2016;97:66–78. doi:10.1016/j.ijimpeng.2016.06.007.
 - [45] Zohdi TI, Powell D. Multiscale construction and large-scale simulation of structural fabric undergoing ballistic impact. *Comput Methods Appl Mech Eng* 2006;195:94–109. doi:10.1016/j.cma.2005.01.011.
 - [46] Grujicic M, Hariharan A, Pandurangan B, Yen CF, Cheeseman BA, Wang Y, et al. Fiber-level modeling of dynamic strength of kevlar® KM2 ballistic fabric. *J Mater Eng Perform* 2012;21:1107–19. doi:10.1007/s11665-011-0006-1.
 - [47] Dippolito M, Wang Y, Ma Y, Yen C, Zheng JQ, Halls V. Simulation of Ballistic Tests for Multi-layer Fabric Body Armors. *ASME Int. Mech. Eng. Congr. Expo.*, 2014.
 - [48] Zhou G, Sun X, Wang Y. Multi-chain digital analysis in textile mechanics. *Compos Sci Technol* 2003;64:239–44.
 - [49] Miao Y, Zhou E, Wang Y, Cheeseman BA. Mechanics of textile composites: Micro-geometry. *Compos Sci Technol* 2008;68:1671–8. doi:10.1016/j.compscitech.2008.02.018.
 - [50] Miao Y, Huang L, Wang Y, Swenson D, Yen C, Cheeseman BA. Explicit Digital Element Approach with Periodic Boundary in Determining Textile Micro-geometry. 24th Annu. Tech. Conf. Am. Soc. Compos. 1st Jt. Can. Tech. Conf. Compos., 2009, p. 1978–90.
 - [51] Ma Y, Huang L, Wang Y, Swenson D, Sullivan B, Yen C. Validation of Explicit Digital

- Element Dynamic Relaxation Approach in Determining Micro-geometry of 3-D Woven Fabrics. 27th Conf. Am. Soc. Compos., 2012.
- [52] Huang L. Determining Micro- and Macro- geometry of Fabric and Fabric Reinforced Composites. Kansas State University, 2013.
 - [53] Johnson KL. Contact Mechanics. Cambridge: 1985.
 - [54] Cook R, Malkus D, Plesha M. Concepts and Applications of Finite Element Analysis. New Yorke: John Wiley & Sons; 1974.
 - [55] Felippa C. Introduction to Finite Element Methods. Boulder: n.d.
 - [56] Sanborn B, Weerasooriya T. Effect of strain rates and pre-twist on tensile strength of Kevlar KM2 single fiber. 2013.
 - [57] Ma Y, Wang Y, Dippolito M, Yen C-F, Zhen J, Halls V. Ballistic strength of Kevlar KM2 fabric using FSP projectiles. 31th Tech. Conf. ASC, 2016, p. 13.